INFORMATION TO USERS

This material was produced from a microfilm copy of the original document. While the most advanced technological means to photograph and reproduce this document have been used, the quality is heavily dependent upon the quality of the original submitted.

The following explanation of techniques is provided to help you understand markings or patterns which may appear on this reproduction.

1. The sign or "target" for pages apparently lacking from the document photographed is "Missing Page(s)". If it was possible to obtain the missing page(s) or section, they are spliced into the film along with adjacent pages. This may have necessitated cutting thru an image and duplicating adjacent pages to insure you complete continuity.

2. When an image on the film is obliterated with a large round black mark, it is an indication that the photographer suspected that the copy may have moved during exposure and thus cause a blurred image. You will find a good image of the page in the adjacent frame.

3. When a map, drawing or chart, etc., was part of the material being photographed the photographer followed a definite method in "sectioning" the material. It is customary to begin photoing at the upper left hand corner of a large sheet and to continue photoing from left to right in equal sections with a small overlap. If necessary, sectioning is continued again — beginning below the first row and continuing on until complete.

4. The majority of users indicate that the textual content is of greatest value, however, a somewhat higher quality reproduction could be made from "photographs" if essential to the understanding of the dissertation. Silver prints of "photographs" may be ordered at additional charge by writing the Order Department, giving the catalog number, title, author and specific pages you wish reproduced.

5. PLEASE NOTE: Some pages may have indistinct print. Filmed as received.

Xerox University Microfilms
300 North Zeeb Road
Ann Arbor, Michigan 48106

Downloaded from SHAREOK. Persistent Handle URL: https://hdl.handle.net/11244/4099

76-15,807

RAO, Prabhakar P., 1944-
TWO DIMENSIONAL CONFIGURATION ANALYSIS OF
A FLAT-PLATE SOLAR COLLECTOR.

The University of Oklahoma, Ph.D., 1975
Engineering, mechanical

Xerox University Microfilms, Ann Arbor, Michigan 48106

THIS DISSERTATION HAS BEEN MICROFILMED EXACTLY AS RECEIVED.

THE UNIVERSITY OF OKLAHOMA

GRADUATE COLLEGE

TWO DIMENSIONAL CONFIGURATION ANALYSIS OF A FLAT-PLATE SOLAR COLLECTOR

A DISSERTATION

SUBMITTED TO THE GRADUATE FACULTY

in partial fulfillment of the requirements for the

degree of

DOCTOR OF PHILOSOPHY

By

PRABHAKAR P. RAO

Norman, Oklahoma

1975

TWO DIMENSIONAL CONFIGURATION ANALYSIS OF A FLAT-PLATE SOLAR COLLECTOR

APPROVED BY

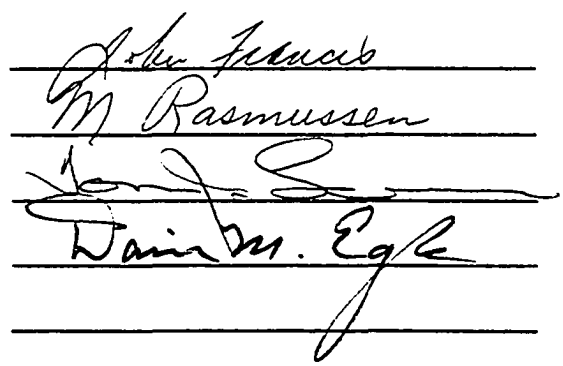

DISSERTATION COMMITTEE

ACKNOWLEDGEMENTS

The author wishes to express his deep indebtedness and appreciation to his co-advisers, Dr. Tom J. Love, Jr., and Dr. John E. Francis under whose guidance, encouragement and extreme patience this work was made possible.

It would be impossible to express appreciation to all who have helped directly or indirectly in this endeavor, however, the author would like to express his thanks to the entire dissertation committee including Dr. M.L. Rasmussen, Dr. D.M. Egle and Dr. D.L. Perkins for having kindly consented and given their time to be on the committee. The author also wishes to thank Dr. Martin Jischke for his help and criticism during the course of the author's graduate studies.

A special word of thanks goes to the author's parents and brother Krishna, for their foresight and encouragement throughout the author's student career. And finally, the author is especially grateful to his wife Vim, for her love, encouragement and understanding. Since she was instrumental in getting the author to do Ph.D., in appreciation this work is dedicated to her.

ABSTRACT

In the present study, a two-dimensional theoretical model of a flat-plate solar collector is developed. By means of this model, it has been shown using hourly values of weather data, that the collector configuration parameters such as length, tube spacing, plate thickness etc., can be optimized based on least cost per Btu of energy absorbed.

The performance model obtained in this study is based on a differential formulation as compared to the existing models of Hottel, Whillier, and Bliss, which are based on a lumped formulation. An explicit expression for the average plate temperature has been obtained. The thermal losses from the plate surface have been considered to be a function of the local plate temperature and the overall loss coefficient has been assumed to be constant for the whole plate.

A Fortran program of the model is developed, whereby, the effects of various parameters on the collector performance and on the cost/Btu of energy absorbed could be studied in a quantitative manner. The present analysis quantitatively verifies the observations made by previous investigators regarding the effects of various parameters on the collector performance and provides a systematic method of evaluating it under different conditions.

NOMENCLATURE

a_n	a constant, defined in equation (3.2.9)
A	surface area of the collector
A_1, A_2, A_3	constants of integration
AST	apparent solar time
b_n	a constant, defined in equation (3.2.9)
B	tube spacing
$\hat{B}_1, \hat{B}_2, \hat{B}_3$	constants of integration
B_n	nth coefficient of the infinite series in the temperature expressions
$B_n^{(K)}$	approximation for B_n according to the Kth truncation
c	correction coefficient for convection from a tilted surface
cc	tenths of sky area covered by clouds (0 = clear sky and 10 = fully covered)
c_i	inequality constraints
C_p	specific heat of the collector fluid
C_1, C_2, C_3	constants of integration
d	nominal diameter of the collector tube
Day	day of the year (Jan. 1 ≡ 1 and Dec. 31 ≡ 365)
D_i	inside diameter of the collector tube
D_o	outside diameter of the collector tube

DST	daylight savings time indicator
D_1, D_2, D_3	constants of integration
e_j	equality constraints
E	constant of integration
$\hat{E}_K$	squared error, defined in equation (3.2.12)
f	ratio of the thermal resistance of the outer plate to that of the inner plate, defined by equation (4.2.4)
F	cost function or objective function
F_i	value of the function at the ith point of the complex
$\bar{F}$	mean value of the function
g_m	a constant, defined in equation (3.2.14)
G_i	lower limit of the constraint
$G(x^*)$	a function of x^*, defined in equation (3.2.9)
Gr_m	arithmetic-mean Grashof's number
Gz_m	arithmetic-mean Graetz's number
$\bar{h}_{base}$	convection heat-transfer coefficient between the bottom of the insulation and the surroundings
$\bar{h}_f$	convection heat-transfer coefficient between the tube wall and the circulating fluid
$\bar{h}_i$	convection heat-transfer coefficient between the ith cover plate and the cover beneath
$\bar{h}_w$	convection heat-transfer coefficient between the top cover and the atmosphere (wind heat-transfer coefficient)
$\bar{h}_1$	convection heat-transfer coefficient between the collector plate and the cover directly above it
H	hour of the day (24 hour time)
$\hat{H}$	a constant, defined in equation (3.2.9)
HA	hour angle of the sun

H_i upper limit of the constraint

i angle of incidence of the direct radiation striking a surface

k thermal conductivity of the collector tube and plate material

$\hat{k}$ points of the initial complex

$\tilde{k}$ pre-assigned number

k_l thermal conductivity of the insulation

L length of collector plate or tube

$\hat{L}$ latitude

$\dot{m}$ mass flow rate of the collector fluid

M a constant defined in equation (2.1.7)

M_f a constant defined in equation (2.1.13)

n number of glass covers of the collector

N a constant defined in equation (2.1.7)

N_f a constant defined in equation (2.1.13)

Nu Nusselt number

Nu_m arithmetic mean Nusselt number

P a constant defined in equation (2.1.13)

Pr Prandtl number

Pr_m arithmetic-mean Prandtl number

$\dot{q}_{dh}$ diffuse solar radiation per unit area on a horizontal surface

$\dot{q}_{Dh}$ direct solar radiation per unit area on a horizontal surface

$\dot{q}_{Dt}$ direct solar radiation per unit area on a tilted surface

$\dot{q}_i$ energy absorbed per unit area by the collector, after optical losses

$\dot{q}_L$	heat loss per unit area from the plate surface
$\dot{q}_{L,base}$	downward heat loss per unit area through the insulation
$\dot{q}_{L,up}$	heat loss per unit area from the plate surface by convection and radiation to the glass cover(s) above
$\dot{q}_{th}$	total incident-radiation per unit area on a horizontal surface
$\dot{q}(x)$	heat flux per unit area in the y-direction
$\dot{Q}_x$	heat flux into element at x
$\dot{Q}_{x+\Delta x}$	heat flux out of the element at $x+\Delta x$
$\dot{Q}_y$	heat flux into element at y
$\dot{Q}_{y+\Delta y}$	heat flux out of the element at $y+\Delta y$
r	angle of refraction of the incident radiation
$r_{i,j}$	pseudo-random numbers
R	reflection loss of direct radiation per unit area from a single surface of glass
Re	Reynold's number
R_r	reflection loss of diffuse radiation per unit area
R_n	reflection loss of direct radiation per unit area from a system of n glass surfaces
S	standard deviation, defined by equation (6.2.5)
$S_K(x^*)$	a sum denoted by equation (3.2.11)
t	thickness of the collector plate
$\hat{T}$	a constant defined in equation (3.2.9)
T_{avg}	average plate temperature
T_f	fluid temperature
$T_{f,avg}$	average temperature of the fluid

T_i temperature of the ith glass cover

T_{in} inlet temperature of the fluid

T_n temperature of the nth cover plate

T_{out} outlet temperature of the fluid

T_p plate temperature

T_∞ ambient temperature

U non-dimensional plate temperature distribution

U_L overall loss coefficient of the collector plate given by equation (4.2.7)

$U_{L,up}$ upward overall loss coefficient of the collector plate given by equation (4.2.5)

U_o overall loss coefficient between the collector fluid and the ambient

v wind speed in knots

W width of the collector plate

x spatial coordinate in the rectangular cartesian system, parallel to the flow direction

x^* dimensionless spatial coordinate

$x_1, x_2 \ldots x_n$ independent variables of the objective function

$x_{i,j}$ coordinates of trial points in a complex

X a function of x^* coordinate

y spatial coordinate in the rectangular cartesian system, normal to the flow direction

y^* dimensionless spatial coordinate

Y a function of y^* coordinate

α absorbtivity of a black non-selective surface

$\hat{\alpha}$ solar elevation above the horizon

α_{nm}	a constant defined by equation (3.2.15)
β	collector orientation in degrees
γ	empirical parameter
δ	ratio of plate length to plate width
$\hat{\delta}$	solar declination
ϵ_c	emissivity of the collector plate for infrared radiation
ϵ_g	emissivity of glass for infrared radiation
θ_{avg}	non-dimensional average plate temperature
θ_f	non-dimensional fluid temperature distribution
$\theta_{f,avg}$	non-dimensional average fluid temperature
θ_p	non-dimensional plate temperature distribution
λ	defined by equation (3.1.13)
μ_b	dynamic viscosity of the fluid at the bulk temperature
μ_w	dynamic viscosity of the fluid at the wall temperature
ν_n	defined in equation (3.1.15)
ν_o	defined in equation (3.1.9)
ξ	dummy variable
ρ_p	density of the plate material
$\phi_n(x^*)$	a function of x^* defined in equation (3.2.9)

TABLE OF CONTENTS

ACKNOWLEDGMENTS iii

ABSTRACT. iv

NOMENCLATURE. v

LIST OF ILLUSTRATIONS xiii

Chapter Page

1. INTRODUCTION 1

1.1 Purpose of Study. 1
1.2 Method of Analysis. 3
1.3 Review of Related Studies 4

2. PROBLEM FORMULATION. 7

2.1 Governing Equations 7

2.1.1 Collector Plate. 7
2.1.2 Fluid Inside the Tube. 10

2.2 Boundary Conditions 12

3. ANALYTICAL SOLUTIONS 14

3.1 Temperature Distribution of the Collector Plate . . . 14
3.2 Temperature Distribution of the Fluid 19
3.3 Average Collector-Plate Temperature 24

4. OPTICAL AND THERMAL LOSSES

4.1 Calculation of the Solar Flux on the Collector Plate Surface. 26

4.1.1 Solar Altitude Angle 27
4.1.2 The Incident Angle 28
4.1.3 Diffuse Solar Radiation on a Horizontal Surface 29
4.1.4 Direct Solar Radiation on a Tilted Surface and the Optical Losses. 29

TABLE OF CONTENTS (Cont'd.)

Chapter		Page
	4.2 Calculation of Thermal Losses from Collector.	31
	4.2.1 Upward Heat Loss Through the Transparent Cover Plates.	31
	4.2.2 Downward Heat Loss Through the Insulation. . . .	34
	4.3 Heat Transfer Coefficient Between the Tube Wall and Collector Fluid.	34
5.	DISCUSSION OF THE EFFECTS OF VARIOUS COLLECTOR PARAMETERS ON THE TEMPERATURE DISTRIBUTIONS AND COLLECTOR PERFORMANCE .	37
	5.1 Effect of Collector Parameters on the Temperature Distribution of the Absorber Plate	37
	5.2 Effect of Collector Parameters on the Temperature Distribution of the Fluid.	51
	5.3 Effect of Collector Parameters on the Short Term Collector Performance.	56
6.	OPTIMIZATION OF COLLECTOR CONFIGURATION.	68
	6.1 Introduction.	68
	6.2 Formulation of the Optimization Problem	69
	6.3 Complex Method of Box	70
	6.4 Formulation of the Cost Function.	74
	6.5 Some Results of the Optimization Scheme	76
7.	CONCLUDING REMARKS	79
BIBLIOGRAPHY		81
APPENDIX		
A.	TEMPERATURE DISTRIBUTION OF COLLECTOR FLUID FOR THE LIMITING CASE OF TUBES SIDE BY SIDE.	83
B.	EXPERIMENTAL DETERMINATION OF THE ISOTHERMS OF THE ABSORBER PLATE USING SCANNING INFRARED CAMERA	87

LIST OF ILLUSTRATIONS

Figure — Page

5.1.1 Plot of plate temperature normal to the tube versus normalized plate width, for $B/D_o = 8$, kt = 0.391 Btu/hr-^oF, $\dot{q}_{th} = 200$ Btu/hr-ft^2, $T_\infty = 50^o$, $T_{in} = 85^oF$ and n=1 38

5.1.2 Plot of plate temperature parallel to the tube versus normalized plate length, for $B/D_o = 8$, kt = 0.391 Btu/hr-^oF, $\dot{q}_{th} = 200$ Btu/hr-ft^2, $T_\infty = 50^oF$, $T_{in} = 85^oF$ and n=1 39

5.1.3a Plot of isotherms of the collector plate for a flow rate of 50 lbs/hr-ft^2, $B/D_o = 8$, kt = 0.391 Btu/hr-^oF, $\dot{q}_{th} = 200$ Btu/hr-ft^2, $T_\infty = 50^oF$, $T_{in} = 85^oF$ and n=1. . 41

5.1.3b Plot of isotherms of the collector plate for a flow rate of 10 lbs/hr-ft^2, $B/D_o = 8$, kt = 0.391 Btu/hr-^oF, $\dot{q}_{th} = 200$ Btu/hr-ft^2, $T_\infty = 50^oF$, $T_{in} = 85^oF$ and n=1. . 42

5.1.3c Plot of isotherms of the collector plate for a flow rate of 2 lbs/hr-ft^2, $B/D_o = 8$, kt = 0.391 Btu/hr-^oF, $\dot{q}_{th} = 200$ Btu/hr-ft^2, $T_\infty = 50^oF$, $T_{in} = 85^oF$ and n=1. . 43

5.1.4a Effect of the product of plate thickness and thermal conductivity on the plate temperature profiles normal to the tube, for a mass flow rate of 11 lbs/hr-ft^2, $B/D_o = 8$, $\dot{q}_{th} = 200$ Btu/hr-ft^2, $T_\infty = 50^oF$, $T_{in} = 85^oF$ and n=1. . 44

5.1.4b Effect of the product of plate thickness and thermal conductivity on the plate temperature profiles parallel to the tube, for a mass flow rate of 11 lbs/hr-ft^2, $B/D_o = 8$ $\dot{q}_{th} = 200$ Btu/hr-ft^2, $T_\infty = 50^oF$, $T_{in} = 85^oF$ and n=1. . 45

Figure Page

5.1.5a Effect of the ratio of tube spacing to tube diameter on the plate temperature profiles normal to the tube, for a mass flow rate of 11 lbs/hr-ft^2, $\dot{q}_{th}$ = 200 Btu/hr-ft^2, kt = 0.391 Btu/hr-^{o}F, T_∞ = 50°F, T_{in} = 85°F and n=1 47

5.1.5b Effect of the ratio of tube spacing to tube diameter on the plate temperature profiles parallel to the tube, for a mass flow rate of 11 lbs/hr-ft^2, $\dot{q}_{th}$ = 200 Btu/hr-ft^2-^{o}F, kt = 0.391 Btu/hr-^{o}F, T_∞ = 50°F, T_{in} = 85°F and n=1. . 48

5.2.1 Effect of mass flow rate on the fluid temperature distribution along the tube for B/D_o = 8, $\dot{q}_{th}$ = 200 Btu/hr-ft^2, kt = 0.391 Btu/hr-^{o}F, T_∞ = 50°F, T_{in} = 85°F and n=1. . 49

5.2.2 Plots of fluid outlet temperature, average plate temperature and collector efficiency versus mass flow rate for L = 10 ft, B/D_o = 8, $\dot{q}_{th}$ = 200 Btu/hr-ft^2, kt = 0.194 Btu/hr-^{o}F, T_∞ = 50°F, T_{in} = 85°F and n=1 50

5.2.3a Effect of the ratio of tube spacing to tube diameter on the fluid outlet temperature for L= 10 ft, $\dot{q}_{th}$ = 200 Btu/hr-ft^2, kt = 0.391 Btu/hr-^{o}F, T_∞ = 50°F, T_{in} = 85°F and n=1. . 52

5.2.3b Effect of the ratio of tube spacing to tube diameter on the non-dimensional fluid outlet temperatures for L = 10 ft, $\dot{q}_{th}$ = 200 Btu/hr-ft^2, kt = 0.391 Btu/hr-^{o}F, T_∞ = 50°F, T_{in} = 85°F and n=1 53

5.2.4 Effect of the product of plate thickness and thermal conductivity on the fluid outlet temperature for L = 10 ft, B/D_o = 8, $\dot{q}_{th}$ = 200 Btu/hr-ft^2, T_∞ = 50°F, T_{in} = 85°F and n=1. 54

5.2.5 Effect of B/D_o ratio and kt on the non-dimensional fluid outlet temperature for $\dot{q}_{th}$ = 200 Btu/hr-ft^2, T_∞ = 50°F, T_{in} = 85°F and n=1 55

5.3.1 Effect of mass flow rate and B/D_o ratio on the collector efficiency for $\dot{q}_{th}$ = 200 Btu/hr-ft^2, kt = 0.194 Btu/hr-^{o}F, T_∞ = 50°F, T_{in} = 85°F and n=1. 57

Figure Page

5.3.2 Effect of the ratio of tube spacing to tube diameter and mass flow rate on the collector efficiency for $\dot{q}_{th}$ = 200 Btu/hr-ft^2, T_∞ = 50°F, T_{in} = 85°F and n=1. . 58

5.3.3 Effect of increasing the value of kt from 0.194 to 0.779 on the collector efficiency for $\dot{q}_{th}$ = 200 Btu/hr-ft^2, kt = 0.779 Btu/hr-^{o}F, T_∞ = 50°F, T_{in} = 85°F and n=1. . 59

5.3.4 Effect of increasing the inlet temperature from 85°F to 135°F on the collector efficiency for $\dot{q}_{th}$ = 200 Btu/hr-ft^2, kt = 0.194 Btu/hr-^{o}F, T_∞ = 50°F, T_{in} = 135°F and n=1 . 61

5.3.5 Effect of fluid inlet temperature and the number of glass covers on the collector efficiency for $\dot{q}_{th}$ = 200 Btu/hr-ft^2, kt = 0.391 Btu/hr-^{o}F, T_∞ = 50°F, $\dot{m}/A$ = 11 lbs/hr-ft^2 and B/D_o = 8 62

5.3.6 Effect of decreasing the ambient temperature from 50°F to 0°F on the collector efficiency for $\dot{q}_{th}$ = 200°Btu/hr-ft^2, kt = 0.194 Btu/hr-^{o}F, T_∞ = 0°F, T_{in} = 85°F and n=1 . . 64

5.3.7 Effect of the number of glass covers on the collector efficiency for $\dot{q}_{th}$ = 200 Btu/hr-ft^2, kt = 0.391 Btu/hr-^{o}F, T_∞ = 0°F, T_{in} = 85°F and B/D_o = 8. 65

5.3.8 Effect of decreasing the incident radiation on the collector efficiency for T_∞ = 50°F, T_{in} = 85°F, kt = 0.194 Btu/hr-^{o}F and n=1. 67

6.3.1 Box (Complex Algorithm) Logic Diagram 73

A.1 Diagram showing the limiting case of tubes side by side and the element of the collector tube referred to in the derivation of the fluid temperature distribution . . . 84

B.1 Diagram showing the experimental set-up used for taking the thermograms of the collector panel 88

B.2 Thermograms of the collector panel with and without water flowing through the tube 90

Figure Page

B.3 Plot of isotherms of the collector plate obtained from the Thermogram for a mass flow rate of 42 lbs/min, T_∞ = 72°F and T_{in} = 67.5°F 91

TWO DIMENSIONAL CONFIGURATION ANALYSIS OF A FLAT-PLATE SOLAR COLLECTOR

CHAPTER 1

INTRODUCTION

1.1 Purpose of Study

The present study is concerned with the detailed two dimensional analysis of a flat-plate solar collector and the subsequent optimization of the collector parameters, viz., the plate thickness, tube spacing and the collector length based on least cost/Btu.

Beginning with the classic work of Hottel and Woertz (1942) and continuing with the studies made by Whillier (1953) and Bliss (1959), many theoretical and experimental investigations have been done to study the effects of various parameters on the collector performance. The theoretical model of the flat-plate collector that is presently in use is basically the one developed by Hottel and Whillier (1958). This model is essentially one dimensional and is based on a lumped formulation. Although numerous experiments have been done to study the effects of various parameters on the collector performance, a rigorous theoretical analysis is lacking in this area. It is the aim of the present study to make up this deficiency.

It has been found by Klein et.al., (1974) that a zero capacitance model is quite adequate when hourly meteorological data are used, and hence in

Figure 1.1 Diagrams showing the collector plate-tube system, dimensions and the coordinate axes.

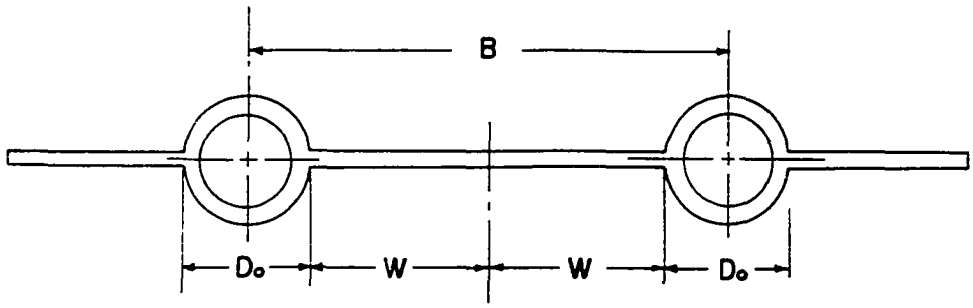
B
D_o
W
W
D_o

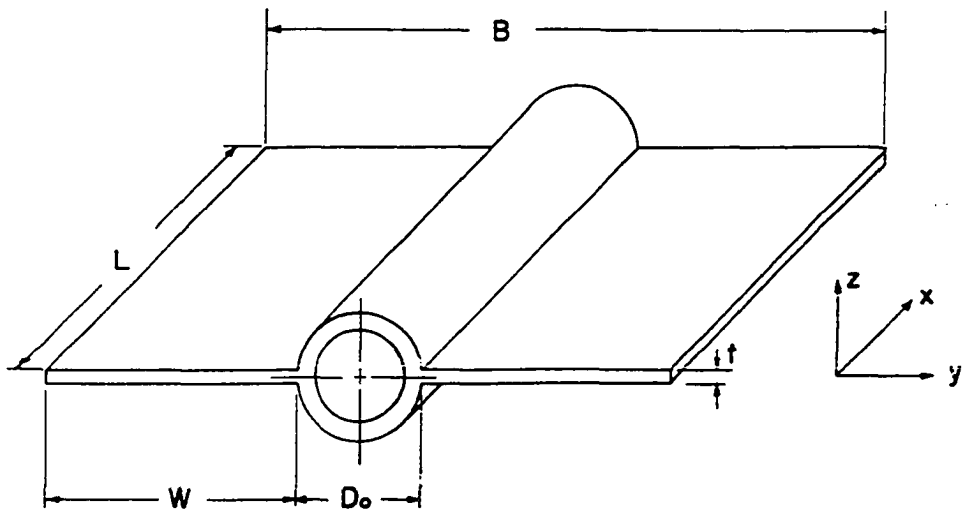
B
L
z
x
y
t
W
D_o

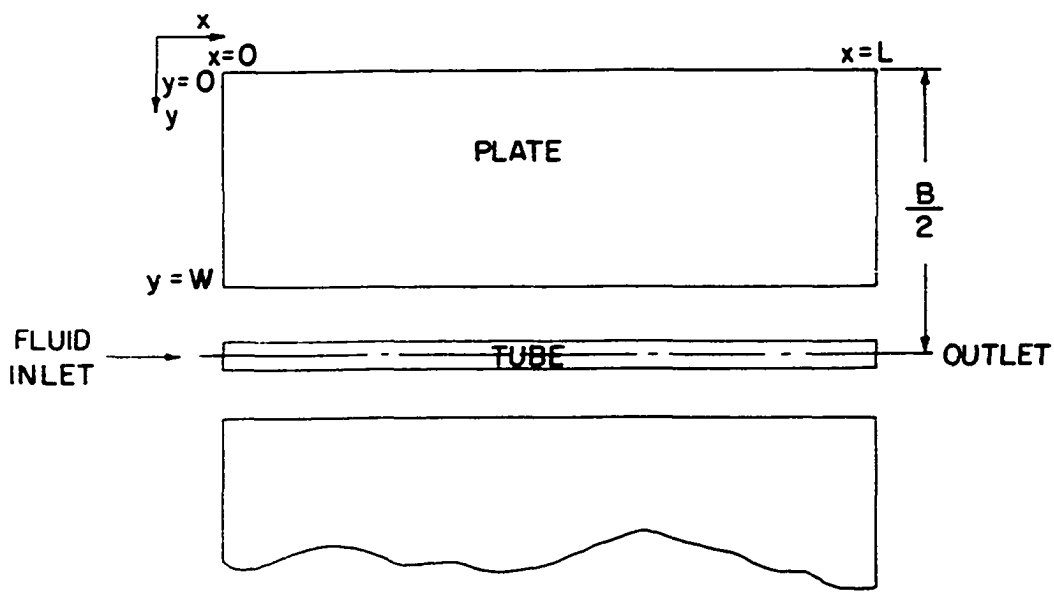
x
x=0
y=0
y
x=L
PLATE
B/2
y=W
FLUID INLET
TUBE
OUTLET

the present study only a steady-state analysis of the collector is made.

Since a typical collector is made up of several tubes with fins in between them, it is sufficient to analyze just a single tube with fins on either side. The particular problem under study is illustrated in Figure 1.1. In the present analysis, the collector plate and the tube are considered as two separate units and an energy balance is made on each of them. Although the analysis is carried out for a tube-in-strip type collector, the assumptions made are not restrictive to the point that they prevent the application of the analysis to other types of collector construction.

1.2 Method of Analysis

This study consists essentially of two parts. In the first part, the collector is idealized and a mathematical model is formulated as a classical heat-transfer problem. Energy balances are made on the collector plate and tube separately, each considered as a separate unit. Separate differential equations describing the temperature distribution of the collector plate and of the fluid inside the tube are obtained. The two coupled differential equations are then solved by means of appropriate transformations, separation of variables and integrating-factor techniques.

In the analysis of the plate, assuming the temperature gradient to be negligible along the thickness, reduces the problem to a two-dimensional one. For the fluid inside the tube, radial variation of temperature is neglected. The assumption of axial-symmetry, renders the problem one-dimensional. The solutions to the two differential equations give the temperature distributions of the plate and the fluid. The collector efficiency can be evaluated when the fluid outlet temperature and mass flow rate are known.

In the second part of this study, be means of the theoretical analysis developed in the first part, the collector design parameters (plate thickness, tube spacing, and the collector length) are optimized on the basis of least cost/Btu. The cost function used in this study is based on the current prices of the collector materials available in the open market. Since the cost function is non-linear, the present problem constitutes a non-linear optimization problem having both equality and inequality constraints. A search of the literature revealed only one method applicable to such a non-linear problem. This was developed by Fiacco and McCormick (1968). Unfortunately, this method requires the analytical derivatives of the objective function with respect to the parameters that are to be optimized. In the present problem it is not possible to obtain such analytical derivatives because of the complex nature of the expressions involved. This makes the method less efficient, and hence another method due to Box (1965) has been utilized. The disadvantage of this method is that it does not handle equality constraints. In spite of this drawback, the method is much simpler than the Fiacco & McCormick's method and also does not require gradients of the objective function. In order to use the method of Box, equality constraints of the problem have been approximated by a set of inequality constraints.

1.3 Review of Related Studies

Beginning more than two centuries ago with the early French work on solar furnaces, many scientists and engineers have endeavored to find ways to use the sun's radiation for technological purposes. Solar water heaters made their appearance in Arizona, California and Florida early in the 1900's. Between World Wars I and II, interest began to rise in the use of solar

radiation for space heating. Until about 1940 attempts at economical utilization of solar energy were experimental and had no theoretical basis.

Based on the pioneering work of Hottel and Woertz (1942), Hottel and Whillier (1953) developed a one-dimensional model of a flat-plate solar collector. Further analytical studies were made by Bliss (1959) using a similar model. Most of the research that is being conducted in solar energy is based on the steady-state models of Hottel, Whillier, and Bliss. The main shortcoming of this early model is that it is basically one-dimensional and is based on a lumped formulation. Various efficiency factors used in the model to account for the multi-dimensional nature of the problem have an implied assumption of infinite conductance in the system. It is not possible to determine the temperature distribution of the collector plate or the fluid using lumped formulation. Although it is known that the thermal losses from the plate surface vary from the inlet to the outlet end of the collector, there is no provision for this factor in the model. There is no way of determining an average plate temperature (essential for estimating an overall heat-loss coefficient) without a knowledge of plate temperature distribution. A value for average plate temperature is generally assumed. Although Hottel's model has been very useful and is widely used to this day, the analysis is not very rigorous.

During the decade beginning with 1970, there has been an increasing interest in the solar energy applications to space heating and cooling. The economics of solar energy systems being a major factor in practical applications, a more detailed and rigorous analysis of the collector model is essential.

In the present study, a two-dimensional model of the collector is formulated and the effects of various parameters on the temperature distri-

bution and efficiency are studied. By means of this two-dimensional model, a method has been developed whereby, for any given set of conditions, one can obtain an optimal collector configuration based on least cost per unit of energy absorbed.

CHAPTER 2

PROBLEM FORMULATION

2.1 Governing Equations

A steady state analysis is made on a portion of a collector consisting of a single tube with a fin attached to it on one side. Energy balances are made on the collector plate and tube separately, and two coupled differential equations governing the temperature distribution of the collector plate and of the fluid are obtained in the following manner.

2.1.1 Collector Plate

It is assumed that the temperature distribution in the plate is two dimensional. Although it is known that the overall heat loss coefficient from the plate to the surroundings is a function of the local plate temperature, an average value of this coefficient valid for the whole plate is used. This average value is estimated iteratively using Hottel's expression for thermal losses from a collector surface and the expression for the average plate temperature.

Consider a differential element of dimensions Δx and Δy of the plate, as illustrated in Figure 2.1.1. An energy balance on this element yields:

$$\begin{bmatrix}\text{Heat conducted into}\\ \text{element at x}\end{bmatrix} + \begin{bmatrix}\text{Heat conducted into}\\ \text{element at y}\end{bmatrix} + \begin{bmatrix}\text{Energy absorbed by the}\\ \text{element after optical losses}\end{bmatrix}$$
$$= \begin{bmatrix}\text{Heat conducted out}\\ \text{of the element at x+}\Delta x\end{bmatrix} + \begin{bmatrix}\text{Heat conducted out}\\ \text{of the element at y+}\Delta y\end{bmatrix} + \begin{bmatrix}\text{Total heat loss from}\\ \text{the element surface}\end{bmatrix} \qquad (2.1.1)$$

$$\dot{Q}_x + \dot{Q}_y + \dot{q}_i \Delta x \Delta y = \dot{Q}_{x+\Delta x} + \dot{Q}_{y+\Delta y} + \dot{q}_L \Delta x \Delta y \qquad (2.1.2)$$

The term $\dot{q}_L$ which represents the heat loss per unit area from the element $\Delta x \Delta y$, takes into account both the upward and downward losses. The

Figure 2.1.1 Diagram of a plate-tube section referred to in the derivation of the plate temperature distribution .

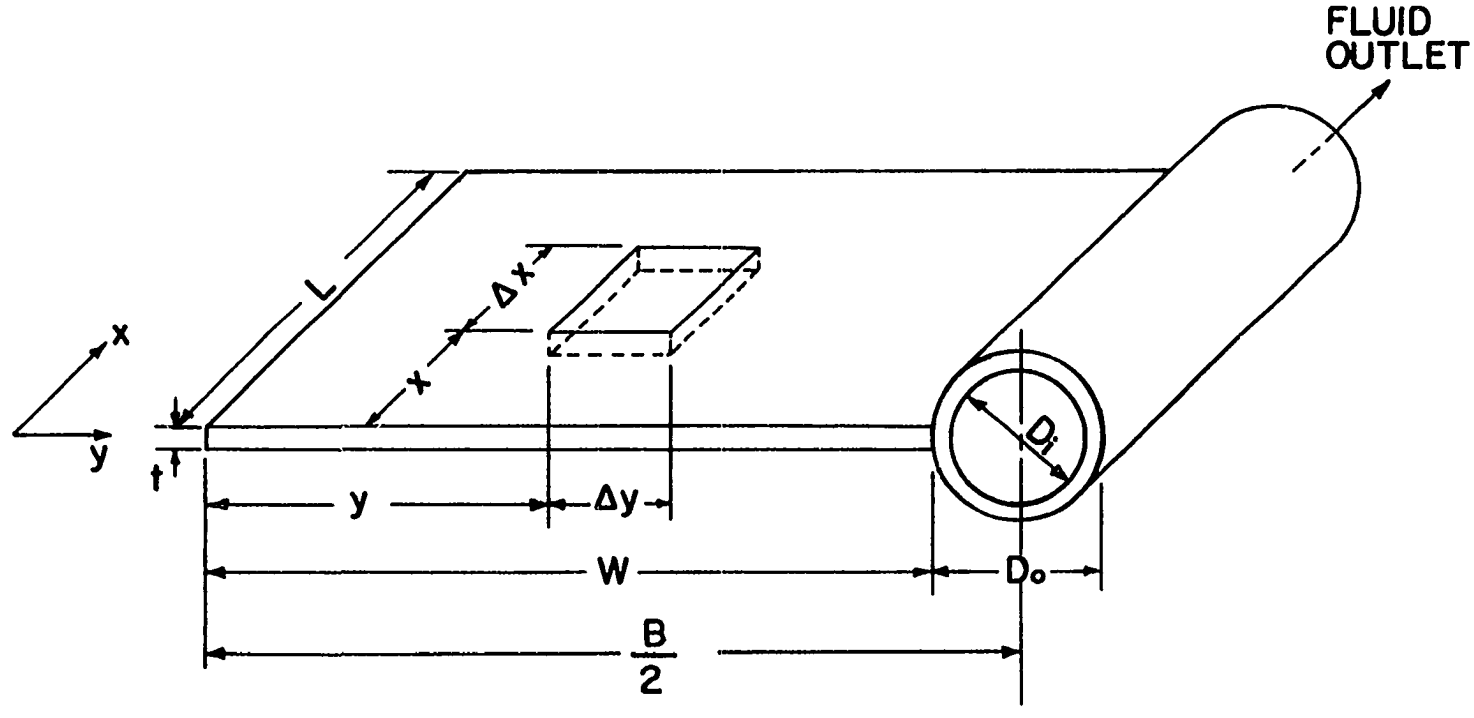
FLUID
OUTLET
L
Δx
x
x
y
t
y
Δy
W
D_i
D_o
B
2

edge losses are neglected in the present analysis.

Now we have

$$k(t\Delta y)\frac{\partial^2 T_p}{\partial x^2}\Delta x + k(t\Delta x)\frac{\partial^2 T_p}{\partial y^2}\Delta y + \dot{q}_i\,\Delta x\Delta y - U_L(T_p - T_\infty)\,\Delta x\Delta y = 0 \qquad (2.1.3)$$

or

$$\frac{\partial^2 T_p}{\partial x^2} + \frac{\partial^2 T_p}{\partial y^2} + \frac{\dot{q}_i}{kt} - \frac{U_L}{kt}(T_p - T_\infty) = 0 \qquad (2.1.4)$$

where T_p is the absorber plate temperature, T_∞ is the ambient temperature, $\dot{q}_i$ is the incident radiation per unit area on the plate after optical losses, kt is the product of thermal conductivity and thickness of the plate and U_L is the overall loss coefficient from the plate to the ambient. This differential equation is non-dimensionalized by substituting the following expressions:

$$\theta_p = \left(\frac{T_p - T_\infty}{T_{in} - T_\infty}\right) \qquad x^* = \frac{x}{L} \qquad y^* = \frac{y}{W} \qquad (2.1.5)$$

where T_{in} is the fluid inlet temperature to the collector, L is the plate length and W is the plate width.

We now obtain

$$\frac{\partial^2 \theta_p}{\partial x^{*2}} + \delta^2\frac{\partial^2 \theta_p}{\partial y^{*2}} - M\,\theta_p = -N \qquad (2.1.6)$$

where

$$\delta = \frac{L}{W} \qquad M = \frac{U_L L^2}{kt} \qquad N = \frac{\dot{q}_i L^2}{kt(T_{in} - T_\infty)} \qquad (2.1.7)$$

This is the governing differential equation for the collector plate.

2.1.2 Fluid Inside the Tube

It is assumed that the temperature distribution of the fluid inside the tube varies only along the axis of the tube. For the flow rates that are generally used, axial conduction in the fluid can be ignored. Neglecting the thermal resistance of the tube and making an energy balance on an differential element Δx of the fluid, as shown in Figure 2.1.2, we have:

[Energy convected into element at x] + [Energy conducted from the plate to the fluid element Δx] + [Energy absorbed by the upper surface of the tube element after optical losses]

= [Energy convected out of the element at $x+\Delta x$] + [Energy lost from the surface of the tube element Δx] (2.1.8)

$$\dot{m}C_p T_f + \dot{q}(x)(2t\Delta x) + \dot{q}_i D_o \Delta x = \dot{m}C_p T_f + \dot{m}C_p \frac{dT_f}{dx}\Delta x + U_o\left(\frac{\pi D_o}{2}\right)(T_f - T_\infty)\Delta x \tag{2.1.9}$$

$$\dot{m}C_p \frac{dT_f}{dx} + U_o\left(\frac{\pi D_o}{2}\right)(T_f - T_\infty) = \dot{q}(x)(2t) + \dot{q}_i D_o \tag{2.1.10}$$

where $\dot{m}$ is the mass flow rate of the fluid, C_p is the fluid specific heat, U_o is the heat loss coefficient from the fluid to the environment and $\dot{q}(x)$ is the amount of heat conducted from the plate to the fluid, per unit area.

This differential equation is non-dimensionalized by substituting the following:

$$\theta_f = \frac{(T_f - T_\infty)}{(T_{in} - T_\infty)}$$
$$x^* = \frac{x}{L} \tag{2.1.11}$$

We now have

$$\frac{d\theta_f}{dx^*} + M_f\theta_f = N_f\,\dot{q}(x^*) + P \tag{2.1.12}$$

Figure 2.1.2 Diagram of the collector tube referred to in the derivation of the fluid temperature distribution.

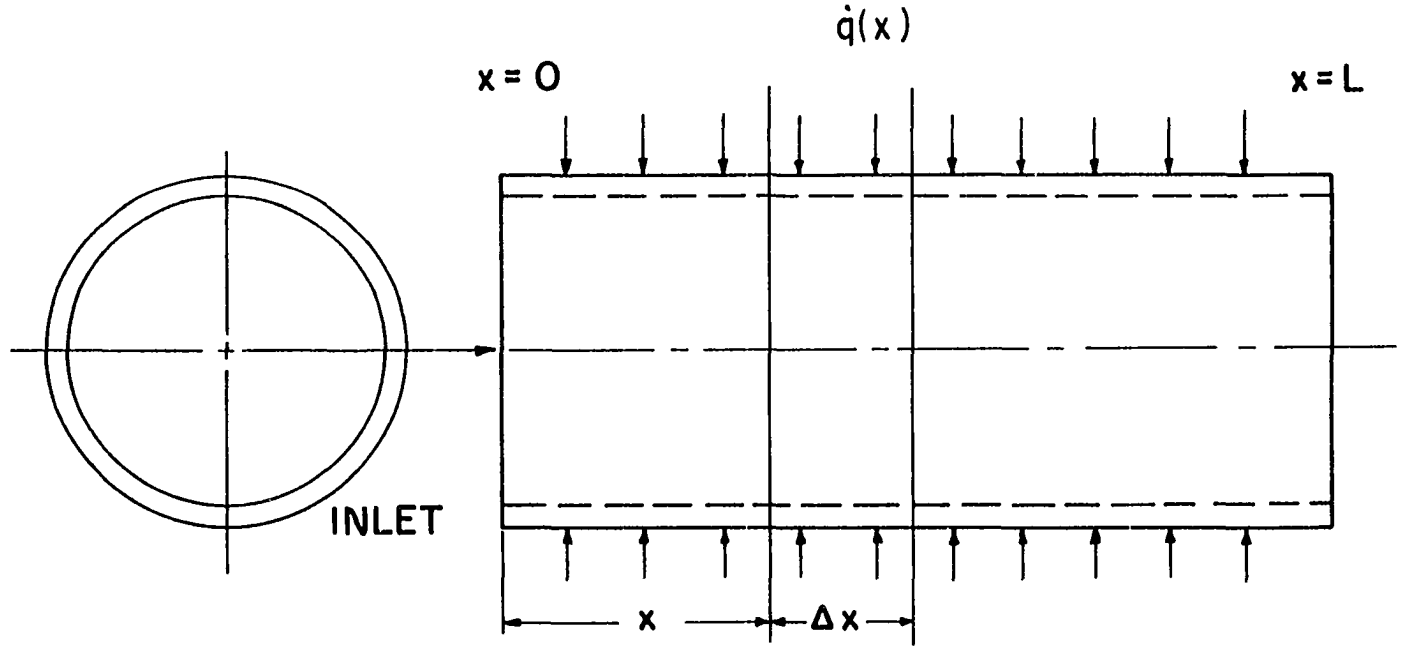
q̇(x)
x = 0
x = L
INLET
x
Δx

where

$$M_f = \frac{U_o \pi D_o L}{2\dot{m} C_p}$$

$$N_f = \frac{2tL}{\dot{m} C_p (T_{in} - T_\infty)} \qquad (2.1.13)$$

$$P = \frac{\dot{q}_i D_o L}{\dot{m} C_p (T_{in} - T_\infty)}$$

This is the governing differential equation for the fluid.

2.2 Boundary Conditions

In an actual collector with the sides well insulated, we can assume that the heat loss at the boundaries x=0 and x=L of the plate is negligibly small. And, since the boundary y=0 is the midpoint of plate between two adjacent tubes, symmetry requires that the slope of the temperature be zero at this boundary. At y=W, which is the boundary between the plate and the tube carrying the fluid, it is assumed that all the heat conducted from the plate is convected away by the fluid. These boundary conditions can now be expressed as:

$$@ \quad x = 0 \quad \frac{\partial T_p}{\partial x} = 0 \qquad (2.2.1)$$

$$@ \quad x = L \quad \frac{\partial T_p}{\partial x} = 0 \qquad (2.2.2)$$

$$@ \quad y = 0 \quad \frac{\partial T_p}{\partial y} = 0 \qquad (2.2.3)$$

$$@ \ y = W \qquad \dot{q}(x)\, t\Delta x = \bar{h}_f \left(\frac{\pi D_i \Delta x}{2}\right)\left(T_p - T_f\right) \qquad (2.2.4)$$

Since the governing differential equation for the fluid is only of first order, it requires only one boundary condition. This condition is that, the temperature of the fluid entering the collector at the boundary x=0 is known. That is

$$@ \quad x = 0 \quad T_f = T_{in} \tag{2.2.5}$$

Non-dimensionalizing the variables using equations (2.1.11), we have

$$@ \quad x^* = 0 \quad \frac{\partial \theta_p}{\partial x^*} = 0 \tag{2.2.6}$$

$$@ \quad x^* = 1 \quad \frac{\partial \theta_p}{\partial x^*} = 0 \tag{2.2.7}$$

$$@ \quad y^* = 0 \quad \frac{\partial \theta_p}{\partial y^*} = 0 \tag{2.2.8}$$

$$@ \quad y^* = 1 \qquad \dot{q}(x^*)t\Delta x = \bar{h}_f \left(\frac{\pi D_i \Delta x}{2}\right)(\theta_p - \theta_f)(T_{in} - T_\infty) \tag{2.2.9}$$

And for the fluid

$$@ \quad x^* = 0 \quad \theta_f = 1. \tag{2.2.10}$$

CHAPTER 3

ANALYTICAL SOLUTIONS

3.1 Temperature Distribution of the Collector Plate

The non-dimensionalized differential equation obtained in equation (2.1.6) is:

$$\frac{\partial^2\theta_p}{\partial x^{*2}} + \delta^2 \frac{\partial^2\theta_p}{\partial y^{*2}} - M\theta_p = -N \tag{2.1.6}$$

By substituting

$$U(x^*,y^*) = \theta_p - \frac{N}{M} \tag{3.1.1}$$

the above differential equation is made homogeneous, that is,

$$\frac{\partial^2 U}{\partial x^{*2}} + \delta^2 \frac{\partial^2 U}{\partial y^{*2}} - MU = 0 \tag{3.1.2}$$

Assuming a product solution of the form

$$U(x^*,y^*) = X(x^*)Y(y^*) \tag{3.1.3}$$

and substituting into equation (3.1.2), we obtain

$$\frac{X''}{X} + \delta^2 \frac{Y''}{Y} - M = 0 \tag{3.1.4}$$

or

$$\frac{X''}{X} = M - \delta^2 \frac{Y''}{Y} = \text{a constant} \tag{3.1.5}$$

where the separation constant is negative, zero or positive.

Case (i) Separation constant = $-\lambda^2$

From equation (3.1.5) we obtain

$$X'' + \lambda^2 X = 0$$
$$Y'' - \left(\frac{\lambda^2 + M}{\delta^2}\right) Y = 0 \tag{3.1.6}$$

The general solutions to these two ordinary differential equations are

$$X(x^*) = A_1 \sin\lambda x^* + \hat{B}_1 \cos\lambda x^*$$
$$Y(y^*) = C_1 \sinh \nu y^* + D_1 \cosh \nu y^* \tag{3.1.7}$$

where

$$\nu^2 = \left(\frac{\lambda^2 + M}{\delta^2}\right) \text{ and } \delta = \frac{L}{W}$$

Case (ii) Separation constant = 0

Equation (3.1.4) now becomes

$$X'' = 0$$
$$Y'' - \left(\frac{M}{\delta^2}\right) Y = 0 \tag{3.1.8}$$

And the general solutions are

$$X(x^*) = A_2 x^* + \hat{B}_2$$
$$Y(y^*) = C_2 \sinh \nu_o y^* + D_2 \cosh \nu_o y^* \tag{3.1.9}$$

where

$$\nu_o^2 = \frac{M}{\delta^2}$$

Case (iii) Separation constant = $+\lambda^2$

In this case we have

$$X(x^*) = A_3 \sinh \lambda x^* + \hat{B}_3 \cosh \lambda x^* \tag{3.1.10}$$

This solution cannot satisfy the homogeneous boundary conditions in the x^* direction and hence cannot be used.

Case (i)

The form of the solution assumed in equation (3.1.3) will now become

$$U(x^*,y^*) = (A_1 \sin \lambda x^* + \hat{B}_1 \cos \lambda x^*)(C_1 \sinh \nu y^* + D_1 \cosh \nu y^*) \tag{3.1.11}$$

The first boundary condition given by equation (2.2.6) will now be used:

$$@\ x^* = 0 \qquad \frac{\partial \theta_p}{\partial x^*} = 0 \quad \text{or} \quad \frac{\partial U}{\partial x^*} = 0$$

or

$$A_1 \lambda (C_1 \sinh \nu y^* + D_1 \cosh \nu y^*) = 0 \tag{3.1.12}$$

$$A_1 = 0 \qquad \text{since } \lambda \neq 0$$

The second boundary condition given by equation (2.2.7) is

$$@\ x^* = 1 \qquad \frac{\partial \theta_p}{\partial x^*} = 0 \quad \text{or} \quad \frac{\partial U}{\partial x^*} = 0$$

or

$$(-\hat{B}_1 \lambda \sin \lambda)(C_1 \sinh \nu y^* + D_1 \cosh \nu y^*) = 0$$

A trivial solution will result if $\hat{B}_1$ is zero. Since $\lambda \neq 0$

$$\sin \lambda = 0$$

$$\text{or} \quad \lambda = n\pi, \qquad \text{where } n = 1,2,3,\ldots\infty \tag{3.1.13}$$

The third boundary condition given by equation (2.2.8) is

$$@\ y^* = 0 \qquad \frac{\partial \theta}{\partial y^*_p} = 0 \quad \text{or} \quad \frac{\partial U}{\partial y^*} = 0$$

or

$$(\hat{B}_1 \cos n\pi x^*)(C_1 \nu) = 0$$

Since $\hat{B}_1$ and $\nu \neq 0$, we should have $C_1 = 0$. (3.1.14)

Now the expression for U becomes

$$U(x^*,y^*) = \sum_{n=1}^{\infty} B_n \cos n\pi x^* \cosh \nu_n y^* \tag{3.1.15}$$

where

$$\nu_n^2 = \left(\frac{n^2\pi^2 + M}{\delta^2}\right)$$

Later on B_n's will be determined using the fourth boundary condition.

Case (ii)

The general solution for this case will be

$$U(x^*,y^*) = (A_2 x^* + \hat{B}_2)(C_2 \sinh \nu_o y^* + D_2 \cosh \nu_o y^*) \tag{3.1.16}$$

$$@\ x^* = 0 \qquad \frac{\partial U}{\partial x^*} = 0 \quad \text{or} \quad A_2 = 0 \tag{3.1.17}$$

$$@\ Y^* = 0 \qquad \frac{\partial U}{\partial y^*} = 0 \quad \text{or} \quad C_2 = 0 \quad \text{since } \hat{B}_2 \neq 0 \tag{3.1.18}$$

Thus we have

$$U(y^*) = B_o \cosh \nu_o y^* \tag{3.1.19}$$

where the two constants $\hat{B}_2$ and D_2 have been combined into a single constant B_o.

Observe that, for this case, the solution U is a function of y* alone.

Case (iii)

The separation constant in this case is positive and when the boundary conditions are applied to the general solution, it will result in a trivial solution.

Hence, the most general solution will be a sum of the two solutions given by equations (3.1.15) and (3.1.19), that is,

$$U(x^*,y^*) = B_o \cosh \nu_o y^* + \sum_{n=1}^{\infty} B_n \cos n\pi x^* \cosh \nu_n y^* \qquad (3.1.20)$$

or

$$\theta_p(x^*,y^*) = \frac{N}{M} + B_o \cosh \nu_o y^* + \sum_{n=1}^{\infty} B_n \cos n\pi x^* \cosh \nu_n y^* \qquad (3.1.21)$$

In this expression, B_o and B_n's are still unknown and have to be determined using the fourth boundary condition.

The fourth boundary condition as given by equation (2.2.9) is:

$$@ \quad y^* = 1 \qquad \dot{q}(x^*)t\,\Delta x = \bar{h}_f\left(\frac{\pi D_i}{2}\right)\Delta x\,(\theta_p(x^*,1)-\theta_f)(T_{in}-T_\infty) \qquad (2.2.9)$$

or

$$\dot{q}(x^*) = \left[\frac{\bar{h}_f \pi D_i}{2t}\right](\theta_p(x^*,1)-\theta_f)(T_{in}-T_\infty)$$

i.e.

$$\frac{-k(T_{in}-T_\infty)}{W}\left.\frac{\partial \theta_p}{\partial y^*}\right|_{y^*=1} = \left[\frac{\bar{h}_f \pi D_i}{2t}\right](\theta_p(x^*,1)-\theta_f)(T_{in}-T_\infty)$$

Substituting for θ_p and $\frac{\partial \theta_p}{\partial y^*}$ from equation (3.1.21) we obtain

$$\left[-\frac{k}{W}\right]\left[B_o\nu_o \sinh \nu_o + \sum_{n=1}^{\infty} B_n\nu_n \sinh \nu_n \cos n\pi x^*\right] = \left[\frac{\bar{h}_f \pi D_i}{2t}\right]\left[\frac{N}{M} + B_o \cosh \nu_o + \sum_{n=1}^{\infty} B_n \cosh \nu_n \cos n\pi x^*\right] - \left[\frac{\bar{h}_f \pi D_i}{2t}\right]\theta_f \quad (3.1.22)$$

An expression for θ_f, which is the temperature distribution of the fluid has to be substituted before B_n's can be evaluated.

It will be seen later on that, since it was not possible to evaluate the B_n's analytically, a colocation scheme had to be utilized.

The plate temperature distribution is now given by:

$$T_p(x^*,y^*) = \theta_p(x^*,y^*)(T_{in}-T_\infty) + T_\infty \quad (3.1.23)$$

3.2 Temperature Distribution of the Fluid Inside the Tube

The non-dimensional differential equation as obtained in equation (2.1.12) is:

$$\frac{d\theta_f}{dx^*} + M_f\theta_f = N_f\, \dot{q}(x^*) + P \quad (2.1.12)$$

The solution to this differential equation using the method of integrating factors is:

$$\theta_f(x^*) = e^{-M_f x^*} \int_0^{x^*} \left[N_f\, \dot{q}(\xi) + P\right] e^{M_f \xi}\, d\xi + E\, e^{-M_f x^*} \quad (3.2.1)$$

where E is the constant of integration.

Applying the boundary condition

$$@\ x^* = 0 \qquad \theta_f = 1$$

We obtain $$E = 1 \quad (3.2.2)$$

Thus, we have

$$\theta_f(x^*) = e^{-M_f x^*} \int_0^{x^*} \left[N_f \dot{q}(\xi) + P \right] e^{M_f \xi} d\xi + e^{-M_f x^*} \tag{3.2.3}$$

In order to carry out the integration of the first term on the right hand side of the above equation an appropriate expression for $\dot{q}(\xi)$ has to be substituted first. Recall that $\dot{q}(\xi)$ is the flux conducted per unit area from the plate evaluated at the boundary $y^* = 1$. This is given by:

$$\dot{q}(x^*) = - \frac{k(T_{in}-T_\infty)}{W} \left(\frac{\partial \theta_p}{\partial y^*} \right)_{y^*=1} \tag{3.2.4}$$

$$= \left[\frac{-k(T_{in}-T_\infty)}{W} \right] \left[B_o \nu_o \sinh \nu_o + \sum_{n=1}^{\infty} B_n \nu_n \sinh \nu_n \cos n\pi x^* \right]$$

This expression is now substituted into the integral of equation (3.2.3). Thus,

$$\theta_f(x^*) = e^{-M_f x^*} + e^{-M_f x^*} \int_0^{x^*} N_f \left[\left(\frac{-k(T_{in}-T_\infty)}{W} \right) \{ B_o \nu_o \sinh \nu_o + \right. \tag{3.2.5}$$

$$\left. \sum_{n=1}^{\infty} B_n \nu_n \sinh \nu_n \cos n\pi \xi \} \right] e^{M_f \xi} d\xi + e^{-M_f x^*} \int_0^{x^*} P e^{M_f \xi} d\xi$$

Carrying out the two integrations, we obtain

$$\theta_f(x^*) = e^{-M_f x^*} + \frac{P}{M_f} (1 - e^{-M_f x^*}) - \left(\frac{N_f k(T_{in}-T_\infty)}{W} \right) \left\{ \frac{B_o \nu_o \sinh \nu_o}{M_f} (1-e^{-M_f x^*}) \right. \tag{3.2.6}$$

$$\left. + \sum_{n=1}^{\infty} \left(\frac{M_f}{M_f^2+n^2\pi^2} \right) B_n \nu_n \sinh \nu_n \left[\cos n\pi x^* + \left(\frac{n\pi}{M_f} \right) \sin n\pi x^* - e^{-M_f x^*} \right] \right\}$$

The fluid temperature distribution is given by:

$$T_f(x^*) = \theta_f(x^*)(T_{in}-T_\infty) + T_\infty \tag{3.2.7}$$

On Determination of B_o, B_1, B_2, ...B_K

Equation (3.1.22) together with (3.2.5) can be recast as

$$\sum_{n=0}^{\infty} B_n \phi_n(x^*) = G(x^*) \tag{3.2.8}$$

where $$\phi_n(x^*) \equiv a_n \cos n\pi x^* + b_n e^{-M_f x^*} \int_0^{x^*} e^{M_f \xi} \cos n\pi\xi \, d\xi$$

$$G(x^*) \equiv -\hat{H}\left[\frac{N}{M} - e^{-M_f x^*} - e^{-M_f x^*} \int_0^{x^*} P\, e^{M_f \xi}\, d\xi\right]$$

$$a_n \equiv \nu_n \sinh \nu_n + \hat{H} \cosh \nu_n$$

$$b_n \equiv \hat{H}\,\hat{T}\,\nu_n \sinh \nu_n \tag{3.2.9}$$

$$\hat{H} \equiv \frac{\bar{h}_f \pi D_i}{2t} \frac{W}{k}$$

$$\hat{T} \equiv \frac{k(T_{in}-T_\infty)}{W} N_f = \frac{2tLk}{\dot{m}C_p W}$$

The problem is to choose the B_n's so that equation (3.2.8) is satisfied identically. Because the functions $\phi_n(x^*)$ are not orthogonal, the B_n's cannot be obtained by a Fourier series analysis.

In the dissertation an approximation is made by means of colocation, that is, solving the K+1 equations

$$\sum_{n=0}^{K} B_n \phi_n(x^*_M) = G(x^*_M), \qquad M = 1,2,\ldots K+1 \tag{3.2.10}$$

It is necessary to assume here that

i) $\sum_{n=0}^{\infty} B_n \phi_n(x^*)$ converges for all x^* between 0 and 1

ii) $\sum_{n=0}^{\infty} B_n \phi_n(x^*)$ converges to $G(x^*)$ for all x^*

In the present study, using colocation scheme with (K+1) = 21, 51 and 81 no significant changes in the fluid outlet temperature were found. The changes were only in the second decimal place and hence in all the theoretical experiments the infinite series was truncated at 21 terms. The computation time (on IBM 370) using 21 and 51 terms of the series is about 14 and 42 seconds respectively.

It is interesting to note the following alternative means of determining the B_n's. Let $S_K(x^*)$ denote the sum

$$S_K(x^*) = \sum_{n=0}^{K} B_n^{(K)} \phi_n(x^*) \tag{3.2.11}$$

where $B_n^{(K)}$ is the approximation for B_n according to the Kth truncation.

Then the squared error between $G(x^*)$ and $S_K(x^*)$ can be represented by

$$\hat{E}_K = \int_0^1 [G(x^*) - S_K(x^*)]^2 \, dx^* \tag{3.2.12}$$

The least squared error is determined by

$$\frac{\partial \hat{E}_K}{\partial B_m^{(K)}} = 0, \qquad m = 0,1,2,\ldots K \tag{3.2.13}$$

This yields

$$\begin{aligned} \sum_{m=0}^{K} B_n^{(K)} \alpha_{nm} &= \int_0^1 G(x^*) \, \phi_m(x^*) dx^*, \quad m = 0,1,2\ldots K \\ &= g_m \qquad\qquad , \quad m = 0,1,2\ldots K \end{aligned} \tag{3.2.14}$$

where $$\alpha_{nm} = \int_0^1 \phi_n(x^*)\, \phi_m(x^*)\, dx^* \tag{3.2.15}$$

This amounts to K+1 equations for $B_o, B_1, \ldots B_K$. Here we must prove, or assume,

i) $S_K(x^*)$ converges as $K \to \infty$ for $0 \le x^* \le 1$

ii) $\hat{E}_K \to 0$ as $K \to \infty$

In the least squares sense, the B_n's determined by this method are better than those determined by colocation, that is,

$$(\hat{E}_K)_{\substack{\text{least}\\ \text{squares}}} \le (\hat{E}_K)_{\text{colocation}} \tag{3.2.16}$$

Now note that

$$\hat{E}_K = \int_0^1 G^2 dx^* - 2 \int_0^1 G\, S_K\, dx^* + \int_0^1 S_K^2\, dx^* \tag{3.2.17}$$

$$\int_0^1 G S_K dx^* = \sum_{n=0}^{K} B_n^{(K)} \int_0^1 G\, \phi_n dx^* = \sum_{n=0}^{K} B_n^{(K)}\, g_n \tag{3.2.18}$$

$$\int_0^1 S_K^2\, dx^* = \int_0^1 S_K \sum_{n=0}^{K} B_n^{(K)}\, \phi_n(x^*)\, dx^* = \sum_{n=0}^{K} B_n^{(K)} \int_0^1 S_K \phi_n dx^*$$

$$= \sum_{n=0}^{K} B_n^{(K)} \sum_{m=0}^{K} B_m^{(K)} \int_0^1 \phi_m \phi_n dx^*$$

$$= \sum_{n=0}^{K} \sum_{m=0}^{K} B_n^{(K)}\, B_m^{(K)}\, \alpha_{mn}$$

$$= \sum_{n=0}^{K} B_n^{(K)}\, g_n \tag{3.2.19}$$

Hence

$$\hat{E}_K = \int_0^1 G^2 dx^* - \sum_{n=0}^{K} B_n^{(K)} g_n$$

$$\hat{E}_K + \sum_{n=0}^{K} B_n^{(K)} g_n = \int_0^1 G^2 dx^* \qquad (3.2.20)$$

This is true for all K. Since $\int_0^1 G^2 dx^*$ is finite, it follows that

$$\sum_{n=0}^{\infty} B_n g_n \quad \text{converges (or diverges negatively)}$$

where $B_n^{(\infty)} \equiv B_n$.

3.3 Average Collector-Plate Temperature

In the formulation of the problem, a single value of the overall loss coefficient was used for the whole plate, in order to account for the thermal losses from the plate. In order to estimate an average value of this coefficient, an average plate temperature is required. An expression for the average plate temperature can be obtained by integrating the plate temperature distribution over the whole area of the plate.

The temperature distribution of the collector plate as given by equation (3.1.21) is

$$\theta(x^*,y^*) = \frac{N}{M} + B_o \cosh \nu_o y^* + \sum_{n=1}^{\infty} B_n \cos n\pi x^* \cosh \nu_n y^* \qquad (3.1.21)$$

Integrating this expression over the whole area of the plate gives

$$\int_0^1\int_0^1 \theta(x^*,y^*)dx^*dy^* = \int_0^1\int_0^1 \left[\frac{N}{M} + B_o\cosh \nu_o y^* + \sum_{n=1}^{\infty} B_n \cos n\pi x^* \cosh \nu_n y^*\right]dx^*dy^* \tag{3.3.1}$$

or

$$\theta_{avg} = \frac{N}{M} + \frac{B_o \sinh \nu_o}{\nu_o} \tag{3.3.2}$$

The average plate temperature is now given by

$$T_{avg} = \theta_{avg}(T_{in}-T_\infty) + T_\infty \tag{3.3.3}$$

CHAPTER 4

OPTICAL & THERMAL LOSSES

4.1 Calculation of Solar Flux on the Collector Plate Surface

The intensity of direct solar radiation on a collector surface depends on the orientation of the collector and the position of the sun. The sun's position in the sky depends on three independent variables; the latitude $\hat{L}$, the solar declination $\hat{\delta}$, which is a function of the date and the time. The earth's tilted axis results in a day-by-day variation of the angle between the earth sun line and the equatorial plane. This angle varies continuously in accordance with the date and is called the declination, $\hat{\delta}$. Numerical values of $\hat{\delta}$ for any particular date can be obtained from tables listed in ASHRAE guide and product directory (1974). In order to facilitate calculations on a computer, it is more convenient to have the expression for declination in a functional form. The following expression has been used in the present analysis:

$$\hat{\delta} = .302 + \cos\left(\frac{2\pi}{360}\cdot \text{Day}\right)(-22.93) - (0.229)\cos\left(\frac{4\pi}{360}\cdot\text{Day}\right)$$
$$+ (-0.243)\cos\left(\frac{6\pi}{360}\cdot\text{Day}\right) + (3.851)\sin\left(\frac{2\pi}{360}\cdot\text{Day}\right)$$
$$+ (0.002)\sin\left(\frac{4\pi}{360}\cdot\text{Day}\right) - (0.055)\sin\left(\frac{6\pi}{360}\cdot\text{Day}\right) \qquad (4.1.1)$$

An approximate but much simpler expression for $\hat{\delta}$ has been suggested by Duffie and Bechman [1973], and is given by

$$\hat{\delta} = 23.45 \sin\left[360 \frac{284+Day}{365}\right] \qquad (4.1.2)$$

4.1.1 Solar Elevation Angle

In order to calculate the diffuse component of the incident solar radiation, the solar altitude angle is required.

Solar time generally differs from Local Standard or Daylight Savings Time and the difference can be significant, particularly when the DST is in effect.

LOCAL STANDARD TIME = LOCAL TIME + DAYLIGHT SAVINGS TIME INDICTOR (4.1.3)

where DST = -1 for summer and +1 for winter. Because the sun appears to move at the rate of 360 degrees per 24 hours, its apparent motion is 4 min. per degree of longitude. The Apparent Solar Time is given by the expression

AST = LOCAL STANDARD TIME + EQN. OF TIME
+ 4 * (No. of Minutes East) or (4.1.4)
- 4 * (No. of Minutes West) of the Local Standard Time Meridians

The longitudes of the six standard time meridians which affect the U.S. are: Eastern ST, 75 deg; Central ST, 90 deg; Mountain ST, 105 deg; Pacific ST, 120 deg; Yukon ST, 135 deg; Alaska-Hawaii ST, 150 deg.

The equation of Time is the measure, in minutes, of the extent by which solar time, as told by a sun dial, runs faster or slower than Civil or Mean Time, as determined by a clock running at a uniform rate.

$$\text{Equation of Time} = (-0.0002) + \cos(\tfrac{2\pi}{360}\cdot\text{Day})(0.4197) - \cos(\tfrac{4\pi}{360}\cdot\text{Day})(3.2265)$$
$$+ \cos(\tfrac{9\pi}{360}\cdot\text{Day})(-0.0903) + \sin(\tfrac{2\pi}{360}\cdot\text{Day})(-7.351) \quad (4.1.5)$$
$$+ \sin(\tfrac{4\pi}{360}\cdot\text{Day})(-9.3912) + \sin(\tfrac{9\pi}{360}\cdot\text{Day})(-0.3361)$$

No. of minutes from solar noon = 60.0 * (12.0-AST)

Solar elevation angle $\hat{\alpha}$, is given by:

$$\sin\hat{\alpha} = \sin\hat{L}\sin\hat{\delta} + \cos\hat{L}\cos\hat{\delta}\cos HA \quad (4.1.6)$$

where $\hat{L}$ is the latitude, $\hat{\delta}$ is the declination and H_A is the hour angle which is given by the relation:

$$\text{Hour Angle} = 0.25(\text{No. of Minutes from solar noon}) \quad (4.1.7)$$

4.1.2 The Incident Angle, i

One additional angle which is very important in solar calculations is the incident angle, i, between the direct solar radiation and a line normal to the irradiated surface. The importance of the incident angle lies in the fact that it determines both the intensity of the direct radiation component striking the surface and the ability of the surface to reflect, transmit, or absorb the sun's rays.

For a surface tilted at an angle β (measured upwards from horizontal), the angle of incidence of solar radiation is given by

$$\cos i = \cos 15(H-12)\cos\hat{\delta}\cos(\hat{L}-\beta) + \sin\hat{\delta}\sin(\hat{L}-\beta) \quad (4.1.8)$$

where H is the hour of the day (twenty-four hour time); $\hat{\delta}$ is the declination angle of the sun; $\hat{L}$ is the latitude of the place, and β is the collector orientation.

4.1.3 Diffuse Solar Radiation on a Horizontal Surface

The diffuse component of solar radiation is difficult to estimate because of its non-directional nature and its wide variations. Diffuse radiation comes from all parts of the sky, and hence we can assume it to be nearly independent of the collector slope. Since only the data on total radiation on a horizontal surface are generally available, a relationship between total and diffusion radiation was given by Löf and Tybout (1972) using both normal incidence (direct) and total horizontal solar data for 3 stations over several thousand hours. Using a multiple regression analysis they have shown that the diffuse component could be satisfactorily represented by

$$\dot{q}_{dh} = 0.78 + 1.07\hat{\alpha} + 6.17cc \qquad (4.1.9)$$

where $\dot{q}_{dh}$ is the diffuse solar radiation on a horizontal surface; $\hat{\alpha}$ is the solar elevation above the horizon as given by equation (4.1.6) and cc is tenths of sky area covered by clouds: 0 = clear and 10 = fully covered.

The direct solar radiation on a horizontal surface is given by:

$$\dot{q}_{Dh} = \dot{q}_{th} - \dot{q}_{dh} \qquad (4.1.10)$$

where $\dot{q}_{th}$ is the total incident radiation on a horizontal surface.

4.1.4 Direct Solar Radiation on a Tilted Surface & the Optical Losses

Direct radiation on the tilted surface of the collector, $\dot{q}_{Dt}$, is then

$$\dot{q}_{Dt} = \dot{q}_{Dh}\left(\frac{\cos i}{\sin \alpha}\right) \qquad (4.1.11)$$

Reflection loss of direct radiation from a single surface of glass is given by the Fresnel equation:

$$R = 0.5\left[\frac{\sin^2(i-r)}{\sin^2(i+r)} + \frac{\tan^2(i-r)}{\tan^2(i+r)}\right] \qquad (4.1.12)$$

The relationship between the angle of refraction, r, and the angle of incidence i, for window glass is:

$$\frac{\sin i}{\sin r} = 1.526 \qquad (4.1.13)$$

Each glass cover plate on the collector has two surfaces, and two or more glass cover plates may be used. The reflection from a system of n transparent plates is:

$$(1-R_n) = \frac{1-R}{1+(2n-1)R} \qquad (4.1.14)$$

Reflection loss of diffuse radiation was calculated by Löf and Tybout (1972) as a function of the number of glass plates by graphical integration over a uniform hemispheric sky, with the following results:

n	1	2	3
R_r	0.16	0.24	0.29

The absorptivity of a good, black, nonselective surface of the collector is a function of solar incidence angle, as represented by the following.

i(Deg)	0-30	30-40	40-50	50-60	60-70	70-80	80-90
α	0.96	0.95	0.93	0.91	0.88	0.81	0.66

A single value of $\alpha = 0.90$ for diffuse radiation was found by (Löf & Tybout (1972)) by integrating over a hemispheric sky. Subtracting the reflection and absorption losses from the solar radiation terms, we

get the amount of solar energy incident on the tilted collector surface, $\dot{q}_i$ after optical losses.

$$\dot{q}_i = \dot{q}_{Dt}(1-R_n)\alpha + \dot{q}_{dh}(1-R_r)(0.90) \qquad (4.1.15)$$

4.2 Calculation of Thermal Losses from Collector

The thermal losses from the collector depend upon a) the average temperature of the collector surface, T_{avg}; b) the emissivity of the absorbing plate, ϵ_c; c) the ambient conditions namely air temperature, T_∞, and wind speed, v; d) the number of transparent cover plates, n, and to a lesser extent - their spacing; e) the transmittance of the transparent cover plates for long-wave radiation; f) the base and edge insulation.

The average temperature of the collector plate T_{avg} further depends upon a number of factors: g) the fluid flow rate through the collector, $\dot{m}$; h) the type of fluid, which is reflected in the specific heat C_p of the fluid; i) the temperature, T_{in}, at which the heat removal fluid enters the collector, j) heat-transfer coefficient between the heat-removal fluid and the flat absorbing plate, $\bar{h}_f$; k) the distance between the fluid-conveying tubes, B; and l) the product of the thermal conductivity times the thickness of the collector plate, kt.

The heat-transfer losses in the collector occur upwards through the transparent cover plates, sideways through the edge insulation and downwards through the rear insulation.

4.2.1 Upward Heat Loss Through the Transparent Cover Plates

The thermal loss upwards from the collector plate is made up of

radiative and convective components. Neglecting the absorption of solar radiation by the glass covers, Hottel and Woertz [1942] have shown the energy loss upwards through the glass cover system can be found by solving the non-linear system of n+1 equations, where n is the number of glass covers. Their equations may now be written as

$$\frac{\dot{q}_{L,up}}{A} = \bar{h}_1(T_{avg}-T_1) + \frac{\sigma(T_{avg}^4-T_1^4)}{\frac{1}{\epsilon_c}+\frac{1}{\epsilon_g}-1}$$

$$= \bar{h}_2(T_1-T_2) + \frac{\sigma(T_1^4 - T_2^4)}{\frac{2}{\epsilon_g}-1} \qquad (4.2.1)$$

$$\vdots \qquad \vdots \qquad \vdots$$

$$\frac{\dot{q}_{L,up}}{A} = \bar{h}_w(T_n-T_\infty) + \sigma\,\epsilon_g(T_n^4 - T_\infty^4)$$

where T_n is the temperature of the nth cover plate and the wind heat transfer coefficient $\bar{h}_w$ is given by,

$$\bar{h}_w = 1 + 0.35\ v \qquad \text{Btu/hr-ft}^2\text{-}^\circ\text{F} \qquad \text{where v is in knots.}$$

The cover to cover heat transfer coefficients, $\bar{h}_i$, are given in Tabor (1955). The foregoing (n+1) simultaneous equations can be solved iteratively to determine $\frac{\dot{q}_{L,up}}{A}$, if the collector plate temperature, T_{avg} and the ambient temperature T_∞, are given. Since the solution to the (n+1) simultaneous equations is very tedius, Hottel has suggested a single expression which replaces the (n+1) equations given above.

$$\frac{\dot{q}_{L,up}}{A} = \frac{(T_{avg}-T_\infty)}{\frac{n}{c\sqrt{\frac{T_{avg}-T_\infty}{n+f}}} + \frac{1}{h_w}} + \frac{\sigma(T_{avg}^4-T_\infty^4)}{\frac{1}{\epsilon_c} + \frac{2n+f-1}{\epsilon_g} - n} \qquad (4.2.2)$$

Although this relation appears rather complicated, Hottel & Woertz have found that for this approximate equation, when tested over normal range of variables involved, the maximum error was 1.8%, with an average value of 1%. When ϵ_c (emissivity of a well blackened surface) is changed from 0.95 to 0.48, the error due to use of equation 4.2.2 instead of 4.2.1 may increase only by about 5%.

The correction coefficient for convection from a titled surface, c, used in equation 4.2.2 is given by,

$$c = 0.19 - 0.000788\ \beta \qquad (4.2.3)$$

where β is the collector tilt in degrees. The ratio of thermal resistance of the outer cover plate to that of the inner plate, f, is a function of the wind speed and is given by:

$$\begin{aligned} f &= 0.76 \times 10^{-0.0374v} && v \le 8.7 \\ f &= 0.36 \times 10^{-0.0202(v-8.7)} && 8.7 < v \le 17.4 \\ f &= 0.24 \times 10^{-0.01132(v-17.4)} && 17.4 < v \end{aligned} \qquad (4.2.4)$$

where v is in knots.

Using equation 4.2.2, we can now estimate the upward overall heat transfer coefficient, $U_{L,up}$.

$$U_{L,up} = \frac{(\dot{q}_{L,up}/A)}{(T_{avg}-T_\infty)} \qquad (4.2.5)$$

Observe that although there is an explicit expression for T_{avg}, as given by equation (3.3.3), it is in turn a function of $U_{L,up}$. Hence an iterative procedure is required in order to estimate the correct value of $U_{L,up}$.

4.2.2 Downward Heat Loss Through the Insulation

The downward heat losses through the insulation of the collector can be expressed as:

$$\dot{q}_{L,base} = \frac{(T_{avg}-T_{\infty})}{\left(\frac{t_1}{k_1} + \frac{1}{\bar{h}_{base}}\right)} \qquad (4.2.6)$$

where t_1 is the thickness of the insulation, k_1 is the thermal conductivity of the insulation and $\bar{h}_{base}$ is the convection coefficient between the bottom of the collector insulation and the ambient. Tabor (1955) recommends a value of 2-4 (Btu/hr-ft^2-^{o}F) for $\bar{h}_{base}$. Whillier (1967) suggests that, if the thermal insulation beneath the collector absorbing plate comprised of a reflective layer of aluminum foil on top of 2" to 4" mineral wool insulation, then the downward losses would only be about 10% of the upward losses. According to his suggestion, the base losses can be accounted for by increasing the value of $U_{L,up}$ obtained iteratively by 10%. Thus, the overall heat-transfer coefficient required to evaluate the thermal losses from the collector surface will now be,

$$U_L = 1.1\ U_{L,up} \qquad (4.2.7)$$

4.3 Heat-Transfer Coefficient, $\bar{h}_f$, Between the Tubewall and Collector Fluid

Whillier (1967) notes that the flow of water through solar heaters

is so slow that in most cases it is laminar. Furthermore, the tube length is usually short enough for the flow not to become fully developed. And he suggests an expression,

$$Nu = 4.36 + \frac{0.067\,[(d/L)Re\ Pr]}{1 + 0.04\,[(d/L)Re\ Pr]^{2/3}} \qquad (4.3.1)$$

where Nu is the Nusselt number, Re is the Reynold's number, Pr is the Prandtl number, d is the nominal diameter and L is the length of the tube.

Based on experimental work, Oliver (1962) suggested the correlations

$$Nu_m = (\mu_b/\mu_w)^{0.14}\ 1.75\,[Gz_m + 0.0083(Gr_m Pr_m)^{0.75}]^{1/3} \qquad (4.3.2)$$

for tubes with $L/d > 70$ and

$$Nu_m = (\mu_b/\mu_w)^{0.14}\ 1.75\,[Gz_m + 0.00056(Gr_m Pr_m \frac{L}{d})^{0.70}]^{1/3} \qquad (4.3.3)$$

for tubes with $L/d < 70$, provided $Gz_m \not< \pi Nu_m$.

Oliver's equations assume that the tube is horizontal and has uniform wall temperature.

Another correlation suggested by Brown and Thomas (1965) is:

$$Nu_m = (\mu_b/\mu_w)^{0.14}\ 1.75\,[Gz_m + 0.012(Gz_m Gr_m^{1/3})^{4/3}]^{1/3} \qquad (4.3.4)$$

where μ_b is the dynamic viscosity of fluid at bulk temperature

μ_w is the dynamic viscosity of fluid at wall temperature

Gr_m is the arithmetic-mean Grashof number

Gz_m is the arithmetic-mean Graetz number

Nu_m is the arithmetic-mean Nusselt number

Pr_m is the arithmetic-mean Prandtl number

This correlation is also based on an assumption of uniform wall temperature.

Baker (1967) from his experimental investigations found that 100 Btu/hr-ft^2-^{o}F was a justifiable value for the film heat-transfer coefficient.

Thus we find that all the values of film heat-transfer coefficients cited in the literature (for apparently similar situations) vary from about 20 to 100 Btu/hr-ft^2-^{o}F and are based either on a constant wall temperature or on a constant wall flux.

From the present analysis it is clear that neither the wall temperature nor the wall flux is constant. But for lack of a more accurate expression for $\bar{h}_f$, as suggested by Baker, a value of 100 Btu/hr-ft^2-^{o}F was used in the analysis. However, values of $\bar{h}_f$ ranging from 25 to 100 Btu/hr-ft^2-^{o}F were tried and no significant variations in the fluid outlet temperatures or the efficiencies were found.

CHAPTER 5

DISCUSSION OF THE EFFECT OF VARIOUS COLLECTOR PARAMETERS ON THE TEMPERATURE DISTRIBUTIONS AND COLLECTOR PERFORMANCE

5.1 Effect of Collector Parameters on the Temperature Distribution of the Absorber Plate

In this chapter, the effects of various collector parameters on the temperature distributions and collector efficiencies are discussed in a quantitative manner. All the theoretical experiments were conducted on a typical winter day (Jan. 15th) at a latitude of 35° (Oklahoma City), 50% cloud cover, at 1300 hours and with an incident radiation of 200 Btu/hr-ft^2.

Plate Temperature Distribution Normal to the Tube

Consider a tube-in-strip type collector configuration as shown in Figure 1.1. The temperature distribution of one half the plate between two tubes has been derived in Chapter 3 and is given by the equation (3.1.23). The width of the plate between two tubes is W, the tube diameter is D_o and the plate thickness is t. Some of the solar energy absorbed by the plate must be conducted across the plate to the region of the tubes. Thus the temperature midway between the tubes will be higher than the temperature near the vicinity of the tubes, as illustrated in Figure 5.1.1. This temperature distribution is highly dependent on the mass flow rate and the inlet temperature

Figure 5.1.1 Plot of plate temperature normal to the tube versus normalized plate width, for $B/D_o = 8$, kt = 0.391 Btu/hr-^oF, $\dot{q}_{th} = 200$ Btu/hr-ft^2, $T_\infty = 50^oF$, $T_{in} = 85^oF$ and n=1.

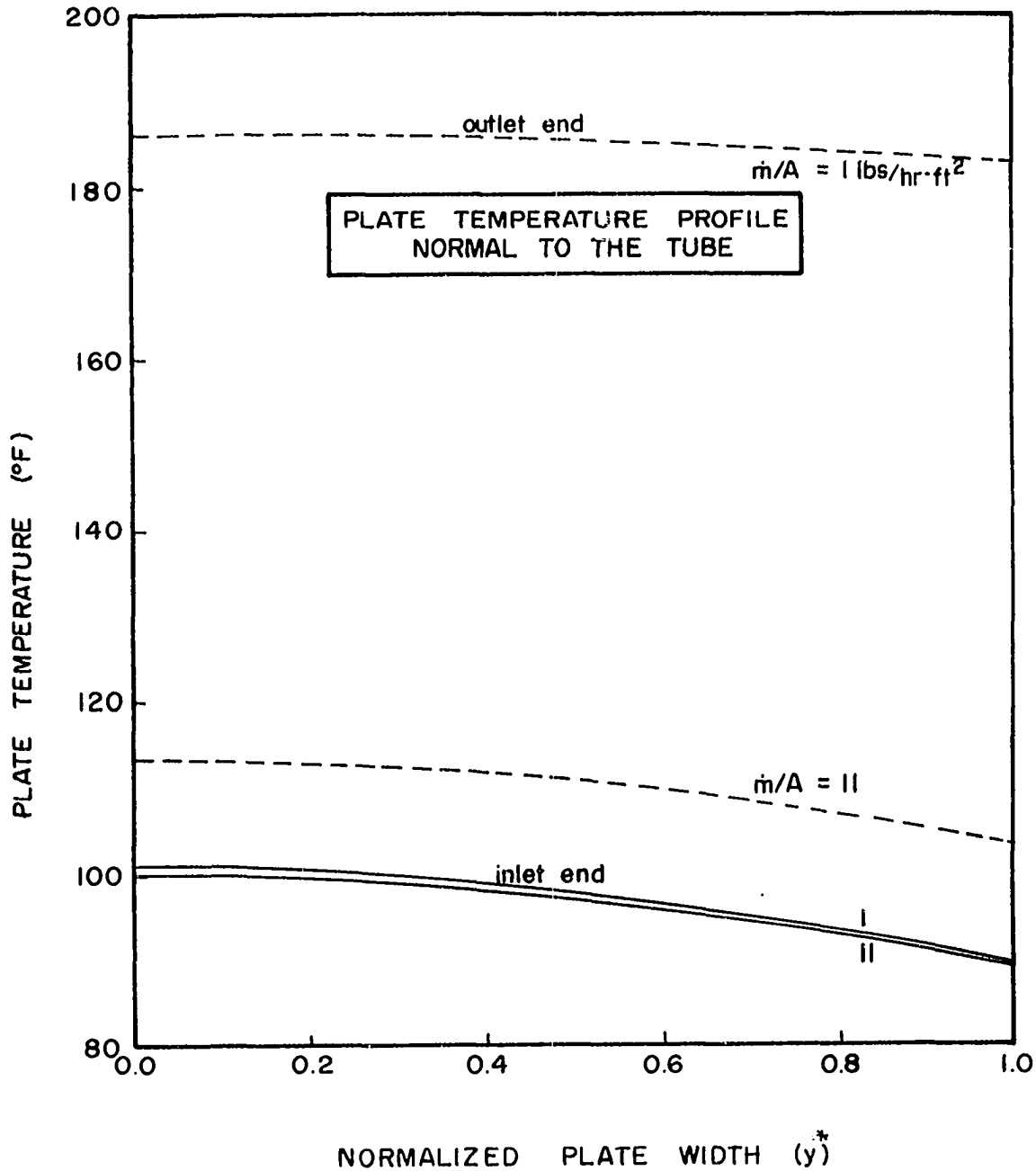
PLATE TEMPERATURE PROFILE
NORMAL TO THE TUBE
outlet end
ṁ/A = I lbs/hr·ft²
ṁ/A = II
inlet end
I
II
PLATE TEMPERATURE (°F)
NORMALIZED PLATE WIDTH (y*)
200
180
160
140
120
100
80
0.0
0.2
0.4
0.6
0.8
1.0

Figure 5.1.2 Plot of plate temperature parallel to the tube versus normalized plate length, for B/D_o = 8, kt = 0.391 Btu/hr-^oF, $\dot{q}_{th}$ = 200 Btu/hr-ft^2, T_∞ = 50^oF, T_{in} = 85^oF and n=1

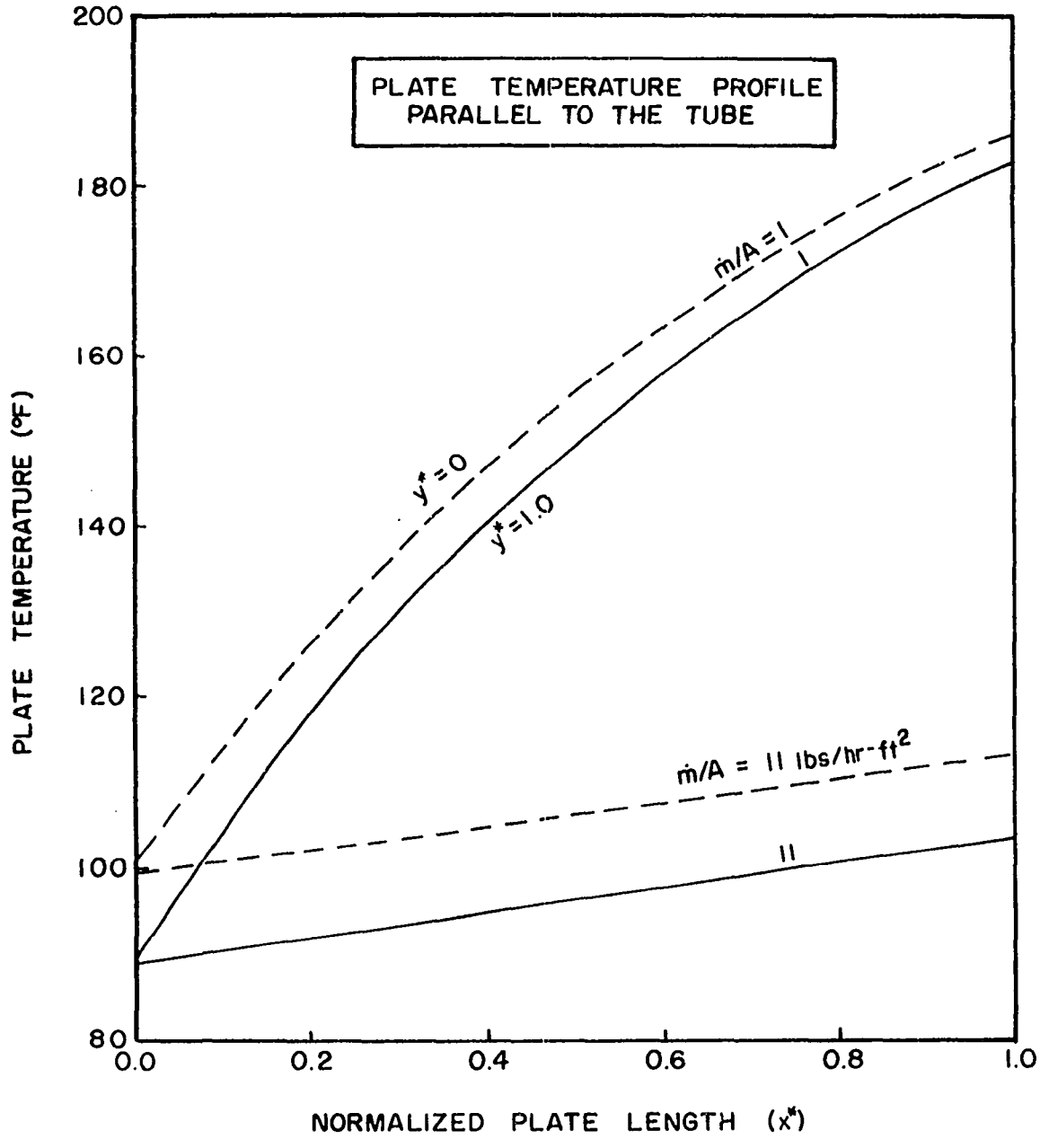
PLATE TEMPERATURE PROFILE
PARALLEL TO THE TUBE
200
180
160
140
120
100
80
PLATE TEMPERATURE (°F)
0.0
0.2
0.4
0.6
0.8
1.0
NORMALIZED PLATE LENGTH (x*)
ṁ/A = 1
1
y* = 0
y* = 1.0
ṁ/A = 11 lbs/hr-ft²
11

of the collector fluid. In Figure 5.1.1, observe that the difference between the center line temperature and the root temperature of the absorber plate is greater at the inlet end than at the outlet of the collector. With increase in mass flow rates, this difference in temperature becomes smaller. Also observe that higher mass flow rates result in lower plate temperatures and gradients and vice-versa.

Plate Temperature Distribution Parallel to the Tube

The energy transferred to the fluid will gradually heat up the fluid causing a temperature gradient to exist in the direction of flow. Since in any region of the plate, the temperature distribution is governed by the local temperature level of the fluid, a situation as shown in Figure 5.1.2 exists. The figure illustrates the strong influence of mass flow rate on the temperature profiles. For extremely low mass flow rates, the plate temperatures are high and the temperature distribution is exponential. For higher mass flow rates, the plate temperature is lower and the temperature profiles become almost linear. Observe that the temperature of the plate midway between the tubes (i.e., @ y=0) is higher than at the root (i.e. @y=W) of the plate.

Isotherms of the Collector Plate

Since the temperature distribution of the collector plate obtained in this analysis is two-dimensional, it can be best illustrated by drawing the isotherms. Figures 5.1.3 (a,b,c) show the isotherms of an absorber plate for three different values of mass flow rate. It is interesting to note that for high mass flow rates the isotherms tend to be parallel to the fluid

Figure 5.1.3a Plot of isotherms of the collector plate for a flow rate of 50 lbs/hr-ft^2, $B/D_o = 8$, kt = 0.391 Btu/hr-^oF, $\dot{q}_{th}$ = 200 Btu/hr-ft^2, $T_\infty = 50^oF$, $T_{in} = 85^oF$ and n=1

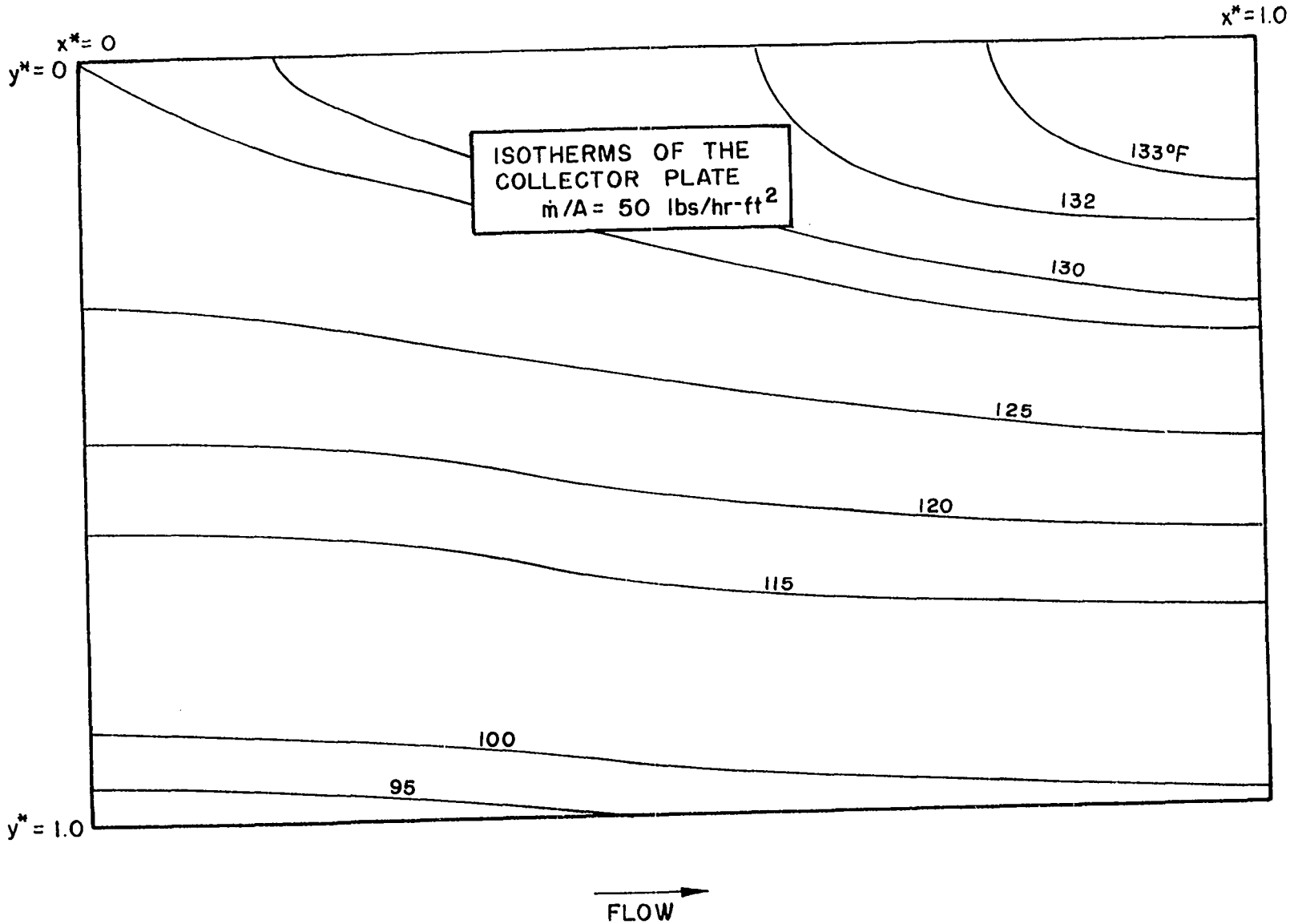
x* = 1.0
x* = 0
y* = 0
ISOTHERMS OF THE
COLLECTOR PLATE
ṁ/A = 50 lbs/hr-ft²
133°F
132
130
125
120
115
100
95
y* = 1.0
FLOW

Figure 5.1.3b Plot of isotherms of the collector plate for a flow rate of 10 lbs/hr-ft^2, $B/D_o = 8$, kt = 0.391 Btu/hr-^oF, $\dot{q}_{th} = 200$ Btu/hr-ft^2, $T_\infty = 50^oF$, $T_{in} = 85^oF$ and n=1

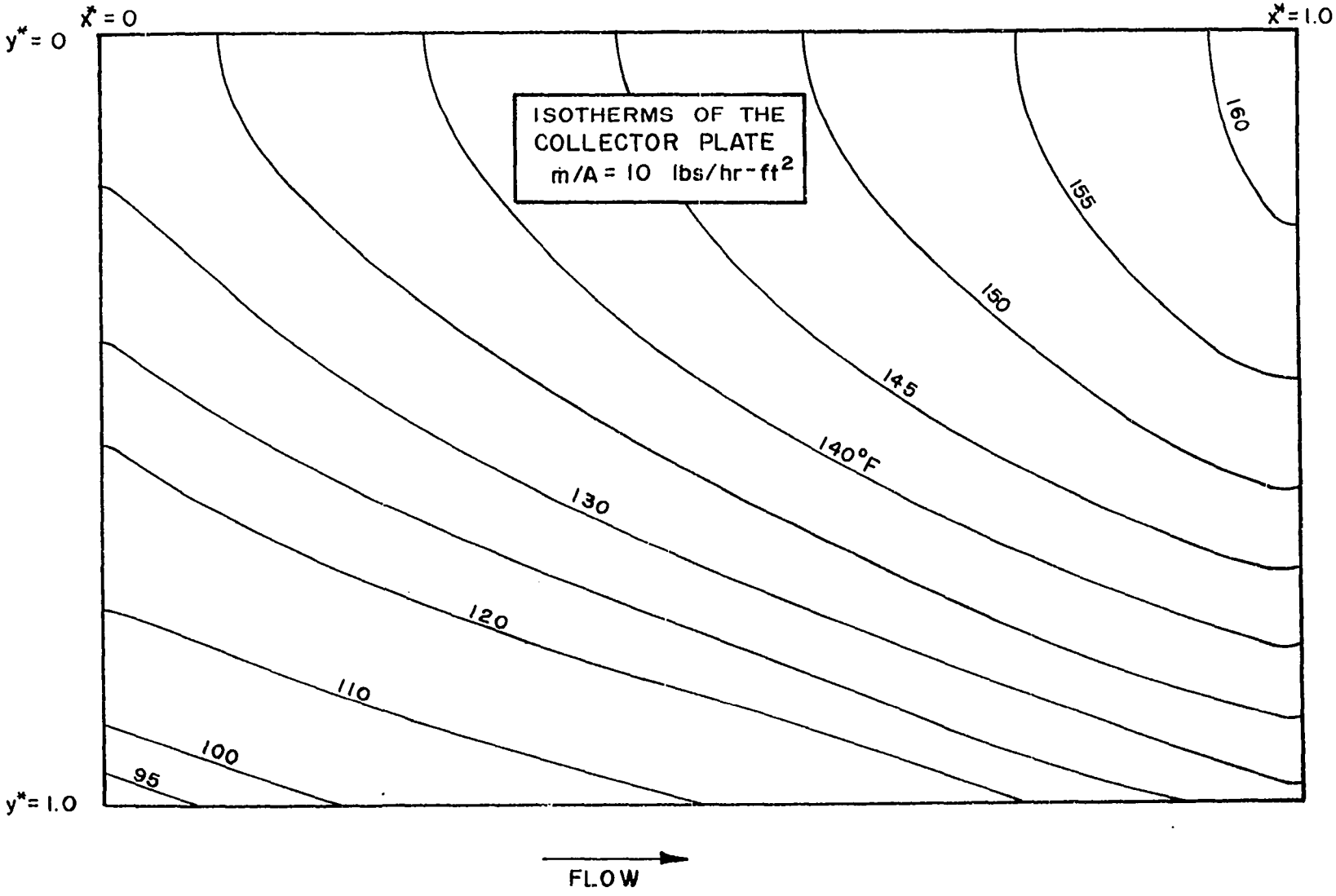
x* = 0
x* = 1.0
y* = 0
y* = 1.0
ISOTHERMS OF THE
COLLECTOR PLATE
m/A = 10 lbs/hr-ft²
160
155
150
145
140°F
130
120
110
100
95
FLOW

Figure 5.1.3c Plot of isotherms of the collector plate for a flow rate of 2 lbs/hr-ft^2, $B/D_o = 8$, kt = 0.391 Btu/hr-^oF, $\dot{q}_{th} = 200$ Btu/hr-ft^2, $T_\infty = 50^oF$, $T_{in} = 85^oF$ and n=1

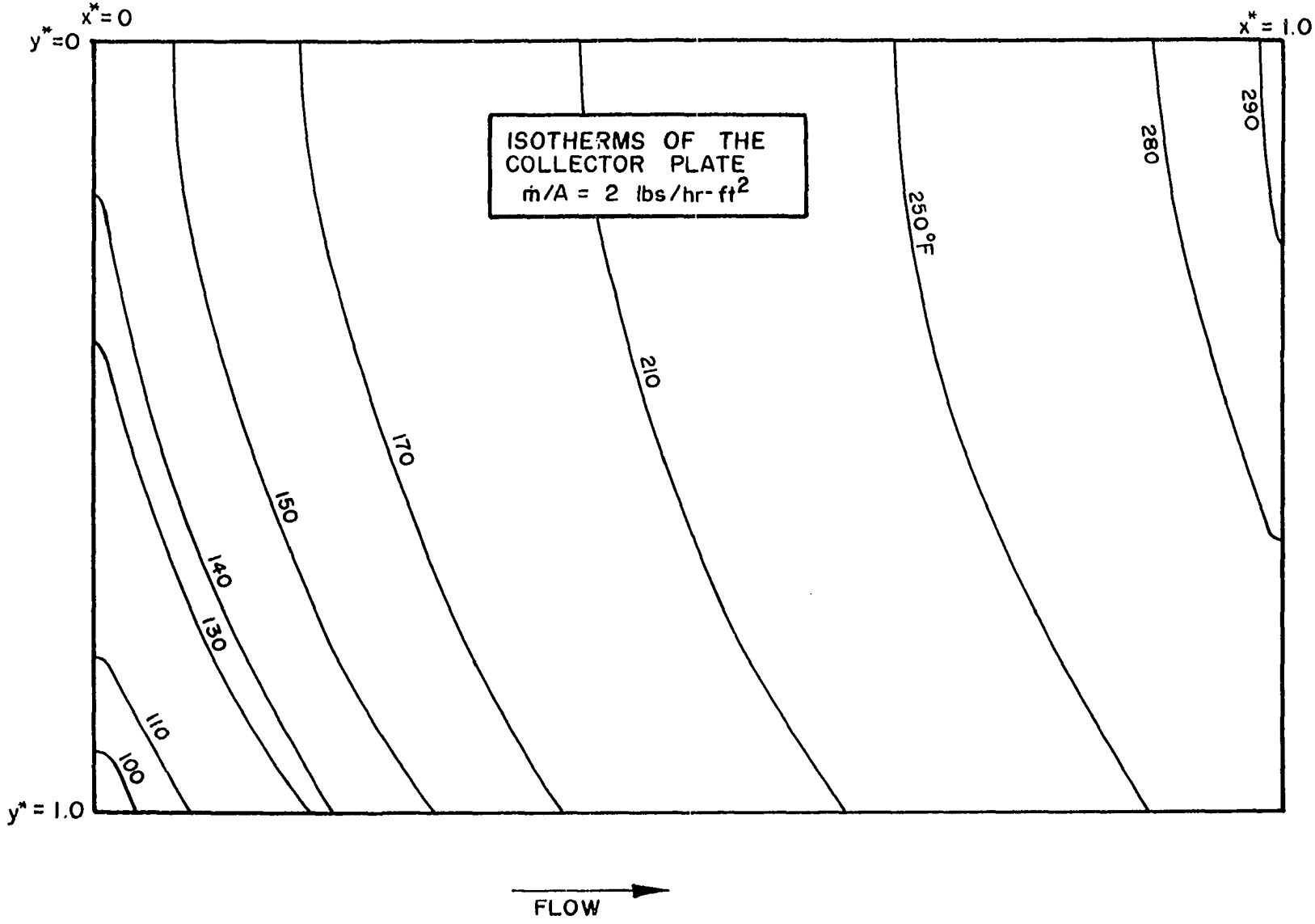
x* = 0
y* = 0
x* = 1.0
y* = 1.0
ISOTHERMS OF THE COLLECTOR PLATE
ṁ/A = 2 lbs/hr-ft²
100
110
130
140
150
170
210
250°F
280
290
FLOW

5.1.4a Effect of the product of plate thickness and thermal conductivity on the plate temperature profiles normal to the tube, for a mass flow rate of 11 lbs/hr-ft^2, $B/D_o = 8$, $\dot{q}_{th} = 200$ Btu/hr-ft^2, $T_\infty = 50^oF$, $T_{in} = 85^oF$, and n=1.

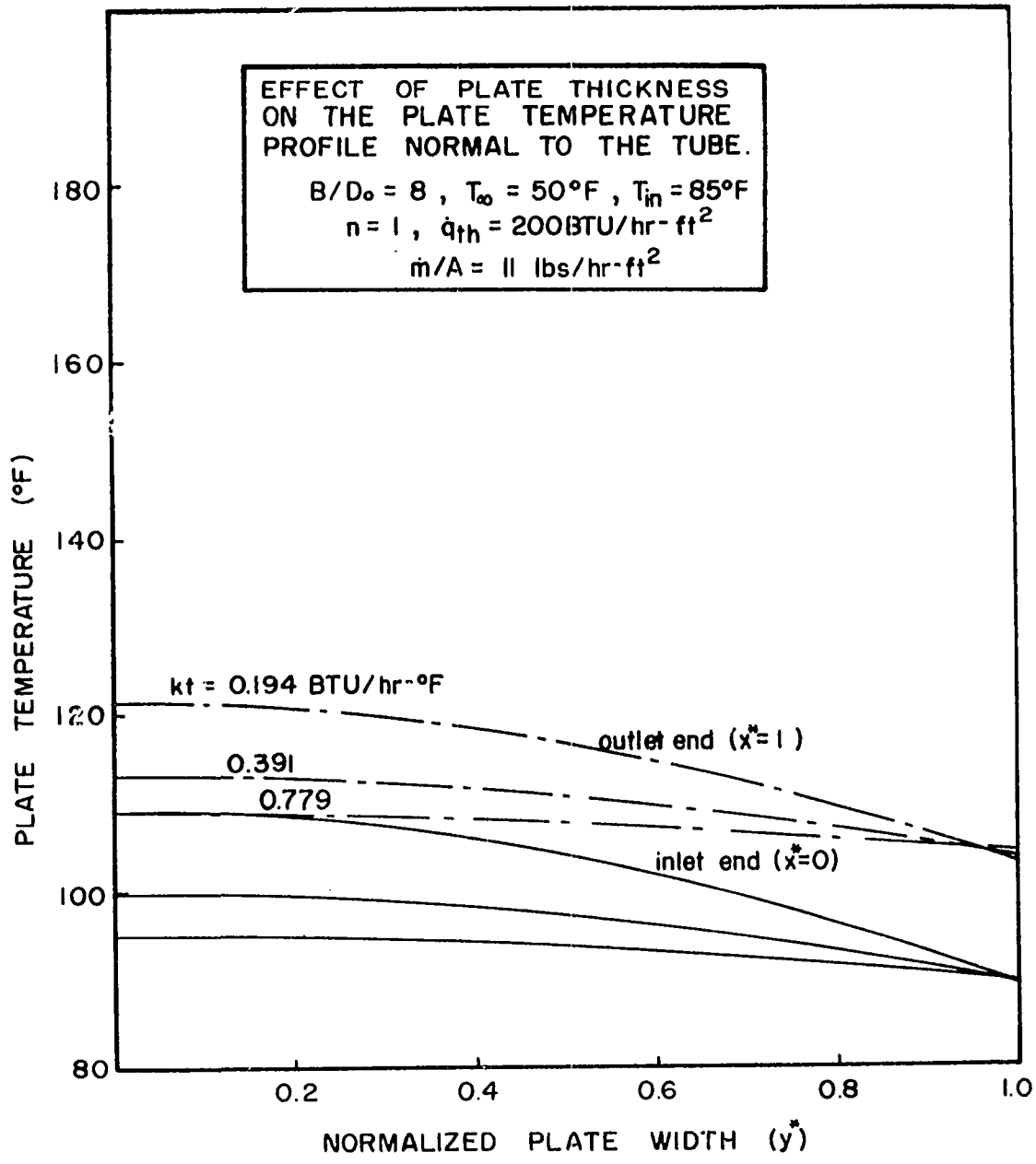
EFFECT OF PLATE THICKNESS ON THE PLATE TEMPERATURE PROFILE NORMAL TO THE TUBE.
B/Do = 8 , T∞ = 50°F , Tin = 85°F
n = 1 , q̇th = 200BTU/hr-ft2
ṁ/A = 11 lbs/hr-ft2
PLATE TEMPERATURE (°F)
180
160
140
120
100
80
kt = 0.194 BTU/hr-°F
outlet end (x*=1)
0.391
0.779
inlet end (x*=0)
0.2
0.4
0.6
0.8
1.0
NORMALIZED PLATE WIDTH (y*)

Figure 5.1.4b Effect of the product of plate thickness and thermal conductivity on the plate temperature profiles parallel to the tube, for a mass flow rate of 11 lbs/hr-ft^2, $B/D_o = 8$, $\dot{q}_{t'h} = 200$ Btu/hr-ft^2, $T_\infty = 50^oF$, $T_{in} = 85^oF$ and n=1.

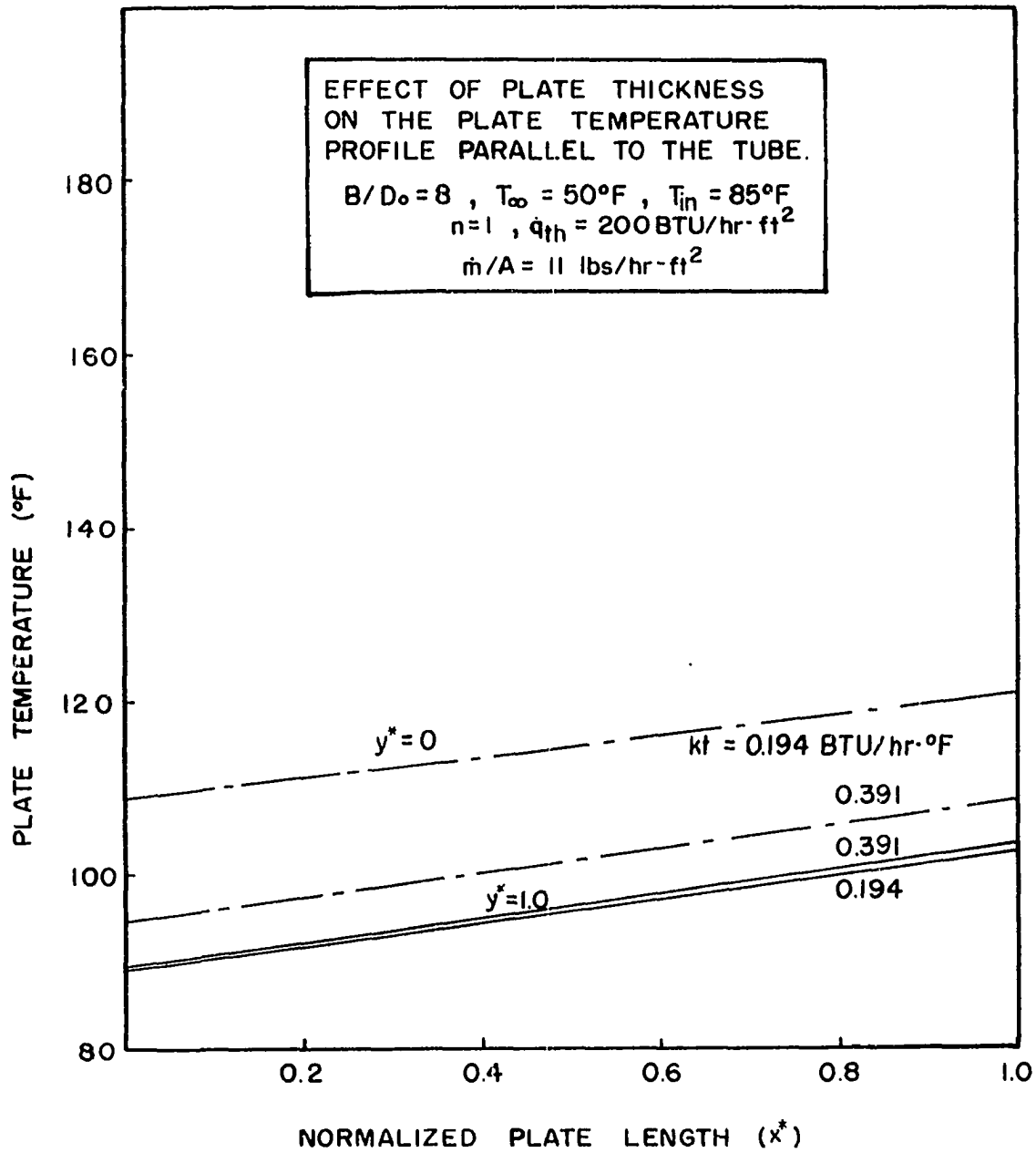
EFFECT OF PLATE THICKNESS
ON THE PLATE TEMPERATURE
PROFILE PARALLEL TO THE TUBE.
B/Do = 8 , T∞ = 50°F , Tin = 85°F
n=1 , qth = 200 BTU/hr-ft2
ṁ/A = 11 lbs/hr-ft2
PLATE TEMPERATURE (°F)
180
160
140
120
100
80
y*=0
kf = 0.194 BTU/hr·°F
0.391
0.391
y*=1.0
0.194
0.2
0.4
0.6
0.8
1.0
NORMALIZED PLATE LENGTH (x*)

direction and gradually become normal to the fluid direction for very low flow rates.

Effect of the Product of Plate Thickness and Thermal Conductivity

Figures 5.1.4 (a,b) illustrate the effect of plate thickness on the plate temperature distribution. As should be expected, thinner plates result in higher temperatures and gradients. And an increase in thickness results in lower plate temperatures and gradients. Such a behavior is due to the fact that an increase in thickness results in a decrease in the thermal resistance and aids heat transfer. Observe that as far as the longitudinal temperature profiles are concerned, plate thickness seems to have very little effect on the temperature gradients, but actual temperatures tend to be much lower for thicker plates, due to an increase in heat transfer.

Effect of the Ratio of Tube Spacing to Tube Diameter

Figures 5.1.5(a,b) illustrate the effect of the ratio of B/D_o on the plate temperature distribution. Observe that wider tube spacing results in higher plate temperatures and higher gradients. The former effect is due to an increase in the total amount of energy absorbed by the plate and the latter effect is due to an increase in the thermal resistance of the plate.

Comparing Figures 5.1.4(a,b) and 5.1.5(a,b) it is interesting to note that an increase in tube spacing has the same effect as a decrease in plate thickness. However, the difference between the two cases is in the magnitudes of temperature and gradients.

Figure 5.1.5a Effect of the ratio of tube spacing to tube diameter on the plate temperature profiles normal to the tube, for a mass flow rate of 11 lbs/hr-ft^2, $\dot{q}_{th}$ = 200 Btu/hr-ft^2, kt = 0.391 Btu/hr-^{o}F, T_{∞} = 50°F, T_{in} = 85°F and n=1

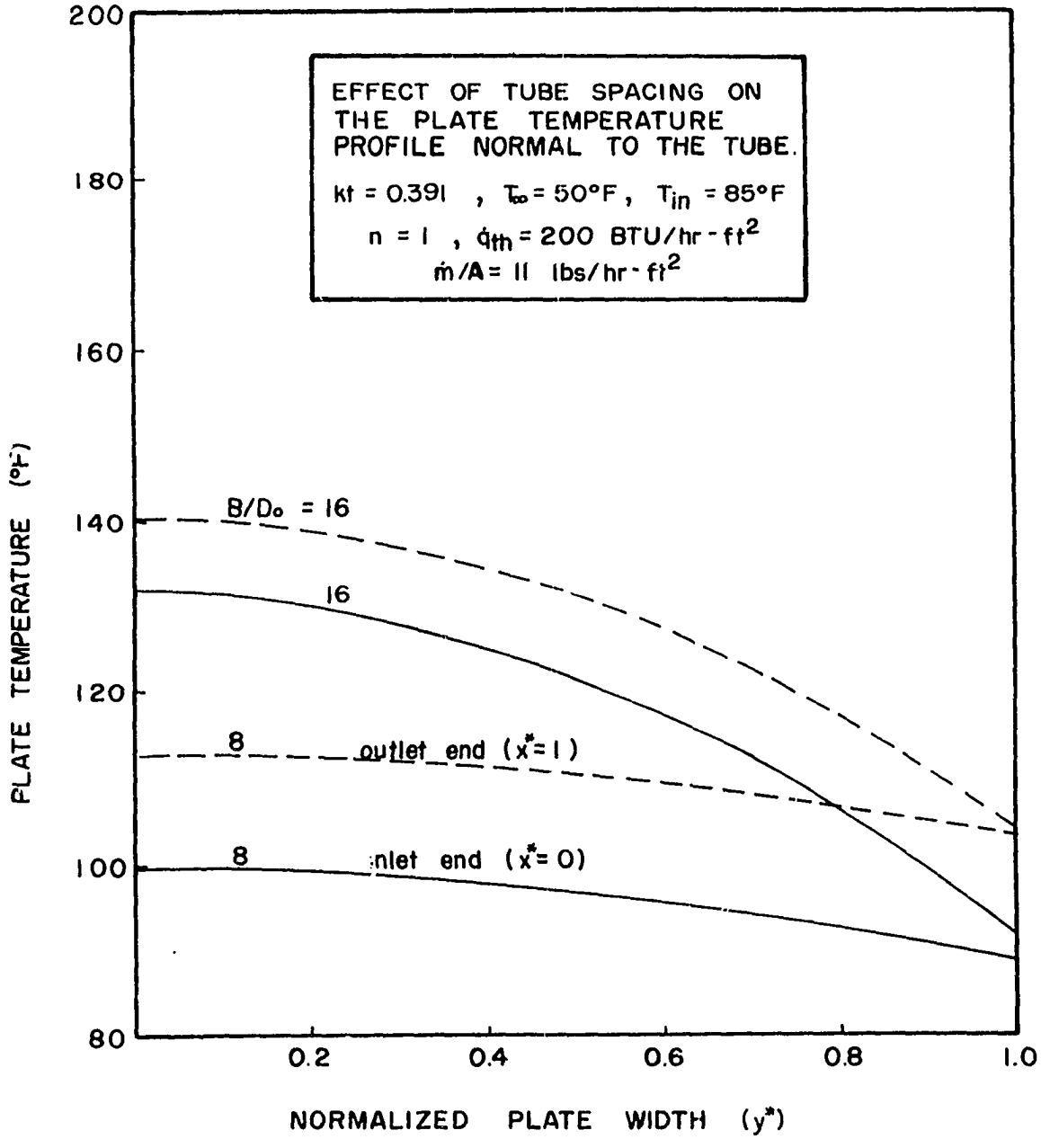
EFFECT OF TUBE SPACING ON THE PLATE TEMPERATURE PROFILE NORMAL TO THE TUBE.
kf = 0.391 , T∞ = 50°F , Tin = 85°F
n = 1 , qth = 200 BTU/hr - ft2
ṁ/A = 11 lbs/hr - ft2
B/Do = 16
16
8 outlet end (x*= 1)
8 inlet end (x*= 0)
PLATE TEMPERATURE (°F)
NORMALIZED PLATE WIDTH (y*)
200
180
160
140
120
100
80
0.2
0.4
0.6
0.8
1.0

Figure 5.1.5b Effect of the ratio of tube spacing to tube diameter on the plate temperature profiles parallel to the tube, for a mass flow rate of 11 lbs/hr-ft^2, $\dot{q}_{th}$ = 200 Btu/hr-ft^2, kt = 0.391 Btu/hr-^{o}F, T_∞ = 50°F, T_{in} = 85°F and n=1

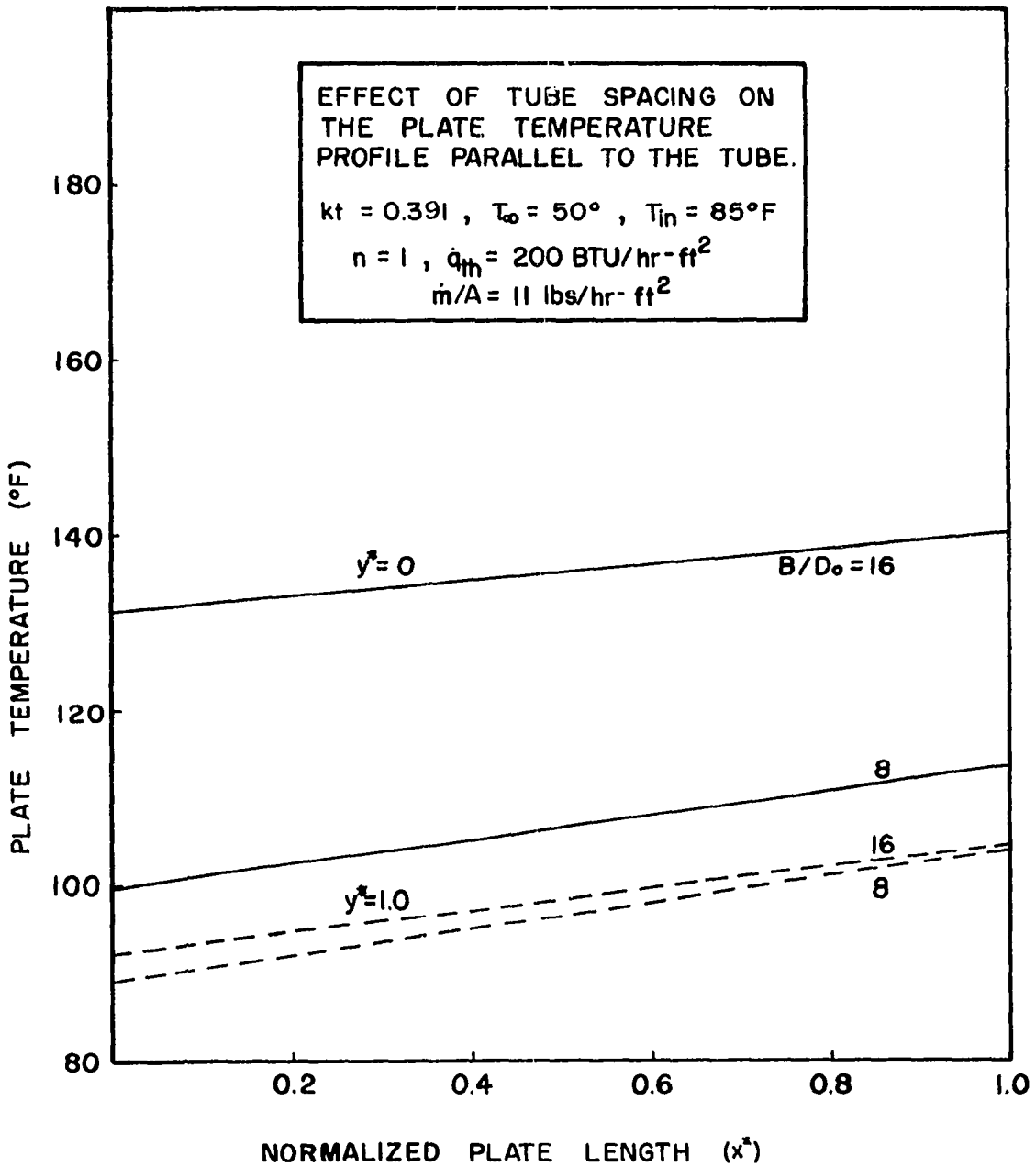
EFFECT OF TUBE SPACING ON THE PLATE TEMPERATURE PROFILE PARALLEL TO THE TUBE.
kt = 0.391 , T∞ = 50° , Tin = 85°F
n = 1 , q̇th = 200 BTU/hr-ft²
ṁ/A = 11 lbs/hr-ft²
PLATE TEMPERATURE (°F)
180
160
140
120
100
80
y*= 0
B/Do = 16
8
16
8
y*=1.0
0.2
0.4
0.6
0.8
1.0
NORMALIZED PLATE LENGTH (x*)

Figure 5.2.1 Effect of mass flow rate on the fluid temperature distribution along the tube for $B/D_o = 8$, $\dot{q}_{th} = 200$ Btu/hr-ft^2, kt = 0.391 Btu/hr-^oF, $T_\infty = 50^oF$, $T_{in} = 85^oF$ and n=1

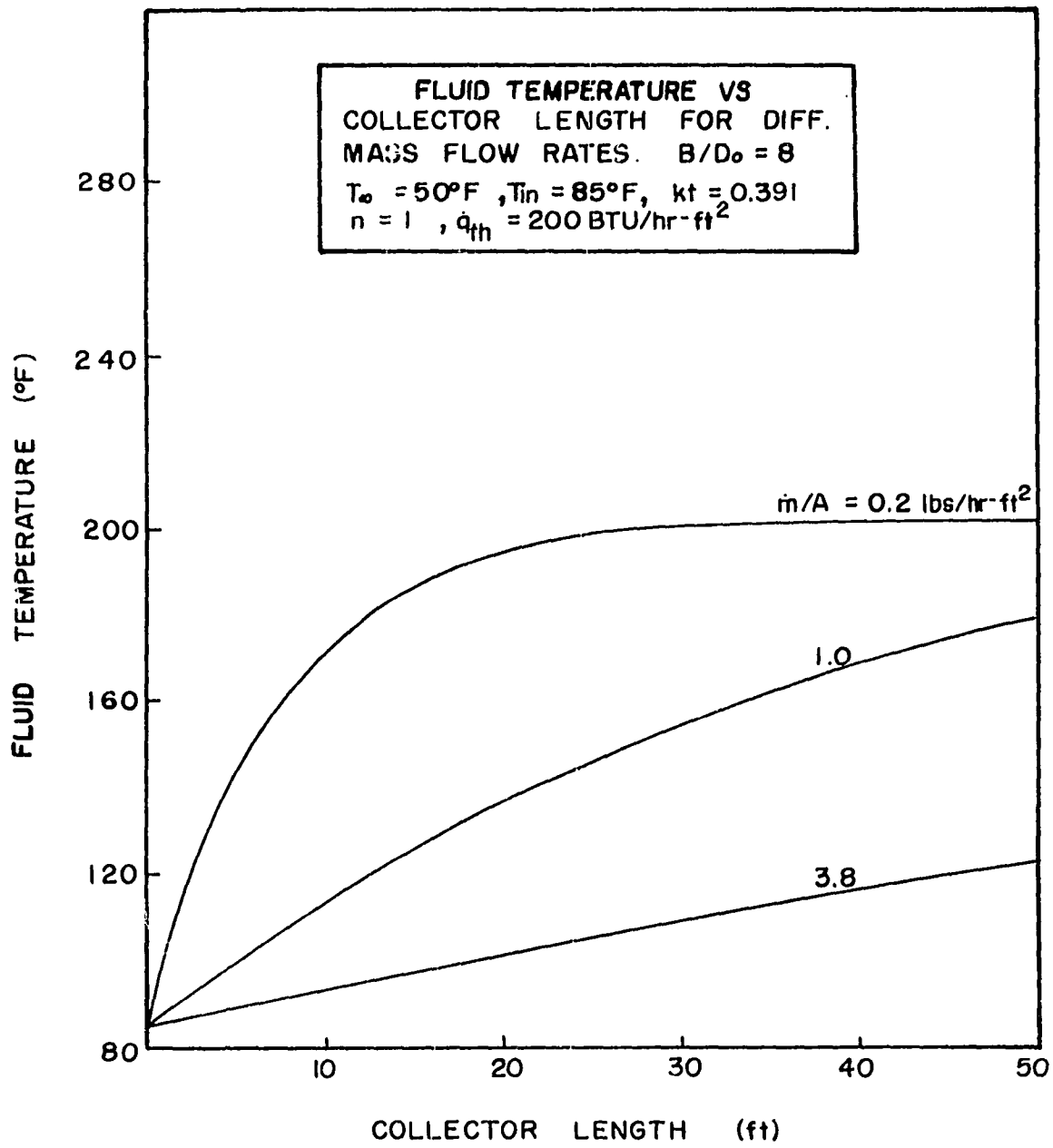
FLUID TEMPERATURE VS
COLLECTOR LENGTH FOR DIFF.
MASS FLOW RATES. B/Do = 8
T∞ = 50°F , Tin = 85°F, kt = 0.391
n = 1 , q̇th = 200 BTU/hr-ft²
FLUID TEMPERATURE (°F)
280
240
200
160
120
80
ṁ/A = 0.2 lbs/hr-ft²
1.0
3.8
10
20
30
40
50
COLLECTOR LENGTH (ft)

Figure 5.2.2 Plots of fluid outlet temperature, average plate temperature and collector efficiency versus mass flow rate for L = 10 ft, $B/D_o = 8$, $\dot{q}_{th} = 200$ Btu/hr-ft^2, kt = 0.194 Btu/hr$^\circ$F, $T_\infty = 50^\circ$F, $T_{in} = 85^\circ$F and n=1

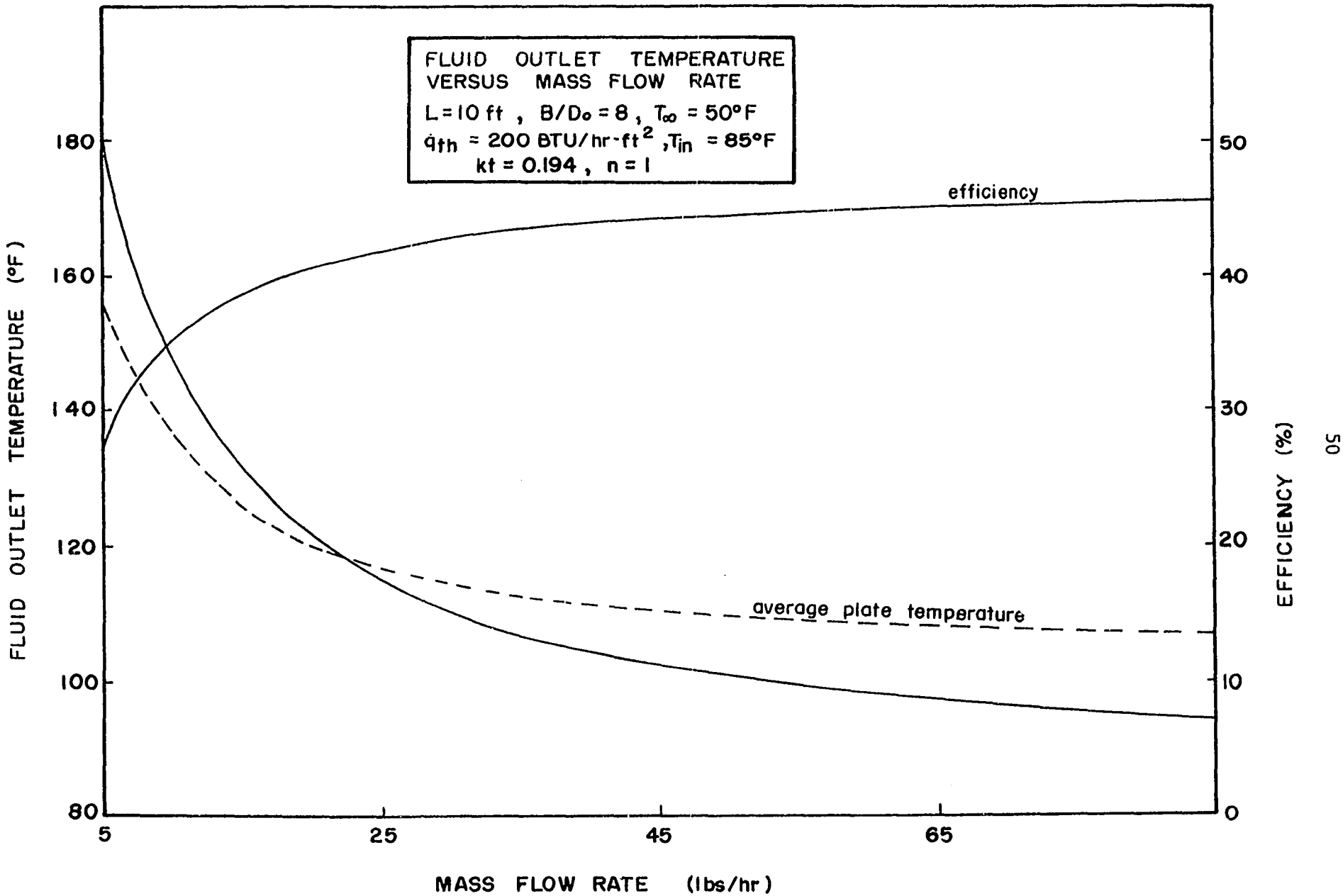
FLUID OUTLET TEMPERATURE VERSUS MASS FLOW RATE
L = 10 ft , B/Do = 8 , T∞ = 50°F
q̇th = 200 BTU/hr-ft², Tin = 85°F
kt = 0.194 , n = 1
efficiency
average plate temperature
FLUID OUTLET TEMPERATURE (°F)
EFFICIENCY (%)
MASS FLOW RATE (lbs/hr)
180
160
140
120
100
80
50
40
30
20
10
0
5
25
45
65

Effect of Collector Length

By plotting the temperature as a function of mass flow rate per unit area of the collector, we obtain the effect of changing the collector length. For a given mass flow rate as the length is increased, the temperature distribution becomes exponential. And, as the length is decreased the temperature distribution becomes almost linear.

5.2 Effect of Collector Parameters on the Temperature Distribution of the Fluid

Effect of Tube Length

The temperature distribution of the fluid inside the tube is given by the equation (3.2.7).

The effect of tube length on the fluid temperature distribution is illustrated in Figure 5.2.1. Observe that foı very low mass flow rates, the temperature profile is exponential and it tends to become linear for higher mass flow rates. For a given length of tube an increase in mass flow rate results in a decrease in fluid temperatures. This effect is illustrated in Figure 5.2.2.

Effect of Tube Spacing

Figures 5.2.3(a,b) illustrate the effect of changing the tube spacing on the fluid outlet temperature. For any given mass flow rate, an increase in tube spacing results in an increase in the fluid outlet temperature. Note that for extremely large flow rates, the tube spacing does not seem to have any effect on the outlet temperature.

Figure 5.2.3a Effect of the ratio of tube spacing to tube diameter on the fluid outlet temperature for L = 10 ft, $\dot{q}_{th}$ = 200 Btu/hr-ft^2, kt = 0.391 Btu/hr-^{o}F, T_{∞} = 50°F, T_{in} = 85°F and n=1

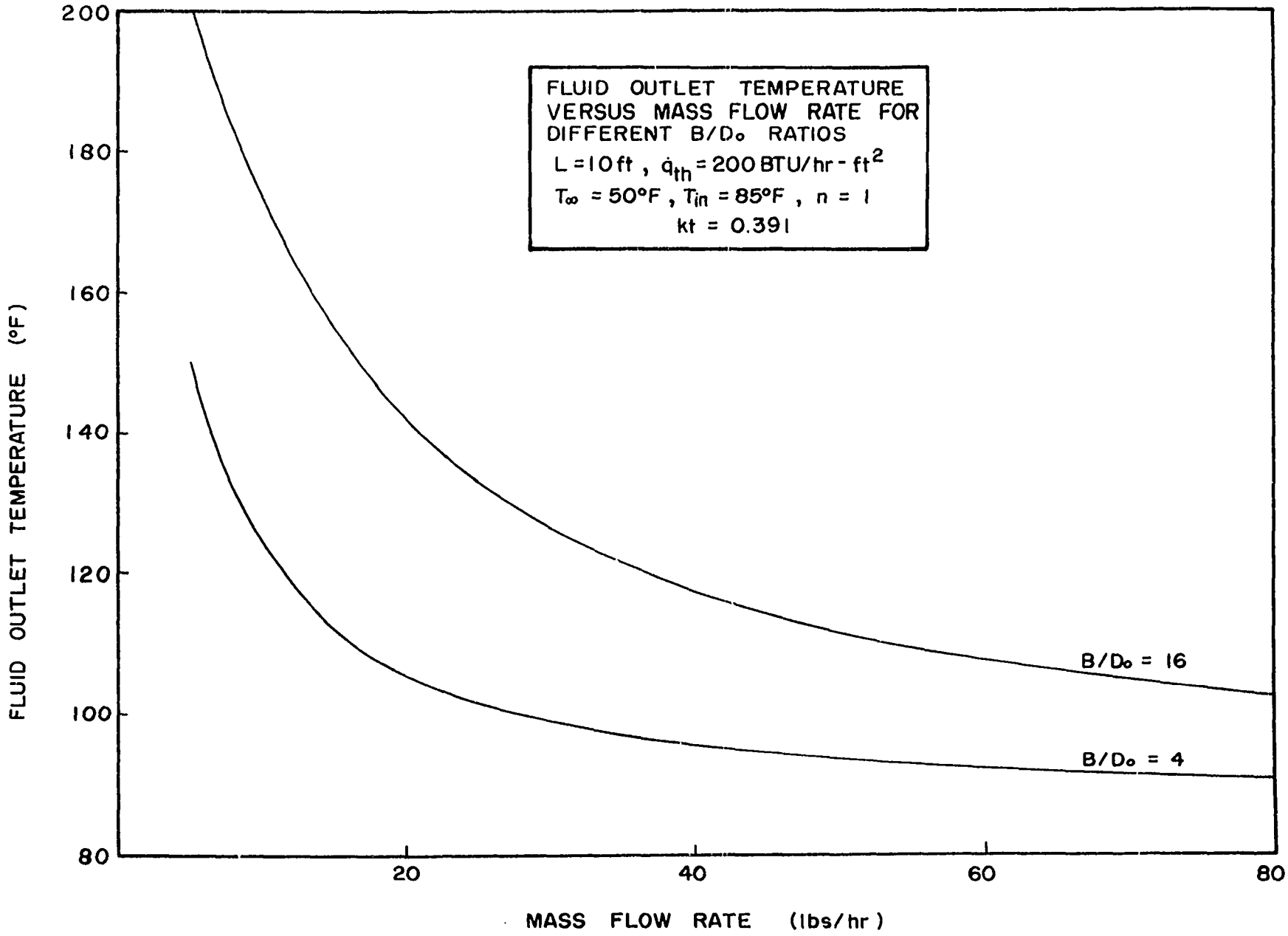
FLUID OUTLET TEMPERATURE VERSUS MASS FLOW RATE FOR DIFFERENT B/Do RATIOS
L = 10 ft , $\dot{q}_{th}$ = 200 BTU/hr - ft^2
T_∞ = 50°F , T_{in} = 85°F , n = 1
kt = 0.391
B/Do = 16
B/Do = 4
FLUID OUTLET TEMPERATURE (°F)
200
180
160
140
120
100
80
20
40
60
80
MASS FLOW RATE (lbs/hr)

Figure 5.2.3b Effect of the ratio of tube spacing to tube diameter on the non-dimensional fluid outlet temperature for L = 10 ft $\dot{q}_{th}$ = 200 Btu/hr-ft^2, kt = 0.391 Btu/hr-^{o}F, T_{∞} = 50°F, T_{in} = 85°F and n=1

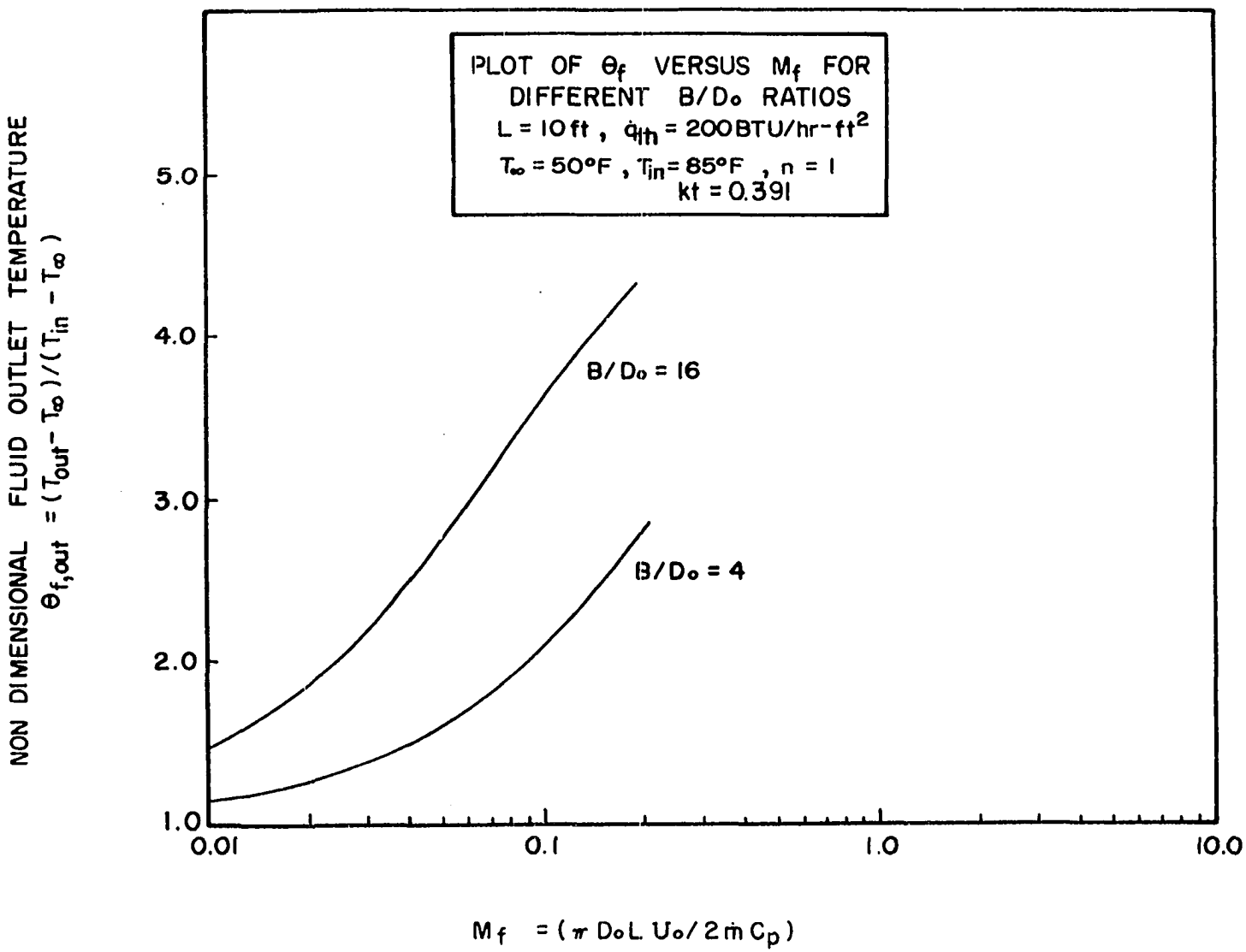
PLOT OF θ_f VERSUS M_f FOR DIFFERENT B/Do RATIOS
L = 10 ft , $\dot{q}_{th}$ = 200 BTU/hr-ft^2
T_∞ = 50°F , T_{in} = 85°F , n = 1
kt = 0.391
B/Do = 16
B/Do = 4
NON DIMENSIONAL FLUID OUTLET TEMPERATURE
$\theta_{f,out} = (T_{out} - T_\infty)/(T_{in} - T_\infty)$
5.0
4.0
3.0
2.0
1.0
0.01
0.1
1.0
10.0
$M_f = (\pi D_o L U_o / 2\dot{m} C_p)$

Figure 5.2.4 Effect of the product of plate thickness and thermal conductivity on the fluid outlet temperature for L = 10 ft, $B/D_o = 8$, $\dot{q}_{th} = 200$ Btu/hr-ft^2, $T_\infty = 50^oF$, $T_{in} = 85^oF$ and n=1.

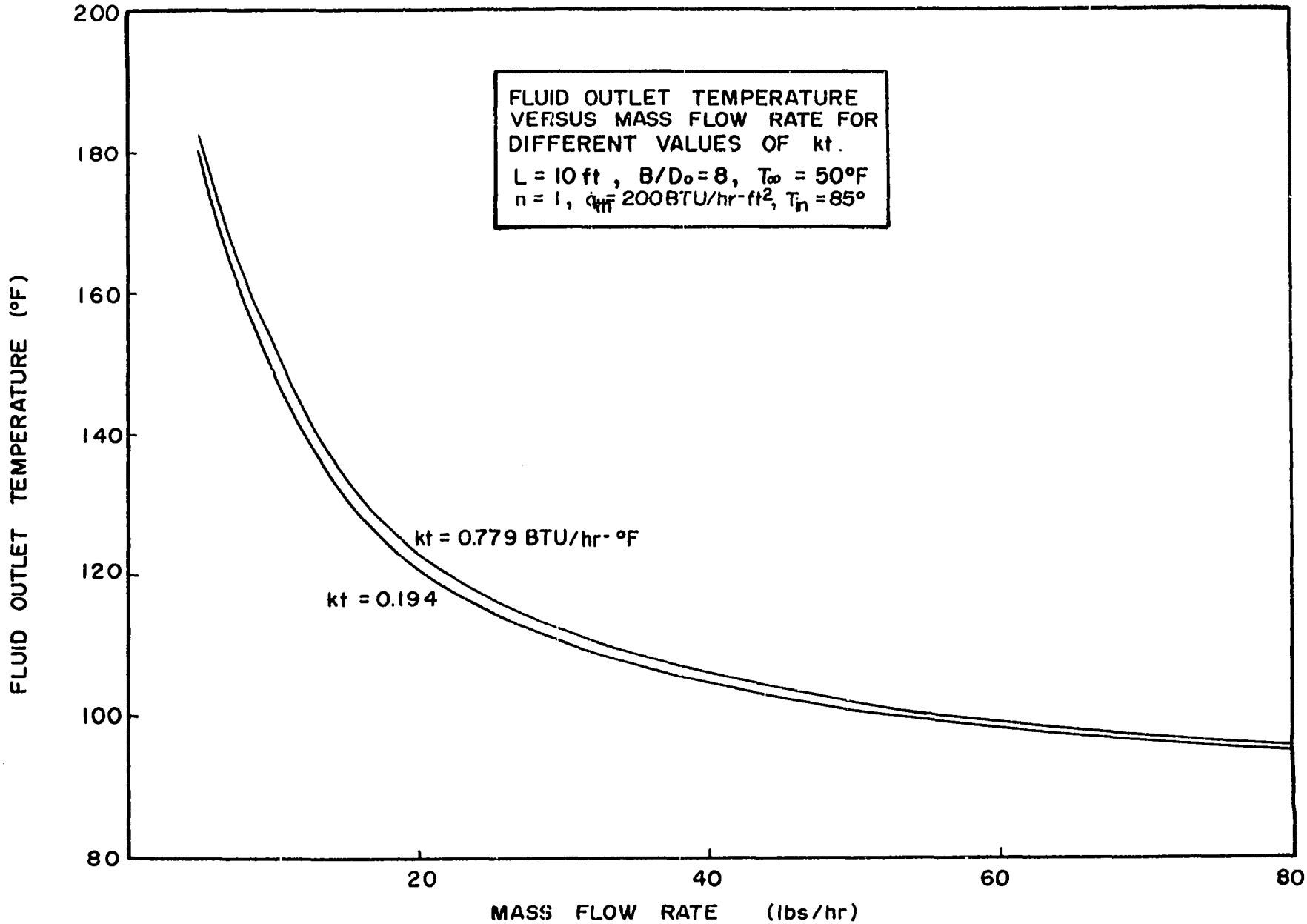
FLUID OUTLET TEMPERATURE VERSUS MASS FLOW RATE FOR DIFFERENT VALUES OF kt.
L = 10 ft , B/Do = 8, T∞ = 50°F
n = 1, qth = 200 BTU/hr-ft², Tin = 85°
kt = 0.779 BTU/hr-°F
kt = 0.194
FLUID OUTLET TEMPERATURE (°F)
200
180
160
140
120
100
80
20
40
60
80
MASS FLOW RATE (lbs/hr)

Figure 5.2.5 Effect of B/D_o ratio and kt on the non-dimensional fluid outlet temperature for $\dot{q}_{th}$ = 200 Btu/hr-ft^2, $T_\infty = 50^oF$, $T_{in} = 85^oF$ and n=1.

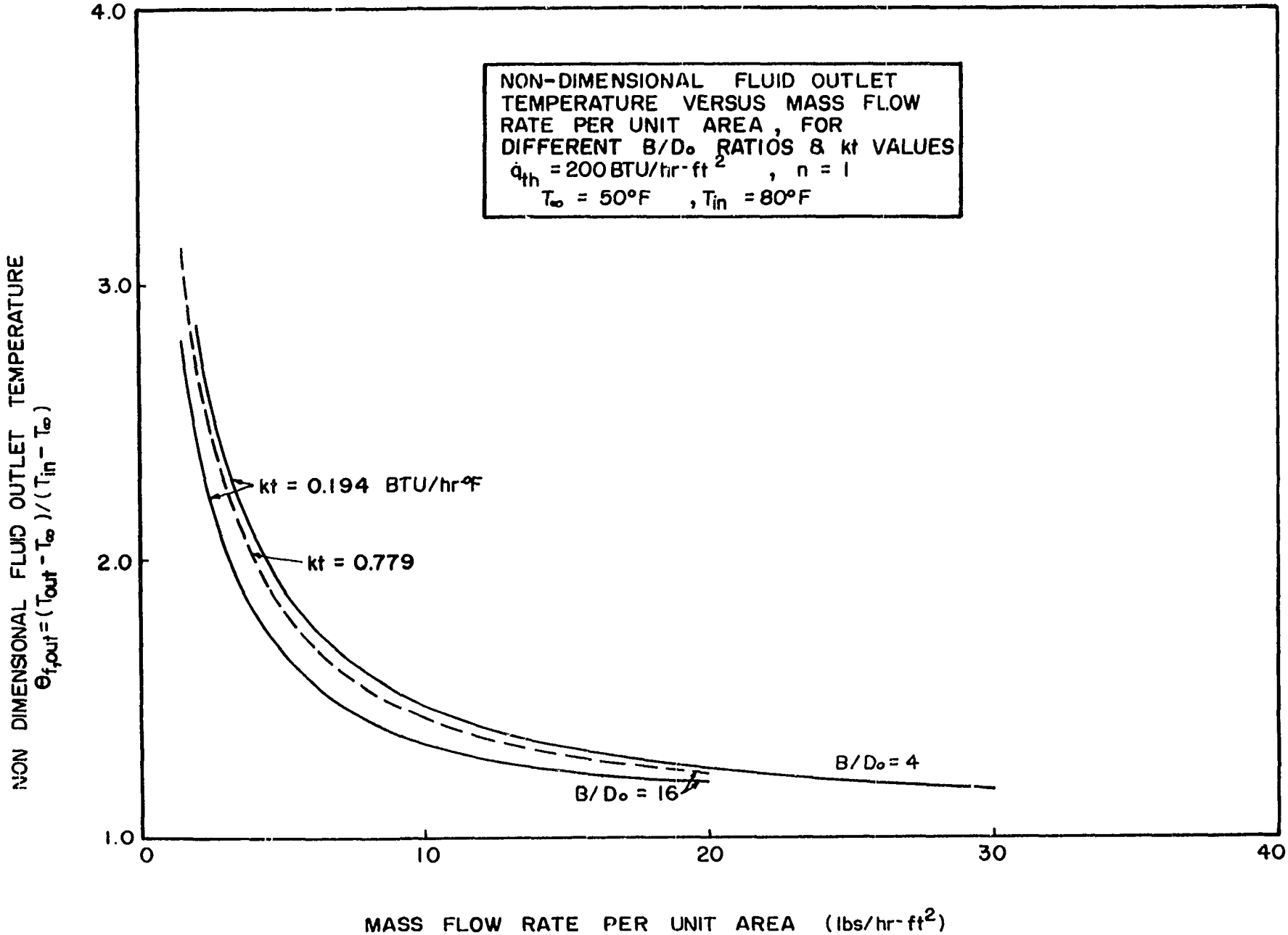
NON-DIMENSIONAL FLUID OUTLET TEMPERATURE VERSUS MASS FLOW RATE PER UNIT AREA, FOR DIFFERENT B/Do RATIOS & kt VALUES
$\dot{q}_{th}$ = 200 BTU/hr-ft^2 , n = 1
T_∞ = 50°F , T_{in} = 80°F
kt = 0.194 BTU/hr-°F
kt = 0.779
B/Do = 4
B/Do = 16
NON DIMENSIONAL FLUID OUTLET TEMPERATURE
$\theta_{f,out} = (T_{out} - T_\infty)/(T_{in} - T_\infty)$
4.0
3.0
2.0
1.0
0
10
20
30
40
MASS FLOW RATE PER UNIT AREA (lbs/hr-ft^2)

Effect of Plate Thickness and Thermal Conductivity

Figure 5.2.4 illustrates the effect of changing the plate thickness and thermal conductivity on the fluid outlet temperature. An increase in the product kt results in a slight increase in the fluid temperature due to increased heat transfer from the plate. However, it should be noted that a four-fold increase in the value of kt results in only about $3^{o}F$ increase in the fluid temperature. Hence, a cost analysis is very essential in order to determine how thick the plate should really be.

In Figure 5.2.5 non-dimensional fluid temperature is plotted against mass flow rate per unit area for different B/D_o ratios and kt values. Observe that an increase in the value of kt causes the curve for $B/D_o = 12$ to approach the curve of $B/D_o = 4$.

5.3 Effect of Collector Parameters on the Short Term Collector Performance

This section is concerned with the prediction of instantaneous collector performance and the effects of various parameters on the collector efficiency. It has been found that basically four parameters dictate the collector performance: mass flow rate, tube spacing, inlet fluid temperature and the overall heat transfer coefficient.

Effect of Mass Flow Rate

As should be expected, the present analysis verifies that the mass flow rate or the mass flow rate per unit area has the greatest influence on the collector performance. Keeping all other parameters constant as the mass flow rate is increased the collector performance rapidly increases at first

Figure 5.3.1 Effect of mass flow rate and B/D_o ratio on the collector efficiency for $\dot{q}_{th}$ = 200 Btu/hr-ft^2, kt = 0.194 Btu/hr-^oF, $T_\infty = 50^oF$, $T_{in} = 85^oF$ and n=1

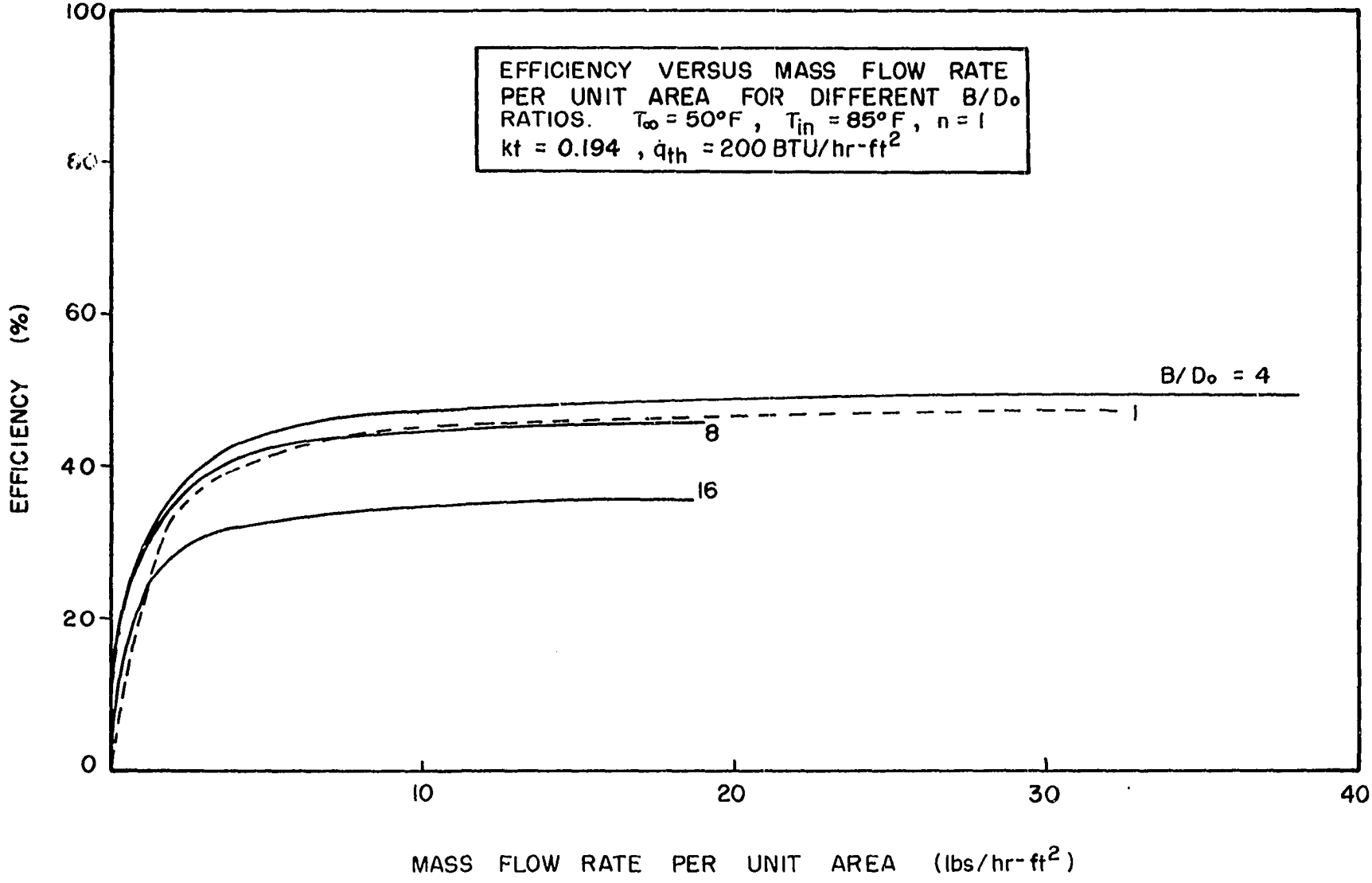
EFFICIENCY VERSUS MASS FLOW RATE PER UNIT AREA FOR DIFFERENT B/Do RATIOS. T∞ = 50°F , Tin = 85°F , n = 1
kt = 0.194 , q̇th = 200 BTU/hr-ft2
EFFICIENCY (%)
100
80
60
40
20
0
10
20
30
40
B/Do = 4
1
8
16
MASS FLOW RATE PER UNIT AREA (lbs/hr-ft2)

Figure 5.3.2 Effect of the ratio of tube spacing to tube diameter and mass flow rate on the collector efficiency for $\dot{q}_{th}$ = 200 Btu/hr-ft^2, $T_\infty = 50^oF$, $T_{in} = 85^oF$ and n=1.

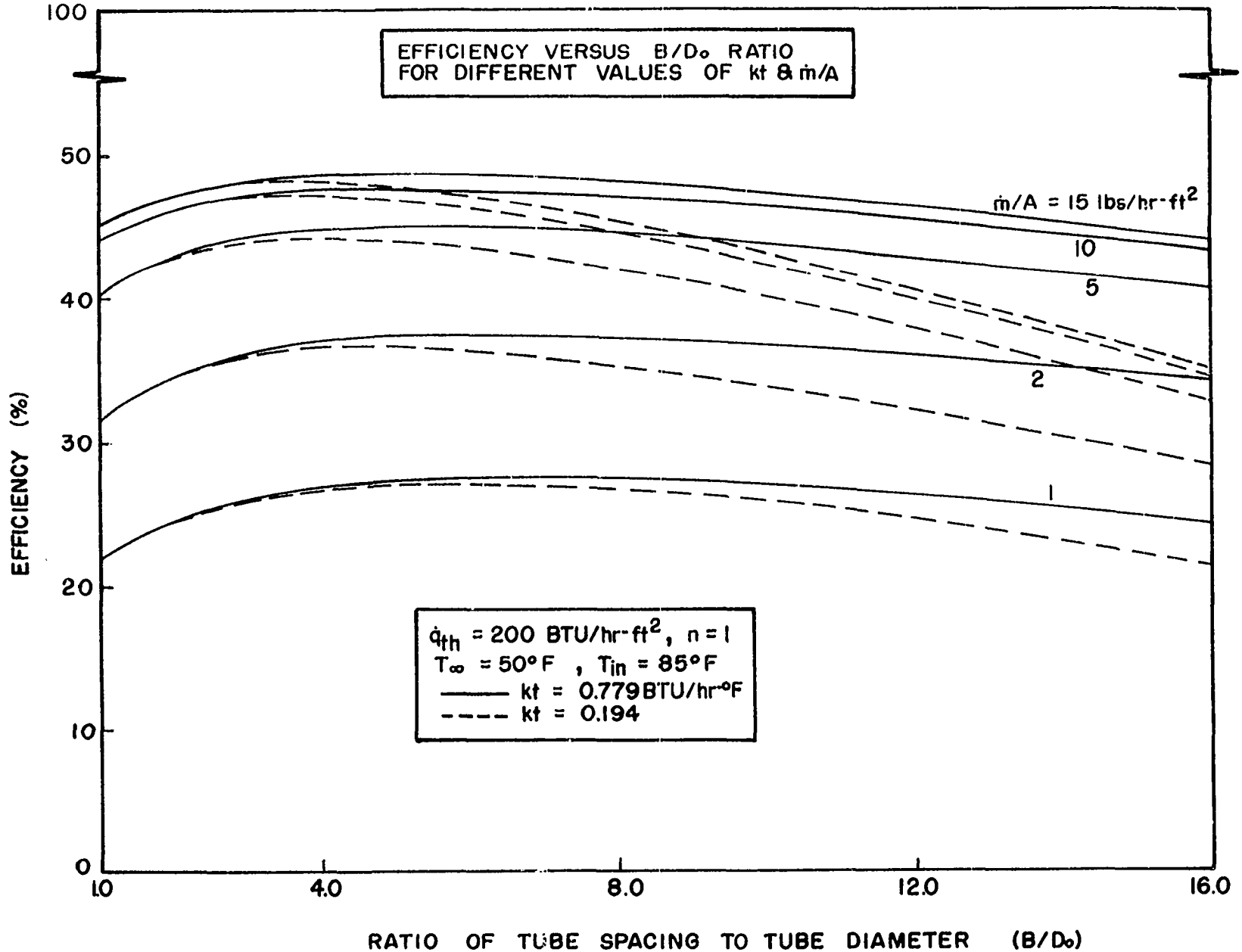
EFFICIENCY VERSUS B/Do RATIO
FOR DIFFERENT VALUES OF kt & ṁ/A
ṁ/A = 15 lbs/hr-ft²
10
5
2
1
q̇th = 200 BTU/hr-ft², n = 1
T∞ = 50°F , Tin = 85°F
kt = 0.779 BTU/hr-°F
kt = 0.194
EFFICIENCY (%)
100
50
40
30
20
10
0
1.0
4.0
8.0
12.0
16.0
RATIO OF TUBE SPACING TO TUBE DIAMETER (B/Do)

Figure 5.3.3 Effect of increasing the value of kt from 0.194 to 0.779 on the collector efficiency for $\dot{q}_{th}$ = 200 Btu/hr-ft^2, kt = 0.779 Btu/hr-^{o}F, T_{∞} = 50°F, T_{in} = 85°F and n=1

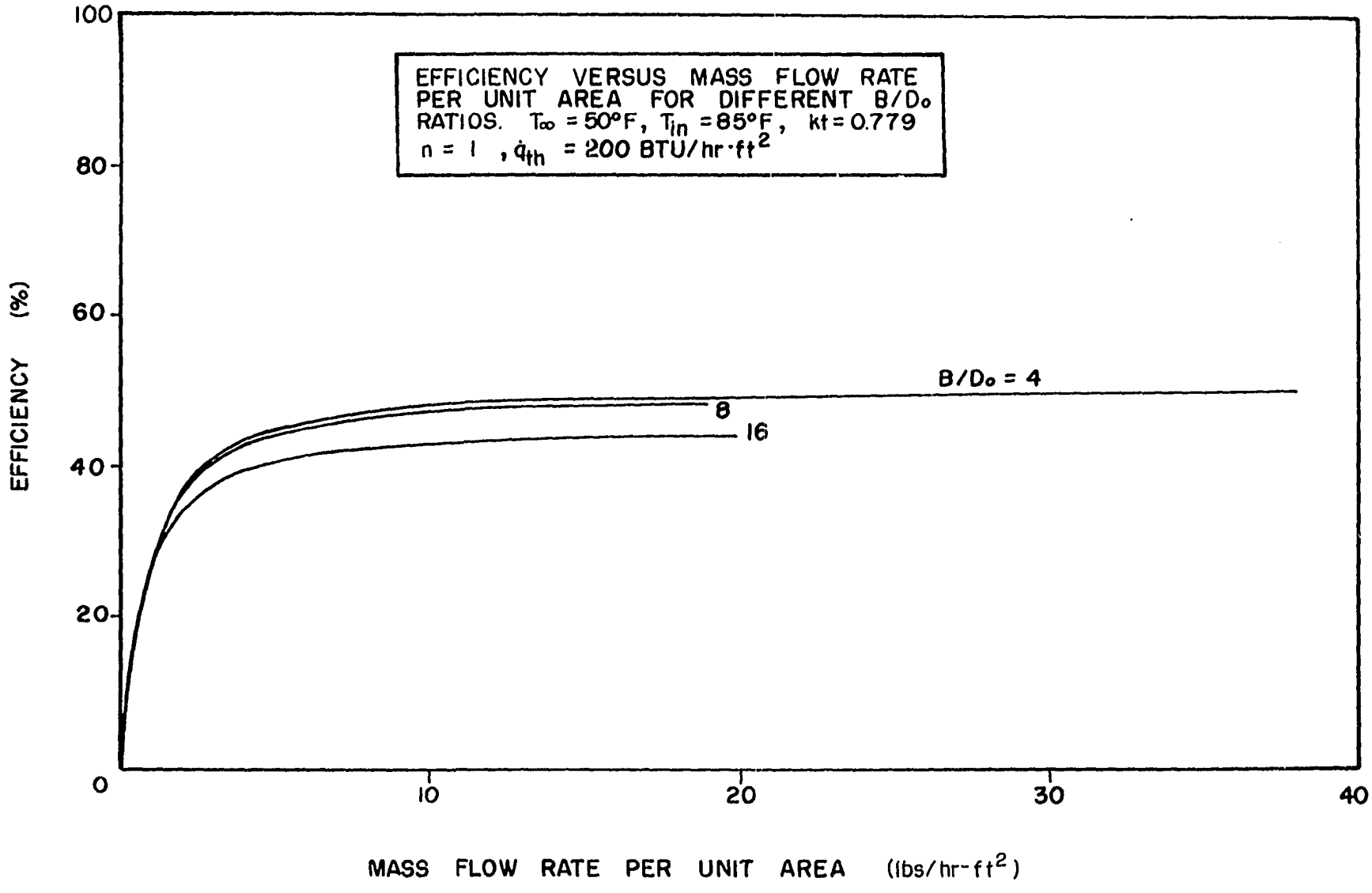
EFFICIENCY VERSUS MASS FLOW RATE PER UNIT AREA FOR DIFFERENT B/Do RATIOS. T∞ = 50°F, Tin = 85°F, kt = 0.779 n = 1 , q̇th = 200 BTU/hr·ft²
EFFICIENCY (%)
100
80
60
40
20
0
B/Do = 4
8
16
10
20
30
40
MASS FLOW RATE PER UNIT AREA (lbs/hr-ft²)

and then levels off and approaches a maximum value asymptotically. This effect is illustrated in Figure 5.3.1. Note that efficiency is plotted as a function of mass flow rate per unit area rather than the total mass flow rate. This eliminates specifying the length of the collector. From the figure it can be seen that around a mass flow rate of about 10 lbs/hr-ft^2 a collector attains most of its efficiency and further increase in mass flow rate does not help much.

Effect of Tube Spacing

An interesting result of the analysis is the effect of the ratio of tube spacing to tube diameter on the efficiency. It was found that for every value of B/D_o ratio, there is a maximum possible efficiency that can be achieved. Figure 5.3.2 illustrates another interesting result. Observe that for each value of mass flow rate, there seems to be an optimum B/D_o ratio that will give maximum efficiency. With increase in mass flow rate, this optimum B/D_o ratio seems to shift to smaller values.

Effect of Plate Thickness and Thermal Conductivity

The effect of plate thickness and thermal conductivity can be observed by comparing Figure 5.3.1 and 5.3.3. Note that the product of kt has very little effect when the B/D_o ratio is small and has greater effect for larger B/D_o ratios. From the heat transfer point of view, this is logical because for wider tube spacings an increase in plate thickness (i.e. an increase in kt) results in a decrease in thermal resistance and helps to increase efficiency.

Figure 5.3.4 Effect of increasing the inlet temperature from $85^{o}F$ to $135^{o}F$ on the collector efficiency for $\dot{q}_{th}$ = 200 Btu/hr-ft^2, kt = 0.194 Btu/hr-^{o}F, $T_{\infty} = 50^{o}F$, $T_{in} = 85^{o}F$ and n=1

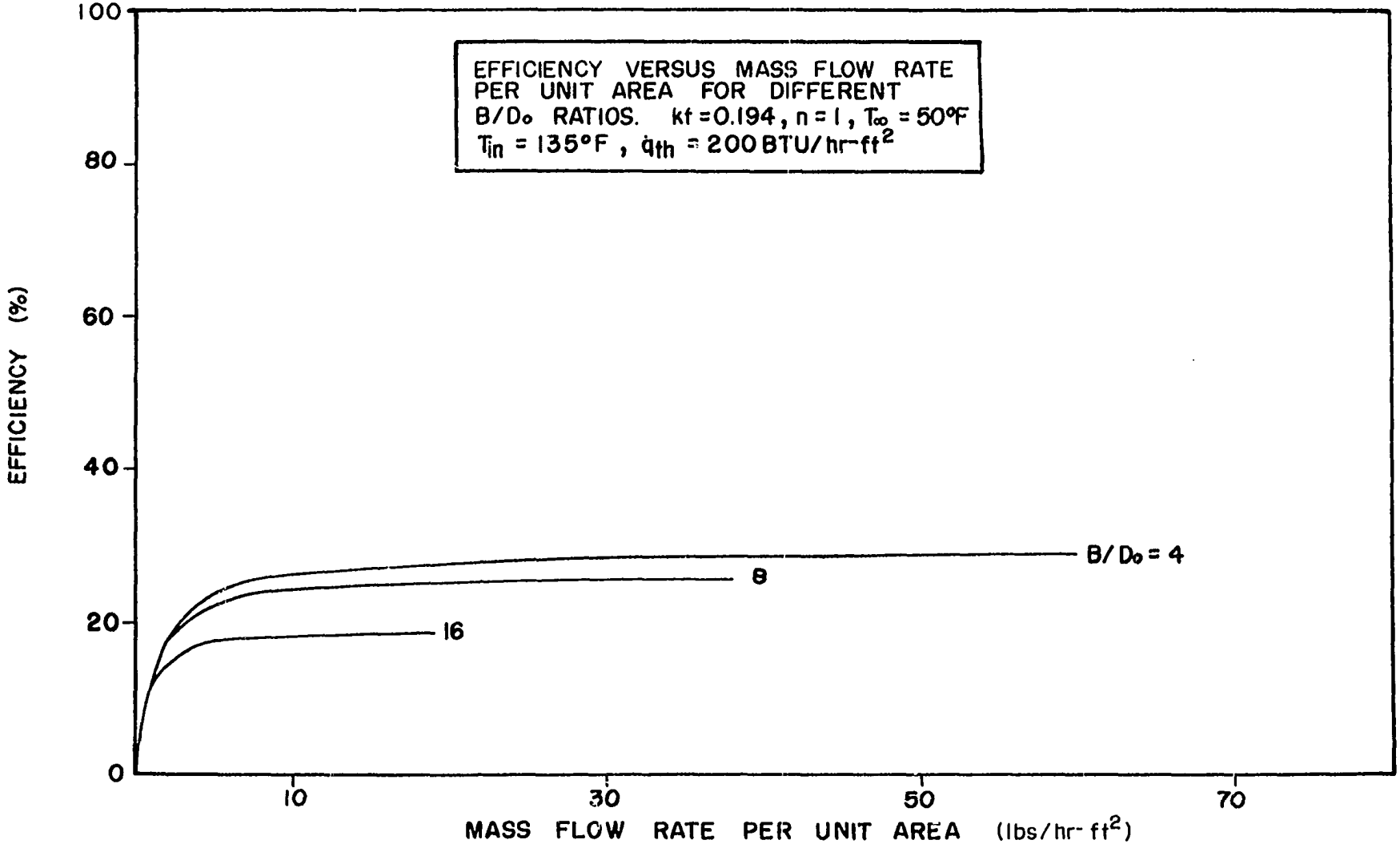
EFFICIENCY VERSUS MASS FLOW RATE PER UNIT AREA FOR DIFFERENT B/Do RATIOS. kf = 0.194, n = 1, T∞ = 50°F
Tin = 135°F, q̇th = 200 BTU/hr-ft²
EFFICIENCY (%)
100
80
60
40
20
0
B/Do = 4
8
16
10
30
50
70
MASS FLOW RATE PER UNIT AREA (lbs/hr-ft²)

Figure 5.3.5 Effect of fluid inlet temperature and the number of glass covers on the collector efficiency for $\dot{q}_{th}$ = 200 Btu/hr-ft^2, kt = 0.391 Btu/hr-^oF, T_∞ = 50^oF, $\dot{m}/A$ = 11 lbs/hr-ft^2 and B/D_o = 8

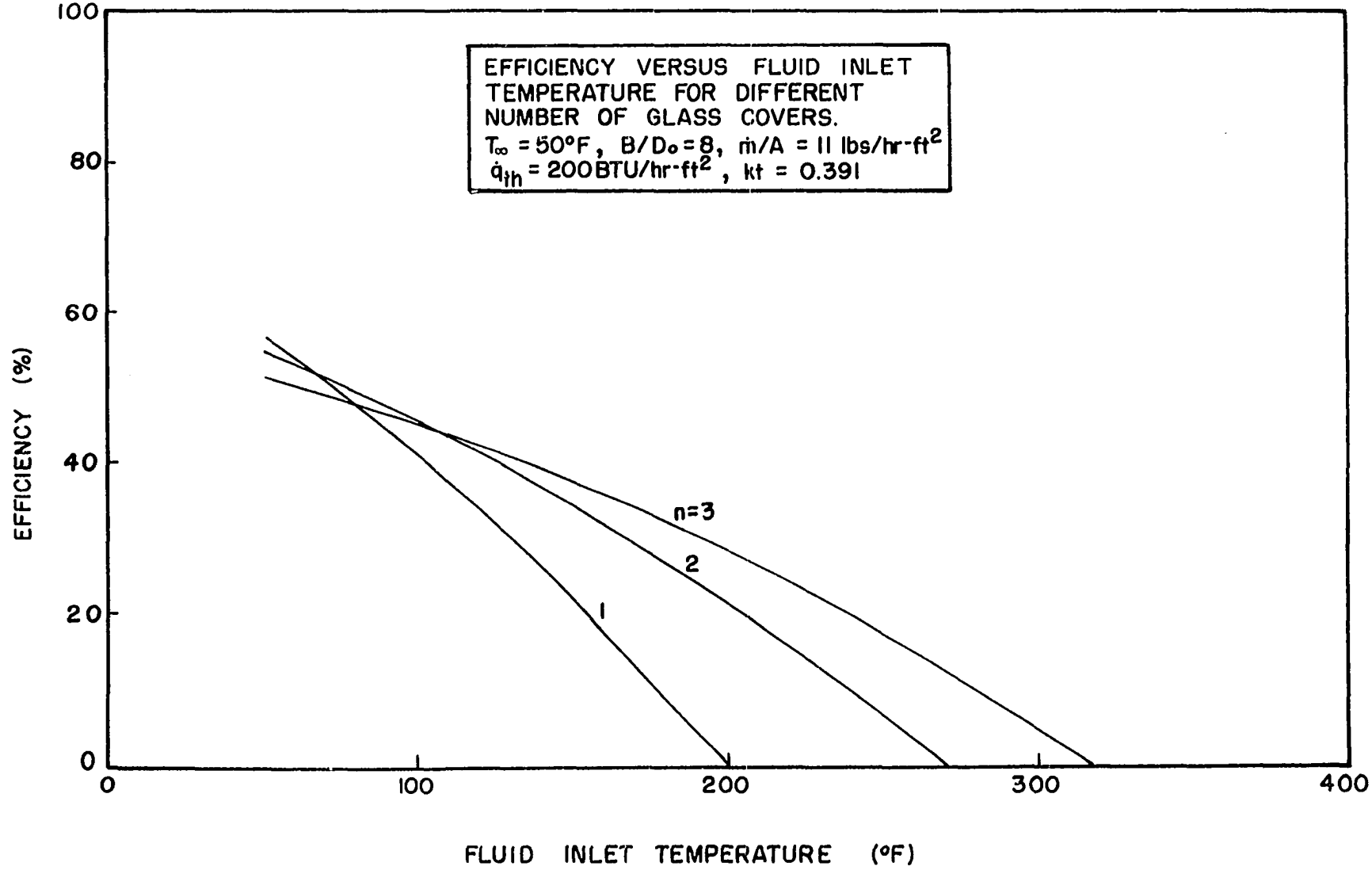
EFFICIENCY VERSUS FLUID INLET TEMPERATURE FOR DIFFERENT NUMBER OF GLASS COVERS.
$T_\infty = 50°F$, $B/D_o = 8$, $\dot{m}/A = 11$ lbs/hr-ft^2
$\dot{q}_{th} = 200$BTU/hr-ft^2, kt = 0.391
n=3
2
1
EFFICIENCY (%)
FLUID INLET TEMPERATURE (°F)
0
20
40
60
80
100
0
100
200
300
400

Effect of Fluid Inlet Temperature

Figures 5.3.1 & 5.3.4 illustrate the effect of increasing the fluid inlet temperature from 85°F to 135°F. The collector efficiency drops appreciably as the fluid inlet temperature is increased. High fluid inlet temperatures result in high plate temperatures, giving rise to increased losses and lower efficiencies.

In Figure 5.3.5 collector efficiency is plotted as a function of fluid inlet temperatures. Observe that when the inlet temperature is equal to the equilibrium plate temperature, efficiency goes to zero. That is, there is no heat gain by the fluid.

Effect of Ambient Temperature

Figures 5.3.1 and 5.3.6 illustrate the effect of decreasing the ambient temperature from 50°F to 0°F. Lower ambient temperatures cause increased collector losses and hence lower efficiencies.

Effect of Glass Covers

Figure 5.3.7 shows an interesting result of the effect of increasing the number of glass covers for an inlet temperature of 85°F. Observe that as the number of covers is increased from 1 to 2, there is a slight increase in efficiency. When the number is further increased to 3, there is a slight drop in efficiency, but is still slightly more efficient than a single cover. Note that for very low mass flow rates, three covers are most efficient. In Figure 5.3.5 collector efficiency is plotted as a function of the fluid inlet temperature. Observe that for temperatures below 80°F, three covers are the least efficient and for temperatures above 100°F, three covers are the most efficient.

Figure 5.3.6 Effect of decreasing the ambient temperature from $50^{o}F$ to $0^{o}F$ on the collector efficiency for $\dot{q}_{th}$ = 200 Btu/hr-ft^2, kt = 0.194 Btu/hr-^{o}F, $T_{\infty} = 0^{o}F$, $T_{in} = 85^{o}F$ and n=1

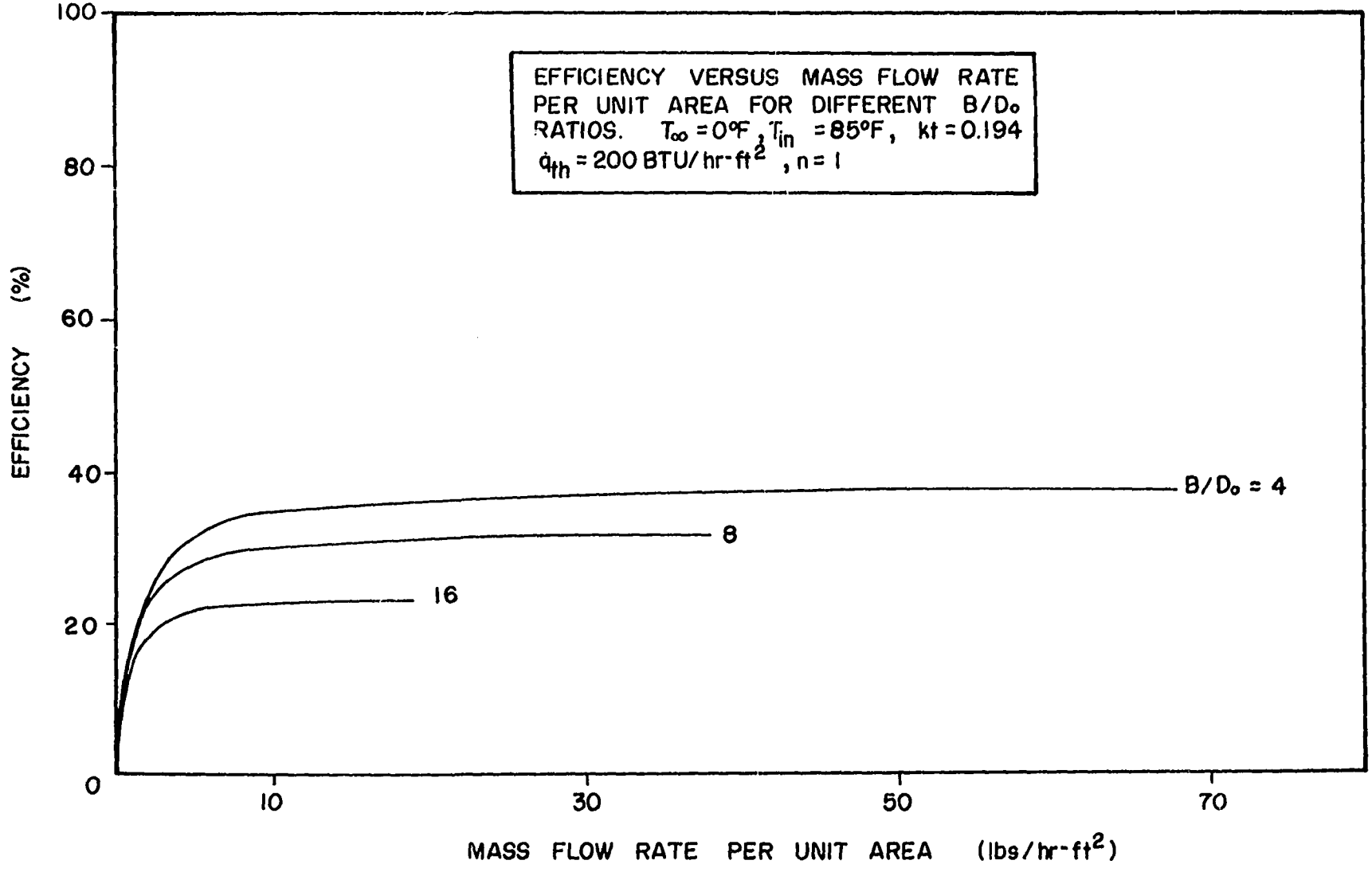
EFFICIENCY VERSUS MASS FLOW RATE PER UNIT AREA FOR DIFFERENT B/Do RATIOS. T∞ = 0°F, Tin = 85°F, kt = 0.194
q̇th = 200 BTU/hr-ft2, n = 1
EFFICIENCY (%)
100
80
60
40
20
0
10
30
50
70
MASS FLOW RATE PER UNIT AREA (lbs/hr-ft2)
B/Do = 4
8
16

Figure 5.3.7 Effect of the number of glass covers on the collector efficiency for $\dot{q}_{th}$ = 200 Btu/hr-ft^2, kt = 0.391 Btu/hr-$^\circ$F, T_∞ = 50°F, T_{in} = 85°F and B/D_o = 8

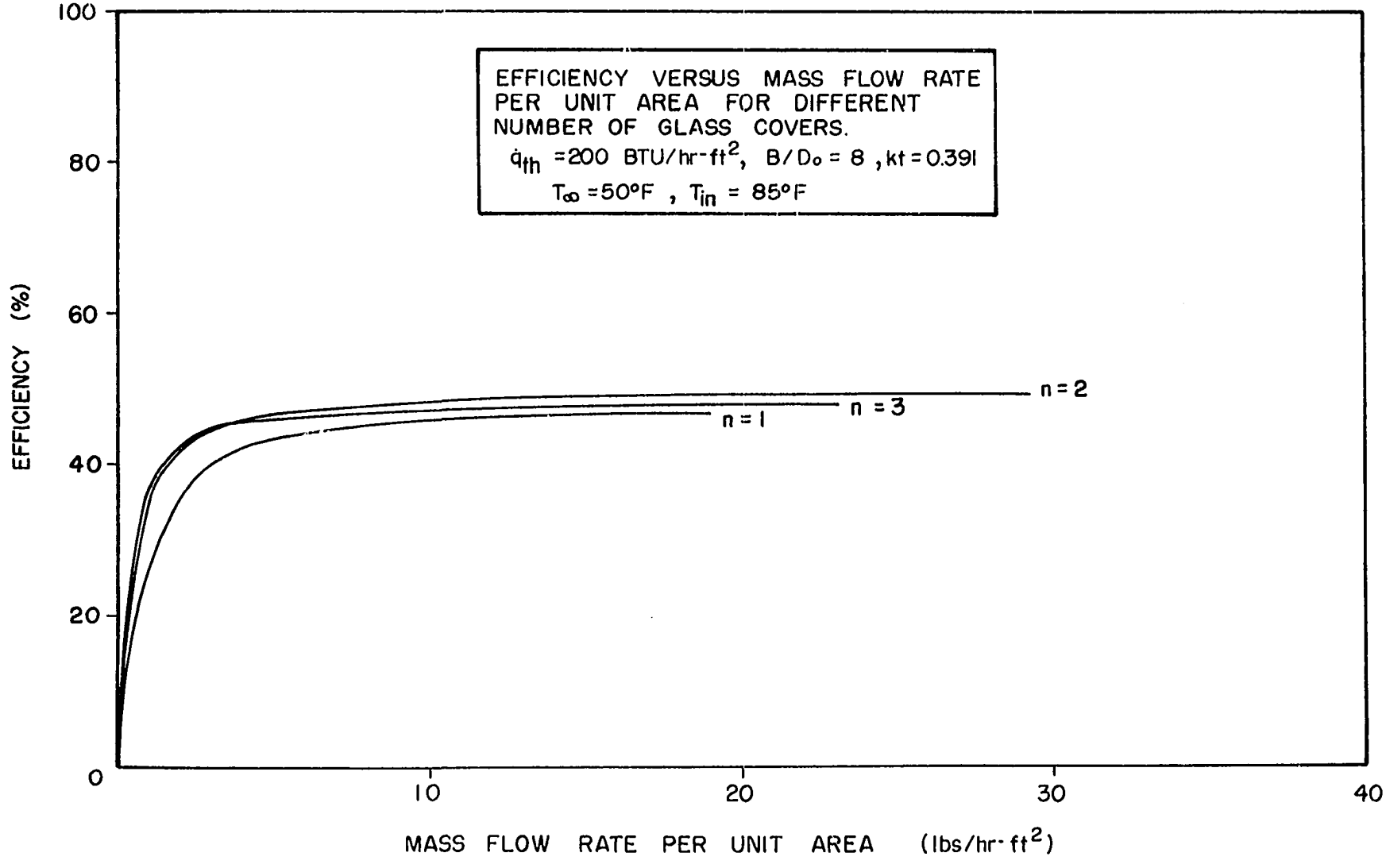
EFFICIENCY VERSUS MASS FLOW RATE PER UNIT AREA FOR DIFFERENT NUMBER OF GLASS COVERS.
$\dot{q}_{th}$ =200 BTU/hr-ft^2, B/Do = 8 , kt = 0.391
T_∞ =50°F , T_{in} = 85°F
n = 2
n = 3
n = 1
EFFICIENCY (%)
100
80
60
40
20
0
10
20
30
40
MASS FLOW RATE PER UNIT AREA (lbs/hr·ft^2)

Effect of Incident Radiation

Figure 5.3.8 illustrates the effect of decreasing the incident radiation by 50%. As should be expected, there is an appreciable decrease in efficiency.

Figure 5.3.8 Effect of decreasing the incident radiation on the collector efficiency for $T_\infty = 50^oF$, $T_{in} = 85^oF$, kt = 0.194 Btu/hr-^oF and n=1

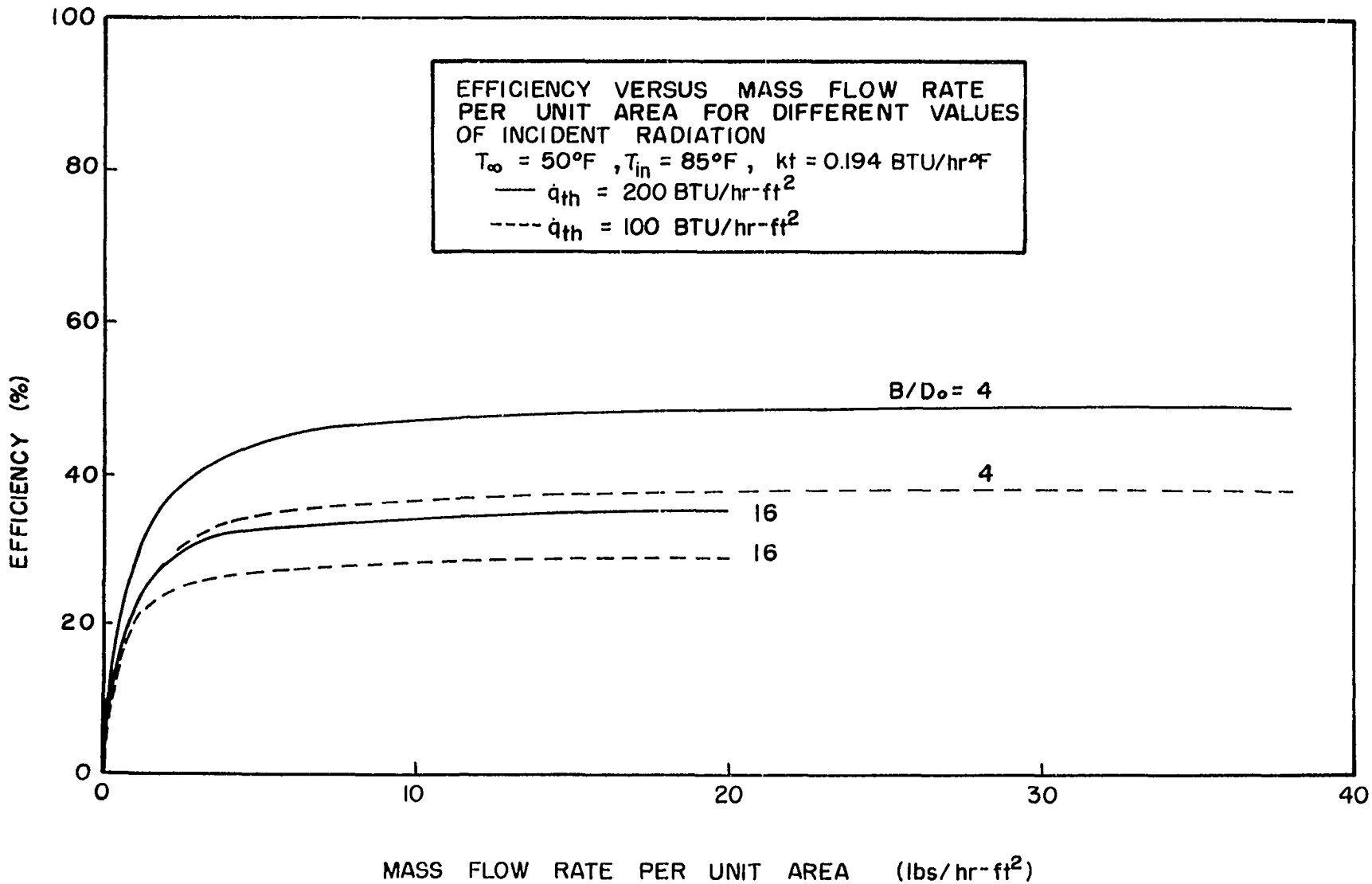
EFFICIENCY VERSUS MASS FLOW RATE PER UNIT AREA FOR DIFFERENT VALUES OF INCIDENT RADIATION
T_∞ = 50°F , T_{in} = 85°F , kt = 0.194 BTU/hr°F
$\dot{q}_{th}$ = 200 BTU/hr-ft^2
$\dot{q}_{th}$ = 100 BTU/hr-ft^2
B/Do= 4
4
16
16
EFFICIENCY (%)
MASS FLOW RATE PER UNIT AREA (lbs/hr-ft^2)
0
20
40
60
80
100
0
10
20
30
40

CHAPTER 6

OPTIMIZATION OF COLLECTOR CONFIGURATION

6.1 Introduction

This chapter describes a method for optimal selection of the collector configuration parameters, viz., the plate thickness, tube spacing and the collector length, based on least-cost per unit of energy collected. The two-dimensional performance model that was developed in the first part of this study is utilized in the optimization process.

In the past, although there have been many studies (Speyer (1958), Buchberg & Roulet (1968), Löf & Tybout (1972)) in which the total collector area is cost optimized, hardly any work has been done in the optimization of the collector configuration itself. Presently, in any collector design, the values of the configuration parameters are arbitrarily chosen, based on experimental observations and general recommendations of Hottel and Whillier (1958). Most investigators consider the collector configuration as a design option, left to the choice of a designer. Due to an increase in the energy awareness and a need for minimal cost solar collector systems, it is felt that the collector configuration is not just a design option; and that, for any given locality and a complete system consisting of a building, storage and a collector unit, there should be an optimum configuration. Such an optimized configuration of the collector should be more economical and efficient.

It should also result in considerable savings, especially when the collectors are mass produced by a manufacturing concern. The reason that there has not been much work in this area is probably due to the fact that the collector model which is currently in use is based on a lumped formulation and hence is not useful for this type of an optimization procedure.

In the present study, using a hypothetical cost model based on retail prices of collector materials, it has been successfully shown that any particular collector design can be cost optimized, depending upon the operating conditions. In this study, even though the collector is optimized as a separate unit, by using a similar procedure it can be optimized as a part of a complete system. Since the computation time required for such an optimization scheme is extremely large, this part of the study has not been carried out.

6.2 Formulation of the Optimization Problem

In the present optimization scheme, the objective function - which is the cost of collector per unit of energy abosrbed, is minimized subject to inequality constraints on length, tube spacing and plate thickness; and equality constraint on the outlet fluid temperature. That is, a combination of length, tube spacing and plate thickness based on minimum cost/Btu that will give a desired outlet temperature is obtained.

Mathematically, the problem may be stated as follows:

$$\text{minimize} \quad F(x_1, x_2, \ldots x_n) \tag{6.2.1}$$

subject to m inequality constraints

$$c_i(x_1, x_2, \ldots x_n) \geq 0 \quad \text{for } i = 1,2,\ldots m \tag{6.2.2}$$

and s equality constraints

$$e_j(x_1,x_2...x_n) = 0 \quad \text{for } j = 1,2,...s \tag{6.2.3}$$

In the general literature associated with optimization schemes (Box, M.J., (1969))the problem as stated in equations 6.2.1 through 6.2.3 is known as a complete optimization problem. Methods such as those due to Fiacco & McCormick (1968) are available to solve this type of problem. Unfortunately, this method cannot be used in the present study, because it requires analytical derivatives of the objective function. In the present problem it is not possible to obtain such analytical derivatives. Hence, another method known as the "complex" method of Box (Box, M.J., (1969)), has been used. The main shortcoming of this method is that it cannot handle equality constraints. In order to use the method of Box, the equality constraint of the problem was approximated by a set of closely spaced inequality constraints.

6.3 Complex Method of Box

The "complex" method of Box is a sequential search technique which has proven effective in solving problems with nonlinear objective functions and subject to nonlinear inequality constraints. The main advantage of using this method in the present problem is that the analytical derivatives of the objective function are not required.

In this method, an original "complex" of $\hat{k} \geq n+1$ points are generated consisting of a feasible starting point and $(\hat{k}-1)$ additional points. The constraints should be of the form as shown in equation (6.2.2). The upper and lower limits of the constraints are either constants or functions of the independent variables of the problem.

The additional ($\hat{k}$-1) points required to set up the initial configuration are found as follows. A tentative trial point is generated with the coordinates

$$x_{i,j} = G_i + r_{i,j}(H_i - G_i) \qquad \begin{matrix} i = 1,2,3...n \\ j = 1,2,3...k-n \end{matrix} \qquad (6.2.4)$$

where the "random numbers" $r_{i,j}$ are pseudo-random rectangularly distributed deviates in the interval (0,1). This point will necessarily satisfy the explicit constraints, but may not satisfy one or more of the implicit constraints. If this is the case, the trial point is moved halfway toward the centroid of those points already selected (of which there is at least one, the initial point), this process being repeated as necessary. Ultimately a permissible point will be found (certainly if the feasible region is convex), and in this way all the $\hat{k}$ points or the vertices of the initial configuration can be constructed.

The objective function is evaluated at each of these points, and the vertex of greatest function value determined. The worst point is replaced by its over-reflection in the centroid of the remaining vertices; where, by over-reflection is meant the point on the produced line joining the rejected point and this centroid, but γ times as far from the centroid as the reflection of the rejected point, γ being an empirical parameter.

Various cases calling for different treatments, arise as follows:

(i) If this trial point satisfies all the constraints, the function is evaluated there, and the whole process repeated. Unless,

(ii) the trial point happens to be the worst point in the new configuration, in which case a move halfway towards the centroid is made instead of the basic iteration of over-reflection.

(iii) If the trial point does not satisfy some explicit constraint, that variable is reset just inside the appropriate boundary (for example by an amount 0.0001) to give a further trial point.

(iv) If some implicit constraint is violated, a further trial point is constructed by a move halfway back towards the centroid, this process being repeated as necessary. These moves could prove unsuccessful if the region were not convex, or if curved valleys were encountered.

Suitable empirically determined values for γ and $\hat{k}$ are $\gamma = 1.3$ and $\hat{k} = 2n$, although this value of $\hat{k}$ is too large when n is as large as ten. $\hat{k} > n+1$ points have been found necessary in order to prevent the configuration from collapsing prematurely into a subspace. The use of the over-reflection factor $\gamma > 1$ enables the complex to expand whenever possible, while the moves toward the centroid allow the complex to contract when necessary.

In general, any iterative minimization technique may converge to a local minimum instead of the required global minimum. With unconstrained problems, a rough check that the global minimum has in fact been found is usually performed by restarting the method from different points, and inferring that if these all lead to the same solution, then this indeed is the global minimum. For constrained optimization, it is not an easy matter to find alternative starting points which satisfy all the constraints, and which differ substantially from each other. With the complex method, this type of check can readily be performed using the same initial point, but different pseudo-random numbers to set up the initial configuration, and the ease with which this can be done is considered to be an advantage of the method. It is also considered that as the initial configuration is generated so as to roughly span the feasible region, the first few iterations will be

Figure 6.3.1 Box (Complex Algorithm) Logic Diagram.

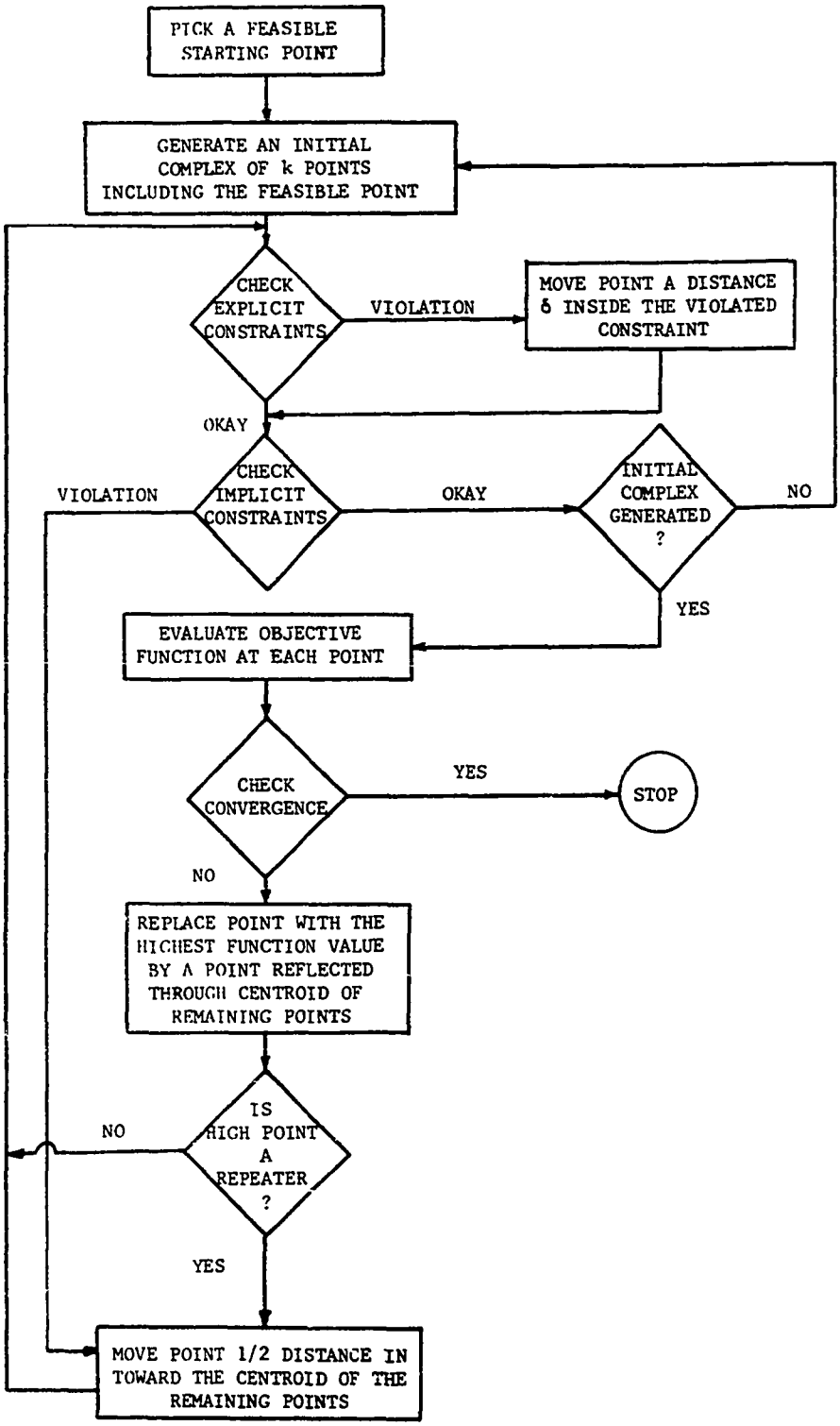
PICK A FEASIBLE STARTING POINT
GENERATE AN INITIAL COMPLEX OF k POINTS INCLUDING THE FEASIBLE POINT
CHECK EXPLICIT CONSTRAINTS
VIOLATION
MOVE POINT A DISTANCE δ INSIDE THE VIOLATED CONSTRAINT
OKAY
CHECK IMPLICIT CONSTRAINTS
VIOLATION
OKAY
INITIAL COMPLEX GENERATED ?
NO
YES
EVALUATE OBJECTIVE FUNCTION AT EACH POINT
CHECK CONVERGENCE
YES
STOP
NO
REPLACE POINT WITH THE HIGHEST FUNCTION VALUE BY A POINT REFLECTED THROUGH CENTROID OF REMAINING POINTS
IS HIGH POINT A REPEATER ?
NO
YES
MOVE POINT 1/2 DISTANCE IN TOWARD THE CENTROID OF THE REMAINING POINTS

even more likely to span the whole of this region. Consequently it seems reasonable to suppose that if several local mimima exist, and one of these corresponds to a very much smaller function value than the rest, then this best local mimimum (the global minimum), will be found. Conversely, if the global minimum is not found, then there would seem to be a high probability that it would not represent much improvement over the minimum actually located.

To test for convergence, the standard deviation

$$S = \sqrt{\left\{ \sum_{i=1}^{n+1} \frac{(F_i - \bar{F})^2}{n} \right\}} \qquad (6.2.5)$$

of the function values at the (n+1) vertices of the current complex is compared with some specified value. A possible improvement on this test would involve the calculation of S after every $\tilde{k}$ evaluations, $\tilde{k}$ being pre-assigned. The requirement would then be that two successive values of S were less than the specified value, and that the corresponding mean values $\bar{F}$ did not differ by some specified amount. This criterion would insure that the search continued until the complex had virtually collapsed onto the indicated minimum.

Figure 6.3.1 shows that logic diagram used in the complex algorithm, which has been reproduced from Kuester and Mize (1973). Further details of the algorithm can be found in this reference.

6.4 Formulation of the Cost-Function

The total cost of the collector per unit of energy absorbed may be expressed in terms of the parameters that describe its configuration and performance. These include collector type, manufacturing process, cost of materials, installation, etc. The actual cost of a flat plate collector can

be broadly divided into four groups:

(i) Fixed cost - Includes framing, insulation, supports, painting, manufacturing process, etc.

(ii) Sheet metal cost - Expressed in dollars per pound of the sheet metal used.

(iii) Cost of tubing - Expressed in dollars per foot length of the tube.

(iv) Cost of glass covers - Expressed in dollars per square foot of the glass used.

The cost function that was developed for the analysis is based on the prices quoted by local hardware suppliers. The total cost per tube of the collector and the associated fin may now be expressed as,

$$\text{(Total cost of collector/tube)} = \text{Fixed cost} + \text{sheet metal cost} + \text{Tube cost} + \text{cost of glass covers} \qquad (6.3.1)$$

Löf and Tybout (1973) have estimated that glass covers cost about $\$0.40/ft^2$ of the collector area. An estimate of $\$2.70/ft^2$ as fixed cost of the collector was obtained from the construction details of C.S.U. solar house. Thus,

$$\text{(Total cost of collector/tube)} = (\$2.70 * \text{Area/tube}) + (\$/\text{lb of plate material})(\text{Weight of the plate/tube}) + (\$1.00/\text{ft})(\text{Tube length}) + (\$0.40/ft^2)(\text{Area/Tube})*n \qquad (6.3.2)$$

where n is the number of glass covers used.

The cost function is now defined as the ratio of the total cost per tube and the associated fin, to the amount of useful energy absorbed per tube. This will be the objective function of the optimization scheme.

$$\text{cost function (F)} = \frac{\text{Total cost per tube and the associated fins}}{\text{Useful energy absorbed per tube}}$$

$$F(B,L,t,n,T_{out}) = \{(\$2.70*BL) + \rho_p(2.0\ WLt)(\$2.00/\text{lb of plate material}) + (\$1.00/ft)*L + (\$0.40*BL)*n\} / (\dot{m}\ C_p(T_{out}-T_{in})) \quad (6.3.3)$$

where ρ_p is the density of the plate material.

Inequality constraints are:

$$G_1 \leq L \leq H_1 \qquad G_2 \leq B \leq H_2 \qquad G_3 \leq t \leq H_3 \quad (6.3.4)$$

and the equality constraint is

$$T_{out} = H_4 \quad (6.3.5)$$

This is converted into an inequality constraint

$$G_4 \leq T_{out} \leq H_4 \quad (6.3.6)$$

where G_i and H_i, i = 1,2,3 & 4 are the lower and upper limits of the constraints respectively. In the present problem $G_4 = 90^oF$ and $H_4 = 95^oF$. The exact values of the upper and lower limits for L, B and t do not really matter as long as they are within practical limits.

6.5 Some Results of the Optimization Scheme

The following data is used as input to the optimization program:

Locality: Oklahoma City Latitude: 35° Longitude: 97°

Date: January 15th Time: 1300 hrs Solar radiation on a horizontal surface: 200 Btu/hr-ft^2 Wind speed: 5 knots

TABLE 6.5

PLATE THICKNESS t (inches)	TUBE SPACING B (inches)	COLLECTOR LENGTH L (feet)	COLLECTOR OUTLET TEMP. T_{out} (^{o}F)	COST/BTU ($/BTU)
	2.0	14.922	90.001	0.0591
	3.0	10.047	90.05	0.0473
0.0107	6.0	5.322	90.03	0.0380
	9.0	4.000	90.008	0.0383
	12.0	3.521	90.07	0.0416
	15.0	3.282	90.05	0.0467
	2.0	14.927	90.01	0.0648
	3.0	9.908	90.01	0.0499
0.0215	6.0	5.457	90.34	0.0426
	9.0	3.871	90.32	0.0413
	15.0	2.849	90.34	0.0463
	2.0	14.920	90.01	0.0764
	3.0	9.866	90.01	0.0642
	6.0	5.016	90.01	0.0535
0.0429	9.0	3.521	90.07	0.0516
	12.0	2.876	90.23	0.0523
	15.0	2.360	90.02	0.0545

Cloud cover: 0.5 Ambient temperature: 50°F Collector material: copper Collector fluid: water No. glass covers: 1

Assuming a collector inlet temperature of 85°F and a mass flow rate of 85 lbs/hr, Table 6.5 gives the optimum collector lengths for obtaining an outlet temperature between 90°F and 95°F. Observe that the results of cost optimization shown in Table 6.5 are based on hourly weather data. The aim of the present optimization study has been to show that a cost optimized collector configuration can be obtained for any particular application. In order to obtain a truly cost optimized system, optimization procedure has to be carried out over a whole year using hourly weather data. The cost function has to be converted into annual cost, and an amortization period has to be assumed. Hopefully this will be the subject of future work.

Since the complex method of Box does not handle equality constraints, a more efficient optimization method should be found to take care of the equality constraints of the problem.

CHAPTER 7

CONCLUDING REMARKS

The present study has sought to develop a method to optimize the configuration of a flat plate collector, based on least cost per unit of energy absorbed. Since the objective function of the optimization scheme is dependent on the collector performance, a theoretical model of the collector that would be suitable to an optimization scheme had to be first developed.

A rational and systematic two dimensional analysis of a flat plate collector is developed, whereby, for any given set of conditions its performance can be evaluated without having to assume any collector parameter, such as the average collector temperature etc.

The nature of the present formulation makes it possible to explicitly study the collector behavior just by inputing hourly weather data and configuration details. Although the present analysis is more complex than the existing one, it is systematic, accurate and more versatile.

Using the two-dimensional performance model of the collector, an optimization scheme is suggested whereby the configuration of a flat plate collector can be cost optimized based on hourly weather data. In the present study it has been shown in principle that it is possible to optimize collector configuration parameters based on least cost per Btu of energy absorbed. In order to obtain a truly optimal collector configuration for a

given locality and operating conditions, the optimization scheme has to be carried out using a whole year's weather data. This part of the problem has not been done and needs further investigation. Such an optimization program should be very interesting and useful in order to study the effects of various parameters such as manufacturing costs, variation in material costs, etc.

Although the cost figures presented in Table 6.5 are highly dependent on the exact nature of the cost function used in the optimization scheme, the trends shown are correct. The absolute values of these optimized cost figures need to be made more realistic using more accurate cost data.

BIBLIOGRAPHY

ASHREA Guide and Product Directory, 1974.

Baker, L.H., "Film Heat Transfer Coefficients in Solar Collector Tubes at Low Reynolds Numbers", Solar Energy, Vol. 11, No. 2, 1967, pp. 78-85.

Bliss, R.W., "The Derivations of Several Plate-Efficiency Factors Useful in the Design of Flat-Plate Solar Heat Collectors", Solar Energy, Vol. 3, No. 4, 1959, pp. 55-69.

Box, M.J., D. Davies and W.H. Swann, "Non-Linear Optimization Techniques", Imperial Chemical Industries Monograph, No. 5, Oliver and Boyd, Edinburgh, 1969.

Box, M.J., "A New Method of Constrained Optimization and a Comparison with Other Methods", Computer Journal, Vol. 8, 1965, pp. 42-52.

Brown, A.R., and M.A. Thomas, "Combined Free and Forced Convection Heat Transfer for Laminar Flow in Horizontal Tubes", Journal of Mech. Eng. Sci., Vol. 7, No. 4, 1965, pp. 440-448.

Buchberg and Roulet, "Simulation and Optimization of Solar Collection and Storage for House Heating", Solar Energy, Vol. 12, 1968, pp. 31-50.

Duffie, J.A. and W.A. Beckman, "Solar Energy Thermal Processes", 1974, John Wiley and Sons, New York.

Fiaco, A.V. and G.P. McCormick, "Nonlinear Sequential Unconstrained Minimization Techniques", John Wiley and Sons, New York, 1968.

Hottel, H.C., and B.S. Woertz, "The Performance of Flat-Plate Solar Heat Collectors", Trans. ASME, Vol. 64, 1942, pp. 91-104.

Hottel, H.C. and Whillier, A., "Evaluation of Flat-Plate Collector Performance", Trans. Conf. on the Use of Solar Energy, Vol. 2, Part 1, 1958, p. 74, University of Arizona Press.

Klein, S.A., J.A. Duffie, and W.A. Beckman, "Transient Considerations of Flat-Plate Solar Collectors", Trans. Am. Soc. Mech. Engrs., J. Eng. Power 96A, 1974, p. 109.

Kuester, J.L. and J.H. Mize, "Optimization Techniques with Fortran", McGraw-Hill Book Company, 1973.

Löf, G.O.G. and R.A. Tybout, "A Model for Optimizing Solar Heating Design", ASME Paper No. 72-WA/Sol-8, Presented at the Winter Annual Meeting of ASME, New York, November 1972.

Oliver, D.R., "The Effect of Natural Convection on Viscous-Flow Heat Transfer in Horizontal Tubes", Chem. Eng. Sci., Vol. 17, 1962, pp. 335-350.

Speyer, E., "Optimum Storage of Heat with a Solar House", Solar Energy, Vol. 3, No. 4, 1959, pp. 26-48.

Tabor, H., "Solar Energy Collector Design", Bull. Res. Coun. Israel, Vol. 5C, 1955, p. 55.

Tabor, H., "Radiation, Convection and Conduction Coefficients in Solar Collectors", Bull. Res. Coun. Israel, Vol. 6C, 1958, p. 155.

Whillier, A., "Solar Energy Collection and its Utilization for House Heating", Sc. D. Thesis, 1953, Dept. of Mechanical Engineering, M.I.T.

Whillier, A., "Design Factors Influencing Solar Collector Performance", Low Temperature Applications of Solar Energy, Chapter III, Edited by R.C. Jordon, 1967.

APPENDIX A

TEMPERATURE DISTRIBUTION OF THE COLLECTOR FLUID FOR THE LIMITING CASE OF TUBES SIDE BY SIDE

Consider an element Δx of a tube containing fluid as illustrated in the Figure A.1. Neglect the thermal resistance of the tube and assume the fluid temperature to vary only along the axis of the tube. Making an energy balance on the element Δx, we have,

$$\dot{m} C_p \frac{dT_f}{dx} + U_o \left(\frac{\pi D_o}{2}\right)(T_f - T_\infty) - \dot{q}_i D_o = 0 \qquad (A.1)$$

where U_o is the overall loss coefficient from the fluid to the ambient. This equation is non-dimensionalized by substituting

$$\theta_f = \left(\frac{T_f - T_\infty}{T_{in} - T_\infty}\right) \quad \text{and} \quad x^* = \frac{x}{L} \qquad (A.2)$$

We now have

$$\frac{d\theta_f}{dx^*} + \left[\frac{U_o \pi D_o L}{2\dot{m} C_p}\right]\theta_f = \left[\frac{\dot{q}_i D_o L}{\dot{m} C_p (T_{in} - T_\infty)}\right] \qquad (A.3)$$

or

$$\frac{d\theta_f}{dx^*} + M_f \theta_f = P \qquad (A.4)$$

Figure A.1 Diagram showing the limiting case of tubes side by side and the element of the collector tube referred to in the derivation of the fluid temperature distribution.

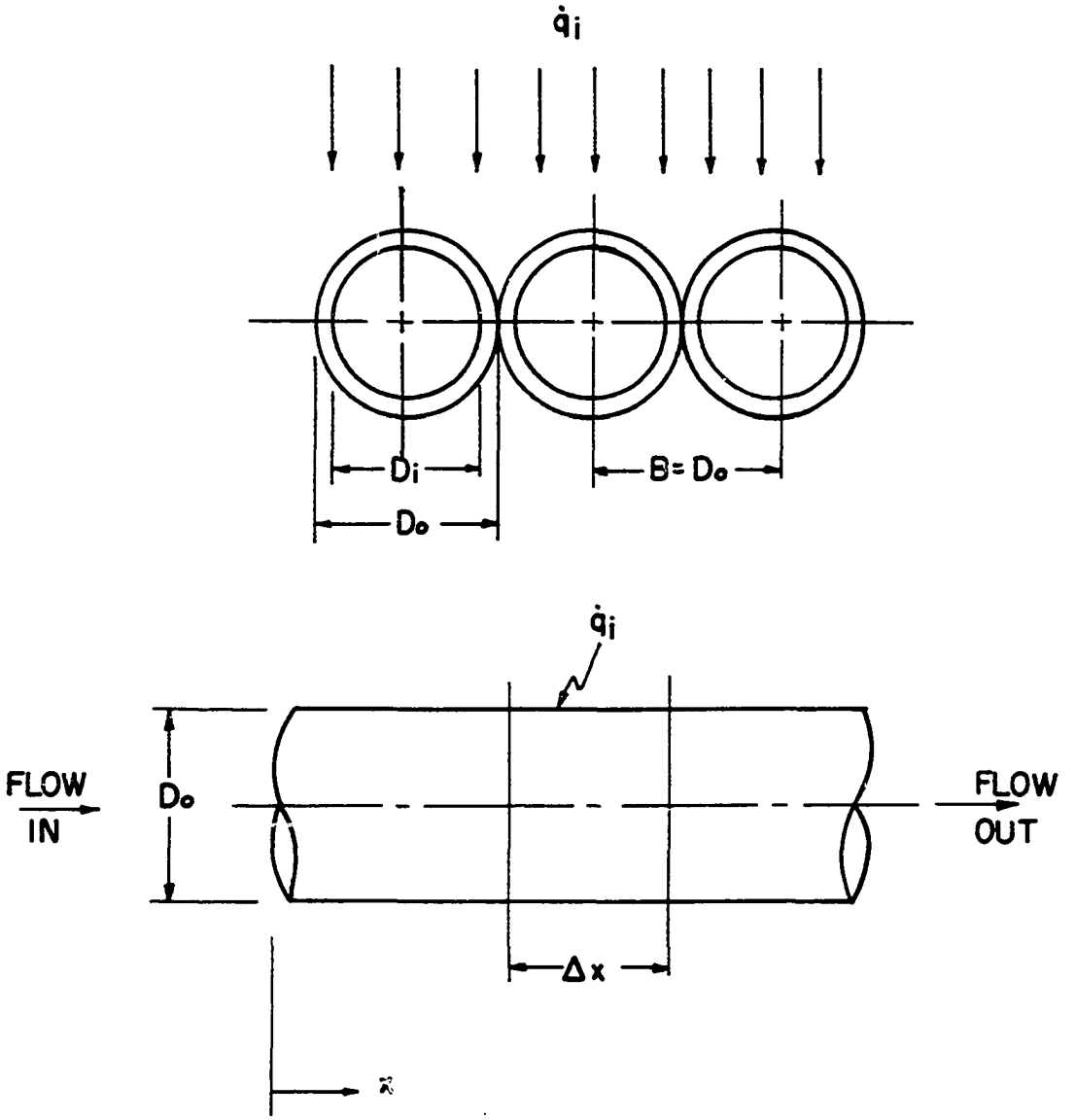
$\dot{q}_i$
D_i
$B = D_o$
D_o
$\dot{q}_i$
FLOW
IN
D_o
FLOW
OUT
Δx
x

where
$$M_f = \left[\frac{U_o \pi D_o L}{2\dot{m} C_p}\right] \tag{A.5}$$

and
$$P = \left[\frac{\dot{q}_i D_o L}{\dot{m} C_p (T_{in} - T_\infty)}\right]$$

The solution to this differential equation is

$$\theta_f(x^*) = e^{-M_f x^*} \int_0^{x^*} P \; e^{M_f \xi} d\xi + E \; e^{-M_f x^*} \tag{A.6}$$

where E is the constant of integration.

Using the boundary condition,

$$@ \; x^* = 0 \quad \theta_f = 1 \tag{A.7}$$

we obtain
$$E = 1$$

Thus,

$$\theta_f(x^*) = \frac{P}{M_f} + e^{-M_f x^*} \left(1 - \frac{P}{M_f}\right) \tag{A.8}$$

The fluid temperature distribution is now given by

$$T(x^*) = \theta(x^*)(T_{in} - T_\infty) + T_\infty \tag{A.9}$$

Average Fluid Temperature

$$\theta_{f,avg} = \int_0^1 \theta_f(x^*) dx^*$$

$$= \int_0^1 \left[\frac{P}{M_f} + e^{-M_f x^*} \left(1 - \frac{P}{M_f}\right)\right] dx^* \tag{A.10}$$

$$= \frac{P}{M_f} + \left(1 - \frac{P}{M_f}\right) \frac{(1 - e^{-M_f})}{M_f}$$

Thus, the average fluid temperature is

$$T_{f,avg} = \theta_{f,avg}(T_{in}-T_{\infty}) + T_{\infty} \qquad (A.11)$$

This average value of fluid temperature is used for evaluating an average value of the overall loss coefficient (U_o), from the fluid to the ambient.

Figure B.1 Diagram showing the experimental set-up used for taking thermograms of the collector panel

APPENDIX B

EXPERIMENTAL DETERMINATION OF THE ISOTHERMS OF THE ABSORBER PLATE USING SCANNING INFRARED CAMERA

An experiment was conducted to verify the analytical results for a single fin attached to the side of a copper tube. The plate-tube segment used in the experiment (Figure 2.1.1) was fabricated from a $\frac{1}{2}$" copper tubing and 0.02" steel sheet metal. The overall dimensions of the fabricated collector panel was 22" X 5 $\frac{7}{8}$". This was insulated on all edges and at the bottom using 2" thick styrofoam. The absorbing surface of the panel was covered with a sheet of saran wrap to reduce upward losses. A spacing of 3/4" was provided between the transparent cover and the absorber plate. The absorber and tube surfaces were painted black using commerically available black paint.

The experiment was conducted on a winter day, late in the afternoon, with clear skies and gusty winds of about 10-15 mph. The collector surface was oriented normal to the direction of sun using visual alignment.

The temperature distribution over the collector surface was monitored with a scanning infrared camera manufactured by Texas Instruments Co. The arrangement of the equipment used in the experiment is shown in Figure B.1. The equilibrium temperature of the plate was beyond the range of the camera and hence extremely high mass flow rate of water had to be used to lower the plate temperature to within the range of the camera. The inlet end of the

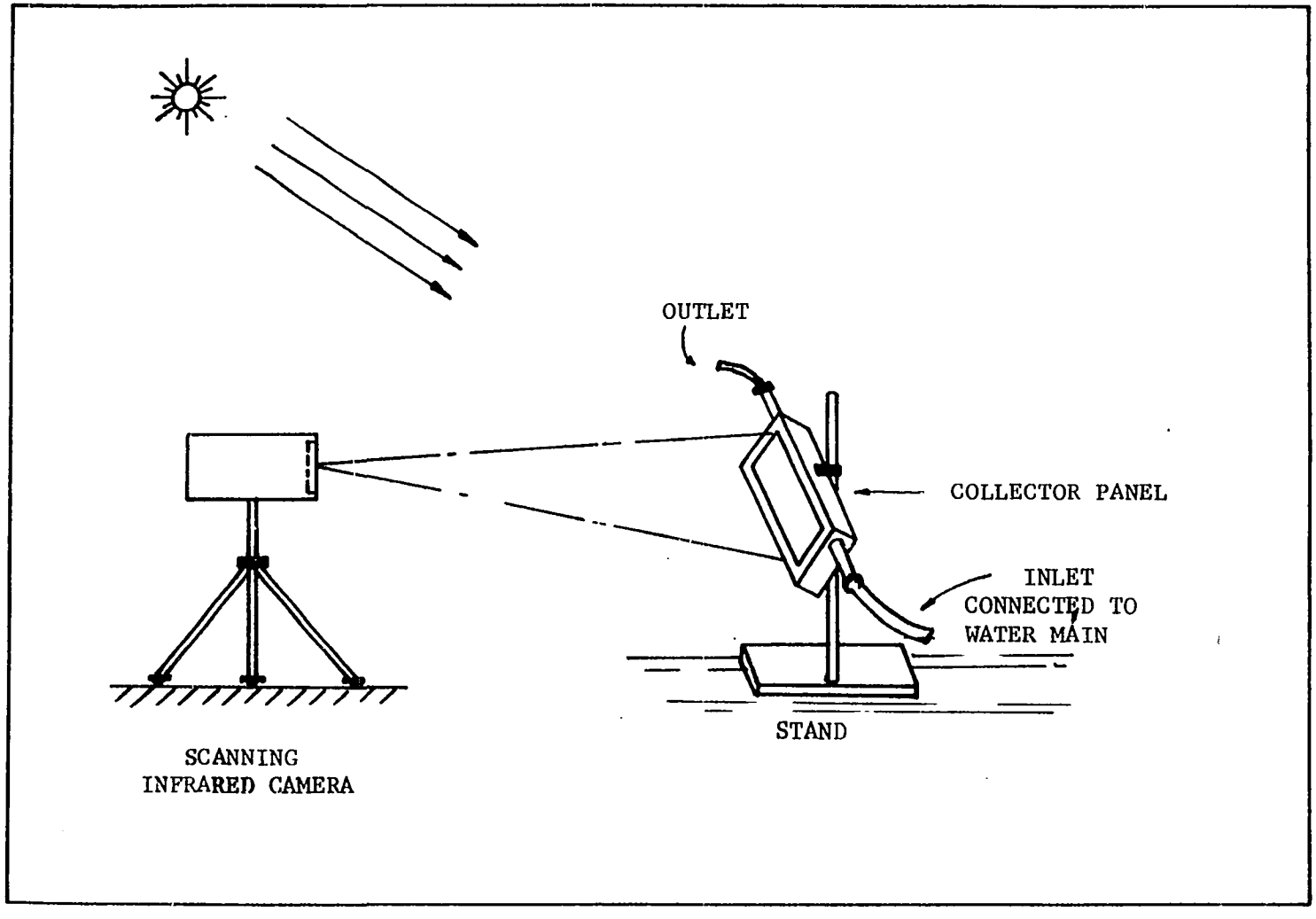
OUTLET
COLLECTOR PANEL
INLET
CONNECTED TO
WATER MAIN
STAND
SCANNING
INFRARED CAMERA

collector panel was connected to a city water supply. The inlet water temperature was 67.5°F, and mass flow rate was 42 lbs/min.

In Figure B.2, thermograms of the collector panel with zero mass flow rate and with a flow rate of 42 lbs/min are shown. In the thermograms white is hotter and black is cooler with shades of gray representing intermediate temperatures. The scale on the side of the thermogram is intended by the manufacturer to indicate temperatures, however, no correction has been made to account for the effect of the plastic cover sheet. Therefore, the readings only depict relative temperatures and the absolute temperatures indicated are not really accurate.

As predicted by the theoretical analysis, the inlet end of the plate is cooler than the outlet end. The cool areas which are visible at the edges of the plate are due to edge losses. Observe that the areas near the inlet and the outlet end are cooler than they should be. This is due to the heat loss along the pipe by conduction.

Microdensitometer traces were taken of the thermogram negatives. The isodensity lines obtained from the densitometer traces correspond to the isotherms. Figure B.3 shows the isotherms obtained from the densitometer traces. It is interesting to note that the general trend of the isotherms compare favorably with the analytical predictions. The analysis indicates that for large flow rates the isotherms would be almost parallel to the fluid flow direction. This is verified in the present experiment. The main reason that the isotherms in Figure B.3 are not smooth curves is due to unequal plate thickness caused by improper welding of the plate and the tube during fabrication.

The present experiment quantitatively verifies the general pattern of the isotherms for large flow rates of the collector fluid. Although

Figure B.2 Thermograms of the collector panel with zero mass flow rate and with a flow rate of 42 lbs/min. $T_{in} = 67.5^{o}F$ and $T_{\infty} = 72^{o}F$

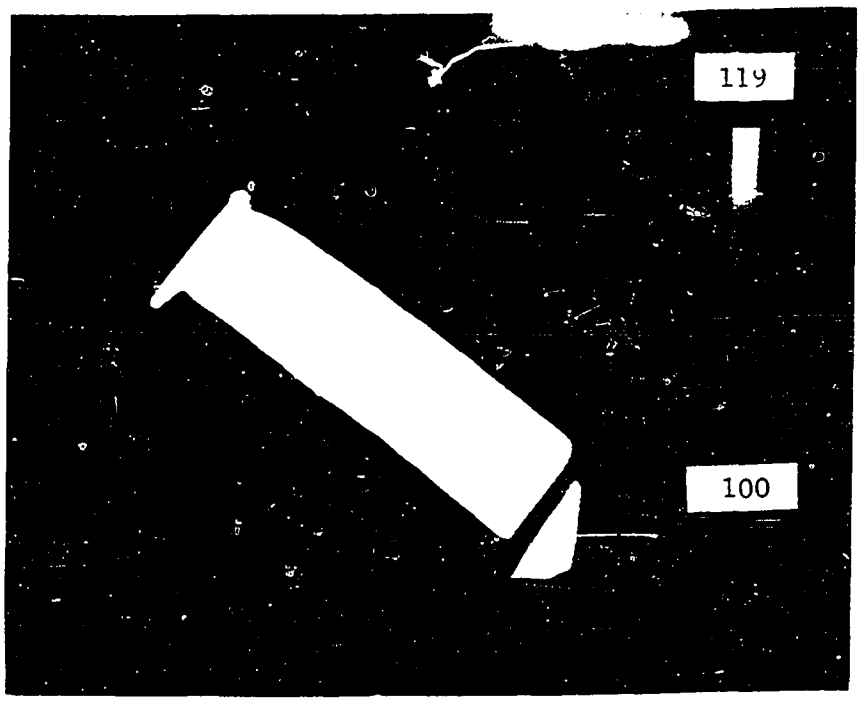

THERMOGRAM OF THE ABSORBER PLATE
FOR ZERO MASS FLOW RATE

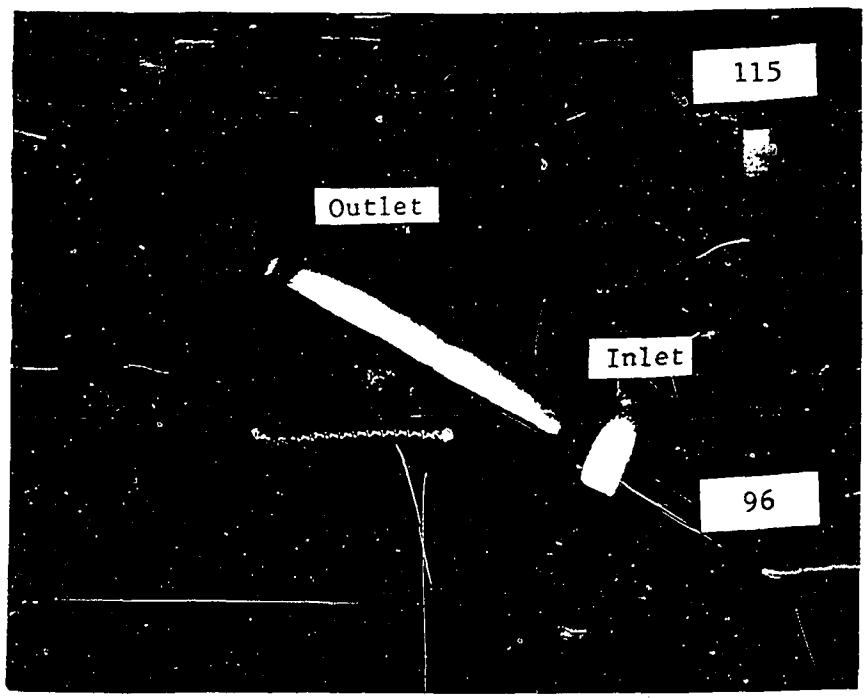

THERMOGRAM OF THE ABSORBER PLATE
FOR A MASS FLOW RATE OF 42 LBS/MIN

Figure B.3 Plot of isotherms of the collector plate obtained from the Thermogram for a mass flow rate of 42 lbs/min, $T_{in} = 67.5^{o}F$ and $T_{\infty} = 72^{o}F$. The temperatures indicated on the isotherms are approximate.

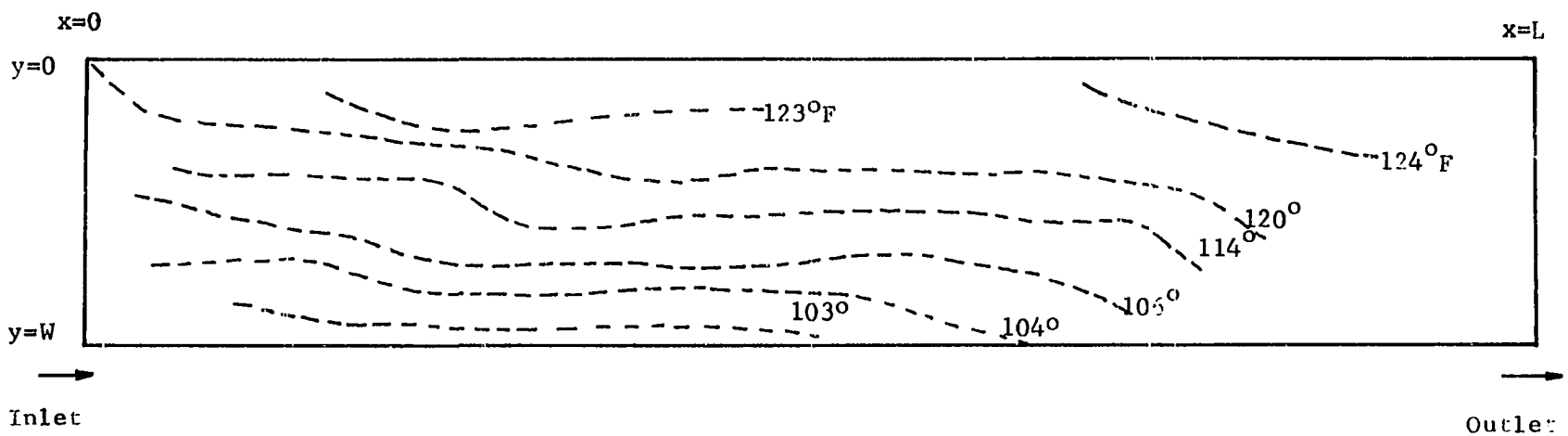

Plot of isotherms of collector plate for
a mass flow rate of 42 lbs/min, T_{in} = 67.5°F and T_{∞} = 72°F

the magnitudes of the temperatures may not be accurate, the trends indicated definitely verify the analytical predictions. Further work needs to be done under more accurately controlled conditions in order to obtain better agreement with the analysis.